INVESTIGATING THE ROLE OF CtBP2 IN REGULATING TUMOR DORMANCY

Kranthi Kumar Chougoni*, Priyadarshan K. Damle[1], Bhaumik Patel[1] and Steven R.Grossman[1]
*C. Kenneth and Dianne Wright Center for Clinical and Translational Research, [1]Division of Hematology, Oncology, and Palliative Care, VCU School of Medicine and VCU Massey Cancer Center, Richmond, VA 23298

Introduction

C-terminal binding proteins (CtBP1 and 2) are transcriptional co-regulators overexpressed in more than 60% of human colorectal tumors, and often involved in promoting activities like tumor survival, proliferation and migration. In addition CtBP2 was specifically shown to promote the self-renewal ability of the cancer stem cell (CSC) population, which is one of the serious limitations to existing anticancer therapies. CtBP2 was shown to up regulate Transcriptional Factor 4 (TCF4) signaling to promote CSC activity. Of note, characteristics of cancer stem cells significantly overlap with those of dormant tumor cells. Tumor dormancy can be defined as cell cycle arrest for prolonged period of time before recurrence. Tumors are heterogeneous in nature which include both therapy resistant and sensitive cells. This phenomenon of tumor dormancy is seen in cancer cells that resist or escape chemotherapy before recurrence. Although, CtBPs role in promoting CSC activity is proven its role in regulating tumor dormancy has not been explored.

The aim of this project is to develop a tumor dormancy model and explore the role of CtBP2 in tumor dormancy.

EXPERIMENTAL SETUP

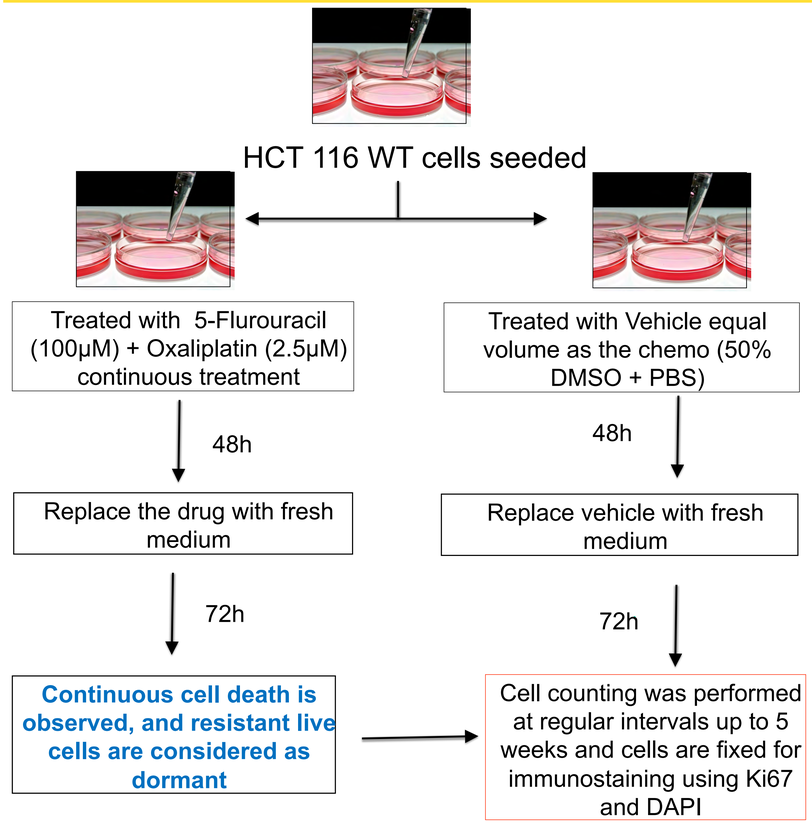

Chemotherapy induces cell growth arrest

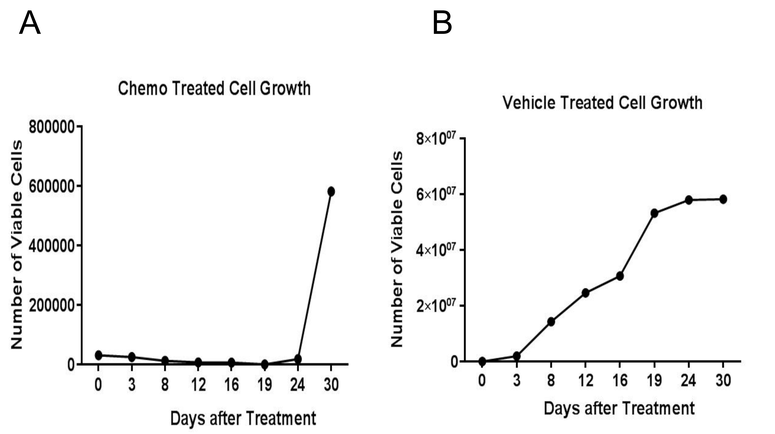

Fig.1 Chemotherapy induces cell growth arrest. Growth pattern of HCT 116 cells treated with **A.** 5FU+ Oxaliplatin and **B.** Vehicle (50%PBS+50%DMSO). Following chemotherapy cell death is observed till day 12, and cell growth arrest is observed between day 12 to day 24, which can be described as the period of dormancy. After day 24, cells start proliferating, which indicates the cells transitioned from the dormant phase to the growth phase.

Dormant cells express low levels of CtBP2

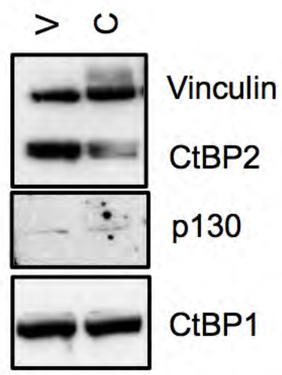

Fig.2 Dormant cells express decreased CtBP2 protein levels. Western blot showing decreased CtBP2 protein levels in cells treated with chemotherapy **C: 5FU+ Oxaliplatin** compared to **V: Vehicle: 50% PBS + 50% DMSO** treated cells, 7 days post vehicle treatment. However no change was observed in CtBP1 protein levels between cells treated with chemotherapy and vehicle. Tumor suppressor p130 was probed to determine its role in promoting tumor dormancy, as its protein levels alter with changes in cell cycle. Vinculin is probed was used as loading control.

Dormant cells lack proliferation ability

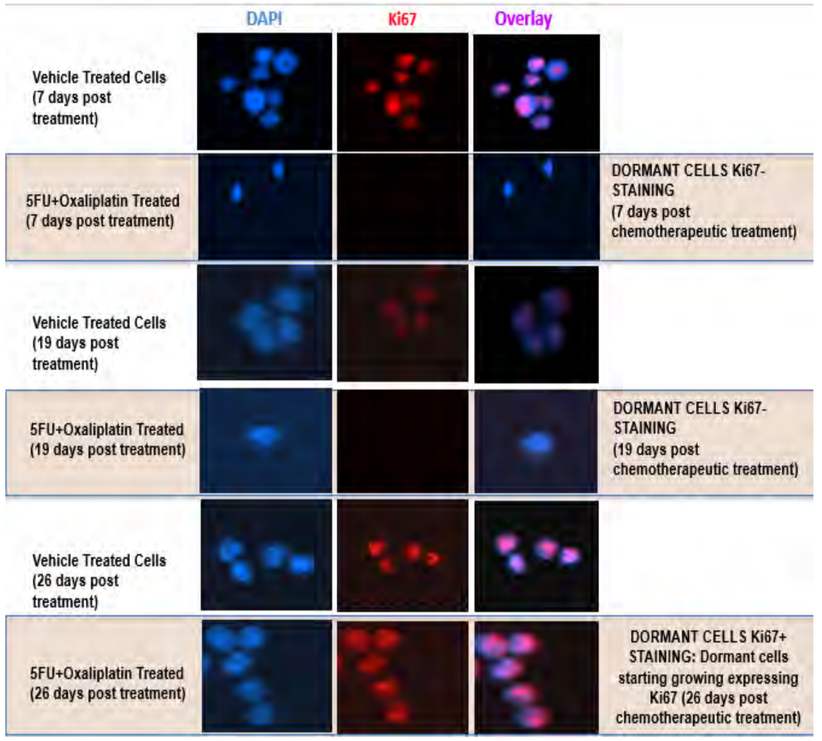

Fig.3 Characterization of tumor dormancy. Following chemotherapy dormant cells lacked Ki67 expression till day 19. After day 19, cells start proliferating as observed by Ki67 expression on day 26.

Conclusion

We developed an *in vitro* tumor dormancy model using chemotherapeutic agents. We further validated our model by performing immunostaining using Ki67. Dormant cells possessed low levels of CtBP2 protein as expected, and we further propose to inhibit CtBP2 activity with chemical inhibitors to induce apoptosis in dormant cells. However, additional studies are needed to validate this hypothesis. In future studies we propose to combine 4-Cl HIPP following chemotherapy either alone or in combination with MEK inhibitor to eliminate chemo-resistant dormant tumor cells.

References

Patel J, Baranwal S, Love IM, Patel NJ, Grossman SR, Patel BB. Inhibition of C-terminal binding protein attenuates transcription factor 4 signaling to selectively target colon cancer stem cells. Cell Cycle. 2014;13(22):3506-3518.
Kleffel S, Schatton T. Tumor dormancy and cancer stem cells: Two sides of the same coin? Adv Exp Med Biol. 2013;734:145-179.
Grooteclaes M, Deveraux Q, Hildebrand J, Zhang Q, Goodman RH, Frisch SM. C-terminal-binding protein corepresses epithelial and proapoptotic gene expression programs. Proc Natl Acad Sci U S A. 2003;100(8):4568-4573.

Mesenchymal cells are main determinants in the therapeutic benefit of hedgehog inhibition in TNBC

[1]Ramos KP, [1]Rodriguez N, [3]Martinez-Montemayor M.,[2]Torres-Garcia W. and [1]Domenech M

[1]Department of Chemical Engineering and [2]Department of Industrial Engineering at University of Puerto Rico-Mayaguez

[3]School of Medicine, Universidad Central del Caribe-Bayamon

Background

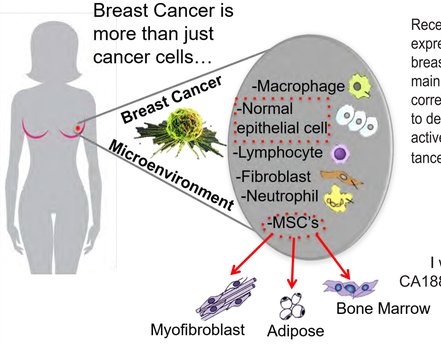

Recent studies have shown that active Hh signaling is over-expressed and decreases survival rates in triple negative breast cancer (TNBC) patients. Mesenchymal cells are main players of paracrine Hh signaling and their abundance correlates with poor prognosis in TNBC. Our main goal is to determine the role of mesenchymal cell sub-types with active Hh signaling in tumor progression and drug resistance mechanisms.

Aknowledgements

I want to extend my thanks to NIH-NCI K01 CA188167 for providing the necessary funds to conduct this investigation.

Methodology

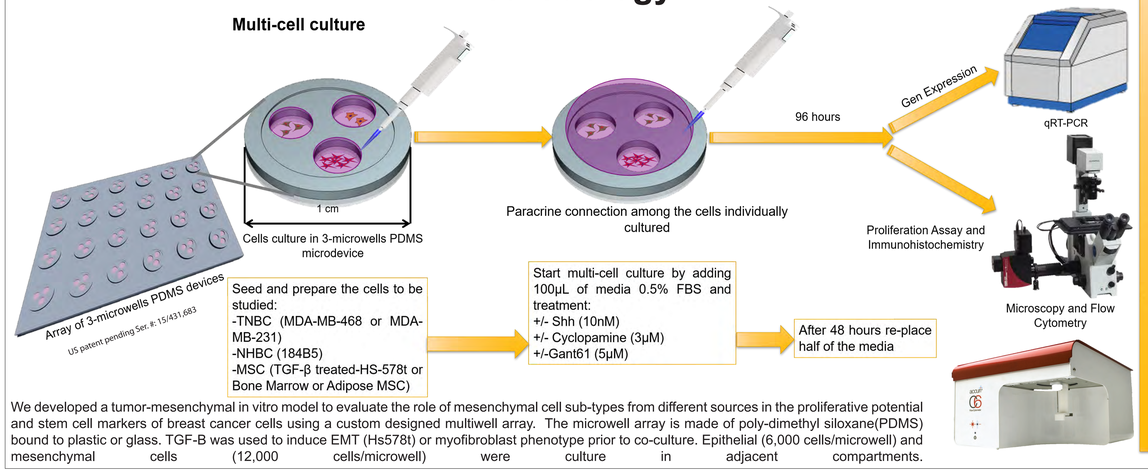

We developed a tumor-mesenchymal in vitro model to evaluate the role of mesenchymal cell sub-types from different sources in the proliferative potential and stem cell markers of breast cancer cells using a custom designed multiwell array. The microwell array is made of poly-dimethyl siloxane(PDMS) bound to plastic or glass. TGF-B was used to induce EMT (Hs578t) or myofibroblast phenotype prior to co-culture. Epithelial (6,000 cells/microwell) and mesenchymal cells (12,000 cells/microwell) were culture in adjacent compartments.

Key Findings

Therapeutic benefit of Hh inhibitors is confined to the mesenchymal compartment in paracrine Hh signaling

Paracrine Hh signaling was confirmed in Hispanic breast tumor samples.

Developed first in vitro model of tumor-mesenchyme Hh signaling in TNBC.

Mesenchymal cells induce a tumorigenic behavior in non-tumorigenic cells.

Paracrine Hh signaling increases the CD44+CD24+ population which is associated to chemo-resistant.

Mesenchymal stem cells are potential targets for Shh-driven metastases.

Hh-mesenchyme 15 gene signature identifies a sub-group with reduced DFS in Basal and Luminal A types

In vivo confirmation and *in vitro* modeling of paracrine Hh signaling

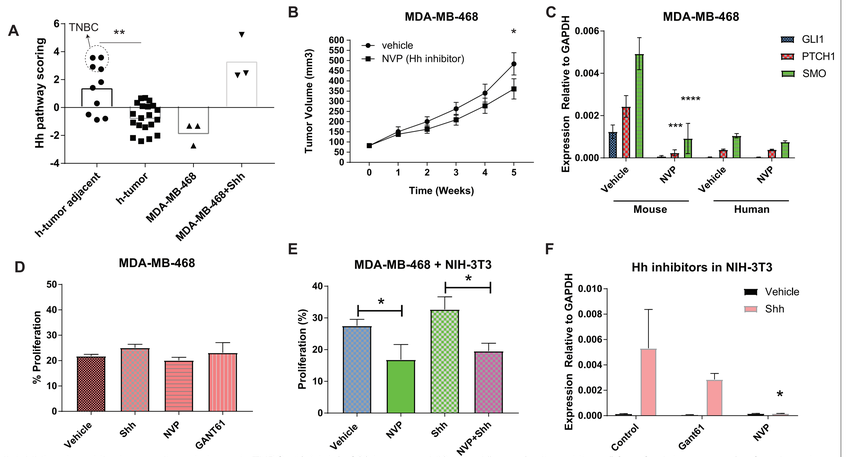

Hh inhibitors target the tumor-adjacent stroma in TNBC. A) A total of 20 tumors and 10 paired "normal-adjacent tissue" from fresh tumor samples from breast cancer patients in Puerto Rico were evaluated using the PanCancer pathways array from Nanostring. MDA-MB-468 xenografted tumors +/- beads with SHH ligand were used as negative and positive controls for Hh signaling. Data analysis and pathway scoring was done with the Nsolver software. Adjusted **P-val <0.005. B) Tumor growth curves in mouse xenograft tumors from MDA-MB-468 treated daily with SMO inhibitor Erismodegib (NVP) or vehicle during the last 4 weeks. Data shows mean +/ SE of 8 animals per treatment. *P-value <0.05 determined by ANOVA analysis C) Evaluation of expression levels of GLI1, PTCH1 and SMO relative to GAPDH using human and mouse specific TAQMAN primers. P-value was determined for comparison between vehicle and NVP groups of the same species using Wilcoxon Man-Whitney test. ***P<0.0005, ****P<0.00001. D-F) Evaluation of cell response to Shh ligand (10nM) and Hh inhibitors, NVP (5uM) and GANT61(5uM) in monoculture (D) or co-culture (E) with NIH-3T3 for 96hrs. F) GLI1 expression levels in NIH-3T3 treated with Shh +/- Hh inhibitors. Data represents mean +/- 1SE of 3 independent studies with n=6-12. P-value determined with Wilcoxon Mann-Whitney test. *P<0.05.

Mesenchymal cells support Hh-driven cell growth and metastasis

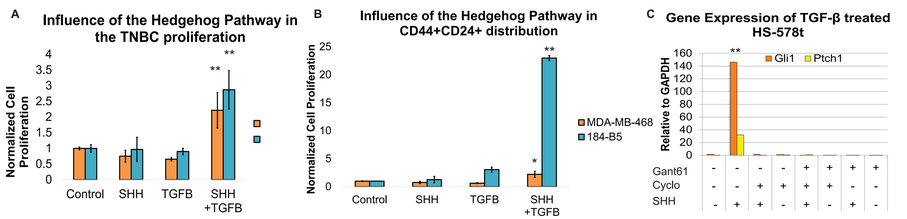

Cell growth (A) and CD44+CD24+ cell profile (B) were evaluated in response to Shh ligand (5nM) in mono and co-culture with EMTfor 96 hrs. Levels of GLI1, a main Hh target gene, were evaluated in cells that undergo EMT (C). Data shown represents average of 3 independent experiments +/- standard error. Student t-test was used to determine significant changes (*p-value <0.05, **p-value<0.005) compared to control.

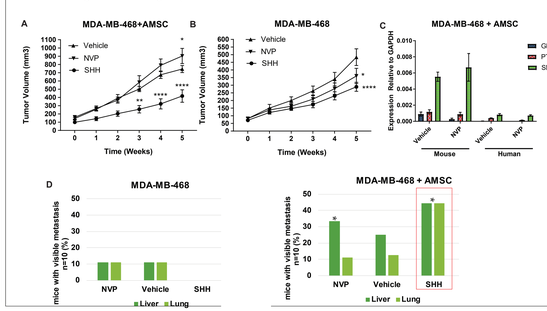

Mesenchymal cells modulate effect of Hh signaling. A-B) Tumor growth curves in mouse xenograft tumors composed by MDA-MB-468 or MDA-MB-468+AMSC were inoculated with beads loaded +/- SHH ligand and treated daily with SMO inhibitor Erismodegib (NVP) or vehicle during the last 4 weeks. Data shows mean +/- SE of 10 mice per treatment. *P-val< 0.05. was determined via ANOVA analysis. C) Evaluation of expression levels of GLI1, PTCH1 and SMO relative to GAPDH in xenografts tumors shown in (B) using human and mouse specific TAQMAN primers. Data represents mean +/- 1SE with n=6 tumors. P-value was determined for comparison between vehicle and NVP groups of the same species using Wilcoxon Mann-Whitney test. D-E) Number of mice with visible metastases from tumors and tissues collected at in (A) and (B). Significance between MDA-MB-468 and MDA-MB-468 +AMSC determine by Fisher's exact test. *P<0.05

Hh-mesenchymal signature uncovers bi-modal prognosis

We examined the mRNA expression levels of a panel of 21 genes involved in Hh signaling (GLI1, GLI2, GLI3, SMO, PTCH1, HHIP), Hh-mesenhyme prostate derived gene signature(CXCL14, FBN2, ANGPT4, TIMP3, IGFBP6, ADAM12, FGF5, HES1 and HSD11B1) and randomly chosen mesenchymal markers (CAV-1, FAP, VIM, ACTA1, CDH1 and CDH2) in gene microarray profiles (GSE3744) to determine the presence of mesenchymal-driven Hh signaling activity in normal, non-TNBC and TNBC breast cancers. We found 15/21 genes were able to discriminate among breast cancer groups (fig.1) and validated our Hh-mesenchyme 15 gene fingerprint using linear discriminant regression analysis in a new set of human breast samples from TCGA database. (table 1). The Hh-mesenchymal gene fingerprint could distinguish with high sensitivity (>70%)among normal, basal and luminal A. ROC analysis was used to determine sensitivity to distinguish among groups. ROC curves (not shown) showed 80% sensitivity.

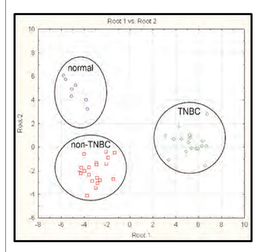

Figure 1. Two-dimensional representations of data from a LDA considering all samples (normal=7, non-TNBC=20 and TNBC=18) and using the 15 gene panel. Axes correspond to the linear discriminant vectors and points represent each sample.

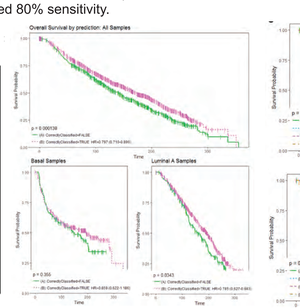

Figure 2. Survival curves for overall survival (months) for METABRIC samples that were correctly (--) vs incorrectly(-) classified for all (p=0.000138), Luminal A (p=0.0343) and Basal (p=0.355) samples.

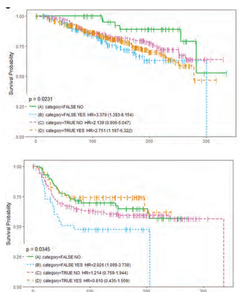

Figure 3. DFS curves for basal and luminal A sub-types +/- hormone therapy (HR). Luminal A (top) and Basal (bottom)samples from the METABRIC datasets respectively; samples sorted based on similarities of a 15-gene Hh-mesenchymal signature (TRUE/FALSE) and if HR was received (YES/NO). Time is in months

Torres-Garcia W. and Domenech, M. (2017). "Hedgehog-mesenchyme gene signature identifies bi-modal prognosis in Luminal and Basal breast cancer sub-types", Molecular BioSystems, DOI: 10.1039/C7MB00416H

Bregs expressing PDL1 are induced by LPS and IFN-α

Epeldegui M[1, 2, 3], Guo Y[3], Penichet M[1, 2, 4, 5, 6] and Martinez-Maza O[1, 2, 3, 4, 7]

[1]UCLA AIDS Institute, University of California, Los Angeles, California, USA, [2]Jonsson Comprehensive Cancer Center, University of California, Los Angeles, California, USA, [3]Department of Obstetrics and Gynecology, David Geffen School of Medicine, University of California, Los Angeles, California, USA, [4]Department of Microbiology, Immunology, and Molecular Genetics, David Geffen School of Medicine, University of California, Los Angeles, California, USA 5Division of Surgical Oncology, Department of Surgery, David Geffen School of Medicine, University of California, Los Angeles, California, USA

6The Molecular Biology Institute, University of California, Los Angeles, California, USA , 7Department of Epidemiology, UCLA Fielding Schoo of Public Health, University of California, Los Angeles, California, USA.

Abstract

HIV infection is associated with a marked increase in risk for B cell lymphoma. While an overall decrease in the incidence of AIDS-related lymphoma (ARL) has been seen in the anti-retroviral therapy (cART) era, the risk for ARL remains elevated. In prior work, we found that B regulatory cells (Bregs) (CD19+CD24+CD38+) and B cells expressing PDL1 (PDL1+) were elevated prior to ARL diagnosis, and that PDL1+ B cells are a subpopulation of Bregs. Here, we aimed to determine whether IFN-α and LPS, both of which are elevated in ARL, in combination with CD40 ligand-positive HIV virions (CD40L+ HIV), induce a Breg cell phenotype and PDL1 expression. Interestingly, when we stimulated B cells with IFN-α, we induced a Breg cell phenotype. However, when B cells were stimulated with LPS or CD40L+ HIV alone, Bregs were induced, but not to the same extent. Furthermore, when we studied the phenotype of these Bregs, we also observed that many of them also express PDL1, and even more interesting, also co-expressed CD71. Expression of both PDL1 and CD71 has been seen to be elevated on B cells before ARL diagnosis. Additionally, when B cells were stimulated with IFN-α, we detected IL-10 production (mean value of 2.84pg/ml of IL-10 in culture supernatants). Moreover, when LPS and CD40L+HIV were added in combination with IFN-α, B cells secreted even higher levels of IL-10 (17.8pg/ml and 5.2pg/ml, respectively). Therefore, exposure of B cells to IFN-α, LPS, and CD40L+ HIV (all of which are elevated in HIV-infection) induces B cells to acquire a Breg cell phenotype, and also, to co-express PDL1 and CD71. Not only B cells acquire a Breg cell phenotype when stimulated with IFN-α and/or LPS and CD40L+ HIV, but they also secrete IL-10, a cytokine that is secreted by Breg cells and mediates their regulatory function.

Material and Methods

Study population. Viable frozen PBMC were obtained from the UCLA Multicenter AIDS Cohort Study (MACS) repository. We obtained 31 samples from individuals who developed NHL, collected prior to their NHL diagnosis. We studied samples from two different MACS study visits: >4 years and 1-4 years prior to NHL diagnosis. We also obtained PBMC from 29 HIV+ controls who did not develop NHL and were matched with cases by: date of birth (within 200 days), study visit (within 250 days) and CD4 count (±175). Lastly, we selected 15 HIV-negative controls.

Flow cytometry. Multicolor flow cytometry was preformed on $1x10^6$ viably thawed PBMC the following immune markers: CD3, CD4, CD19, CD24, CD38, CD71, CD1d, PDL1 (eBiosicnece) and CD10 (Becton Dickenson, BD), conjugated with: FITC, PE, APC, PerCp-Cy5.5, PE-Cy7, APC-Alexa750, Pacific Blue™, 605eFluor or 650 eFluor (nano-crystals). Stained samples were run in a LSR Fortessa. Flow cytometry was also preformed in B cells previously isolated from healthy donor controls and then exposed to CD40L-HIV, IFN-α a

Statistics. Log-transformed means were compared between NHL HIV+ individuals and HIV+ controls using linear mixed models with a random effect for each match pair. Each visit (>4 years and 1-4 years prior to NHL diagnosis) was analyzed independently and together to investigate the change in values across visits via an interaction term. When analyzed together, an additional random effect for each individual was included to account for multiple observations per individual. For the comparison of log-transformed means between HIV+ controls with HIV-negative controls, linear models were used controlling for age. When appropriate, least-square means are presented. Analyses were done using the R statistical language.

Conclusions

- Breg (CD19+CD24+CD38+) cells and CD19+PDL1+ cells are elevated prior to AIDS-NHL 1-4 years, but not >4 years prior to NHL diagnosis
- CD40L-expressing HIV, IFN-α and/or LPS induce Bregs.
- PDL-1 and CD71 is elevated in Bregs induced by CD40L-expressing HIV, IFN-α and/or LPS. All these markers are elevated prior to ARL therefore Future work will focus on determining if these cells are, in fact, pre-tumor cells

Results

- **Bregs are elevated prior to AIDS-NHL diagnosis and CD19+PDL1+ are elevated prior to AIDS-NHL diagnosis**

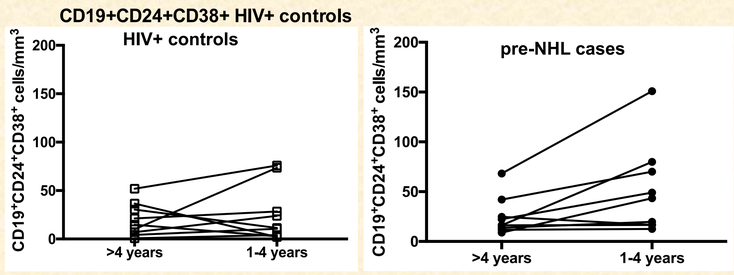

Figure 1. Numbers of B regulatory cells (Breg) are elevated in the peripheral blood prior to AIDS-NHL diagnosis. a) Multi-color flow cytometry for Breg phenotype ($CD19^+CD24^+CD38^+$) was performed from prospectively collected PBMC from AIDS-NHL cases, and matched HIV+ and HIV-negative controls. Bregs were gated as $CD19^+CD24^+CD38^+$; absolute numbers of Bregs (cells/mm^3) were measured 1-4 years and more than 4 years prior to AIDS-NHL diagnosis. Lines in figure (A) represent means. **B)** Absolute numbers of Bregs in PBMC from HIV+ controls are shown at the two different visits; lines represent each individual changes across visits. **C)** Absolute numbers of Bregs in PBMC from AIDS-NHL cases are shown at the two different visits; lines represent each individual changes across visits. p-values were calculated using either an F-test or t-test for the difference in log means in a linear mixed model, respectively.

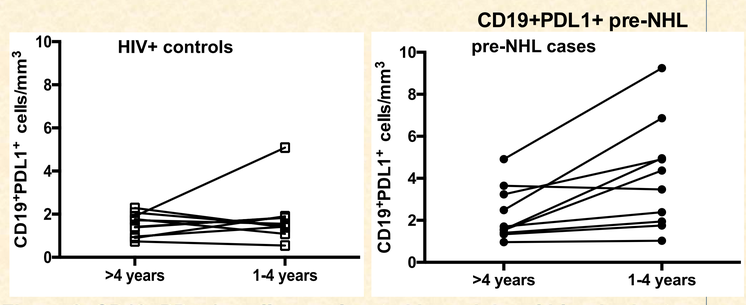

Figure 2. CD19+PDL-1+ cells are elevated in peripheral blood prior to AIDS-NHL diagnosis. A) Multi-color flow cytometry was performed in prospectively collected PBMC from AIDS-NHL cases (circles), matched HIV+ controls who did not develop NHL (squares) and HIV-negative controls (triangles). Absolute numbers of $CD19^+PDL1^+$ (cells/mm^3) were measured 1-4 years before AIDS-NHL and more than 4 years prior to AIDS-NHL. **B)** Absolute numbers of $CD19^+PDL1^+$ cells in PBMC from HIV+ controls are shown at the two different visits; lines represent each individual changes across visits **C)** Absolute numbers of $CD19^+PDL1^+$ in PBMC from AIDS-NHL cases are shown at the two different visits. lines represent each individual changes across. p-values were calculated using either an F-test or t-test for the difference in log means in a linear mixed model, respectively.

- **Bregs, PDL1 and CD71 are induced by IFN-α and CD40L+HIV and/or LPS**

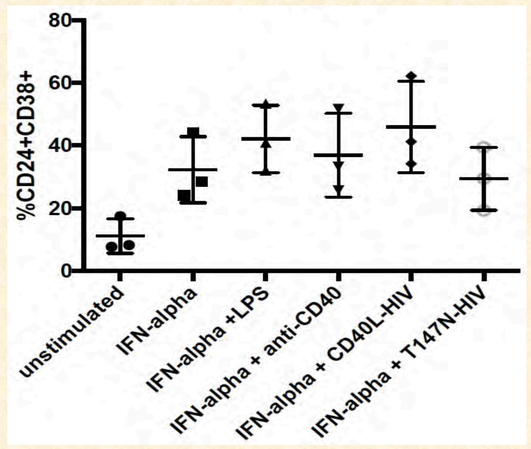

Figure 3. Bregs are induced by IFN-α and CD40L+HIV and/or LPS. Multicolor flow cytometry was preformed in isolated B cells from PBMC after they were exposed to: IFN-α, LPS, CD40L+HIV, T147N-HIV to detect levels of Bregs (CD24+CD38+) CD40L-HIV induces PDL-1 expression on B cells and they secrete IL-10.

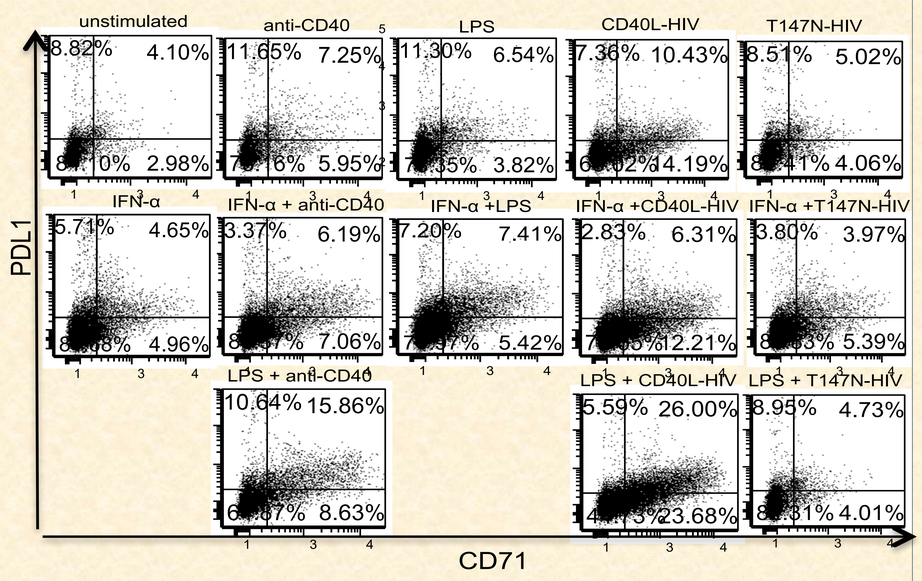

Figure 4. PDL 1 and CD71 is induced Bregs that are stimulated with IFN-α and CD40L-HIV and/or LPS. Multicolor flow cytometry was preformed in isolated B cells from PBMC after they were exposed to: IFN-α, LPS, CD40L+HIV, T147N-HIV to detect levels of Bregs (CD24+CD38+), then levels of PDL1 and CD71 were measured in gated Breg cells.

Acknowledgements

This work was supported in part by the following NIH grants: R01-CA168482-S, R01-CA168482, R01-CA196266, P30-AI028697 supplement and the UCLA AIDS Institute and UCLA Center for AIDS Research NIH grant (P30-AI028697).

Disclosures: Dr. Manuel L. Penichet is a shareholder of Klyss Biotech, Inc. The Regents of the University of California are in discussions with Klyss to license Dr. Penichet's technology to this firm.

HuR ubiquitination by BRCA1/BARD1 and its role in controlling gene expression during DNA damage response.

Gamage Aruggoda, Danae Fonseca, Emral Devany, Tamara Yakubova and Frida E. Kleiman
Chemistry Department, Hunter College, City University of New York, New York

Abstract:

During DNA damage response (DDR), control of mRNA stability is essential for regulation of gene expression and DNA repair. Human antigen R (HuR) is a ubiquitously expressed RNA binding protein (RNA-BP) that targets mRNAs by binding AU-rich elements (ARE) in the 3'UTR, usually increasing target mRNAs stability. HuR has been associated with carcinogenesis, cell proliferation, and DDR. Posttranslational modifications of HuR regulate its function in controlling mRNA stability. Ubiquitination has been implicated in not only regulating HuR stability but also remodeling HuR interaction with target mRNAs. Under non-stress conditions, non-degradative ubiquitination of HuR signals its dissociation from target mRNAs, such as p21 and MKP-1, resulting in mRNA destabilization. The E3 ubiquitin (Ub) ligase responsible for HuR modification has not been identified yet.

Our results indicate that the E3 Ub ligase BRCA1/BARD1 can modify HuR in *in vitro* ubiquitination reactions. Furthermore, siRNA-mediated knockdown of BRCA1/BARD1 decreased HuR ubiquitination in HCT116 cells. A similar reduction in HuR ubiquitination was observed after UV treatment. Studies from our lab indicate that both the mRNA processing factor CstF-50 and the escort factor p97 play a role regulating the ubiquitination of BRCA1/BARD1 substrates. Our endogenous-immunoprecipitation assays showed that p97, CstF-50, HuR, and BRCA1/BARD1 can form (a) complex(es) in HCT116 cells. Interestingly, both GST-CstF-50 and p97 inhibited *in vitro* HuR ubiquitination by BRCA1/BARD1. Consistent with this, both siRNA-mediated depletion of CstF-50 and inhibition of p97 activity increased HuR ubiquitination in HCT116 cells. Interestingly, the binding of HuR to TP53 3'UTR allows not only its ubiquitination by BRCA1/BARD1 but also its release from the target mRNA. Consistent with this, HuR ubiquitination decreased binding of HuR to TP53 mRNA, allowing the binding of mRNA destabilizing factors, such as PARN deadenylase and microRNA-induced silencing complex. Using different HuR derivatives, we determined that BRCA1/BARD1-mediated ubiquitination of HuR mostly occurs in the RNA recognition motif RRM3. Furthermore, the binding of GST-CstF-50 to the hinge region of HuR inhibited BRCA1/BARD1-mediated ubiquitination of HuR.

Based on these results, we propose a model where under non-stress conditions BRCA1/BARD1 ubiquitinates HuR, inducing release of HuR from target mRNAs involved in DDR resulting in mRNA destabilization. After UV treatment, HuR ubiquitination by BRCA1/BARD1 is inhibited by CstF-50/p97. This results in HuR binding to target mRNAs involved in DDR, which increases target mRNAs stability, and allows the progression of the response.

Introduction:

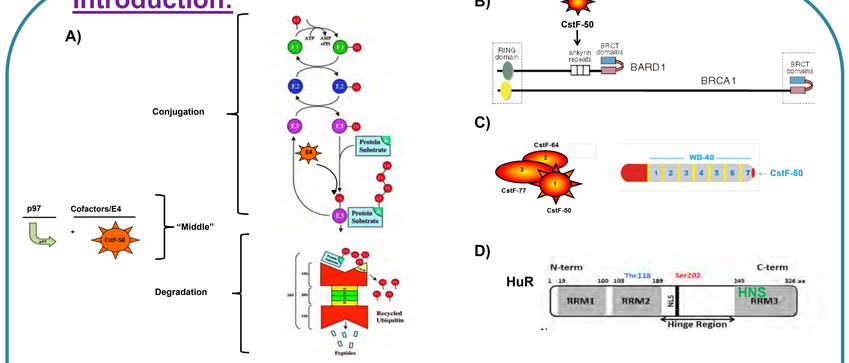

Figure 1: A) The ubiquitin-degradative pathway. The ATP-dependent pathway occurs via a three-step enzymatic reaction and regulates the degradation of cellular proteins. **B) Schematic representation of the BRCA1/BARD1 heterodimer.** The RING and BRCT domains for both proteins and ankyrin repeats for BARD1 are shown. The BARD1 binding site for CstF-50 is also depicted (Modified from Baer and Ludwig, 2001). **C) Schematic representation of polyadenylation factor CstF-50**. **D) Schematic representation of HuR structure**. HuR has 3 RNA recognition motifs (RRM, grey), and a hinge region (white) containing unique nuclear-cytoplasmic shuttle sequence (HNS, green). Phosphorylation sites are highlighted in green. Modified from Venigalla and Turner, 2012.

Results:

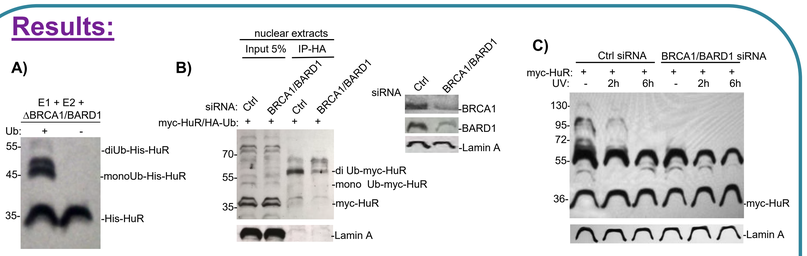

Figure 2: BRCA1/BARD1 ubiquitinates HuR *in vitro and in vivo* in HCT 116 cells. (A) *In vitro* ubiquitination reactions were conducted in the presence of ATP, recombinant ΔBRCA1/BARD1, E1, UbcH5c, His-Ub, and His-HuR. Samples were fractionated and immunoblotted with anti-HuR antibodies. **(B)** HCT116 cells were transfected with myc-HuR and HA-Ub constructs and BRCA1/BARD1 expression was knocked-down using siRNA. Nuclear extracts were IPed with rabbit anti-HA antibody and immunoblotted by mouse anti-myc antibody. **(C)** BRCA1/BARD1 dependent ubiquitination of HuR is inhibited after UV induced DNA damage. HCT116 cells were transfected concomitantly with myc-HuR constructs and with either control or BRCA1/BARD1 siRNA. Cells were also treated with 40 J/m^2 UVC irradiation and allowed to recover for the indicated times. Nuclear extracts were immunoblotted by mouse anti-myc antibody.

Results:

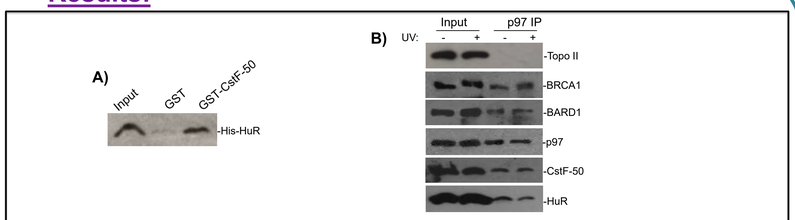

Figure 3: HuR binds directly to the mRNA processing factor CstF-50 and associates to other factors of the ubiquitination pathway, such as BRCA1/BARD1 and p97.

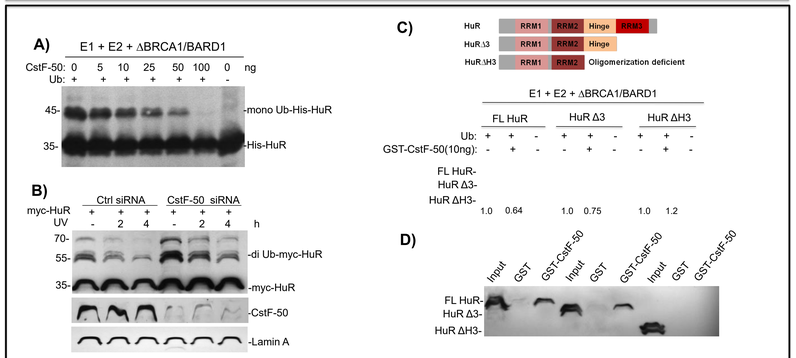

Figure 4: CstF-50 inhibits HuR ubiquitination by BRCA1/BARD1 by binding to HuR hinge region. A) *In vitro* ubiquitination reactions were conducted as in Fig. 2 but with increasing amounts of GST-CstF-50. Samples were fractionated by SDS-PAGE and immunoblotted with anti-HuR antibodies. **B)** HCT116 cells were transfected with myc-HuR construct and with either control or CstF-50 siRNA. Cells were exposed to 40 J/m^2 UVC irradiation and allowed to recover for the indicated times. Nuclear extracts were immunoblotted with anti-myc antibody. **C)** CstF-50 inhibits BRCA1/BARD1-mediated ubiquitination of HuR derivatives encompassing the hinge region. HuR derivatives with different combinations of RRM, and hinge regions were used in the ubiquitination reactions described in (A). **D)** CstF-50 binds to the hinge region of HuR. Purified His-HuR derivatives were pulled-down by either GST or Gst-CstF-50.

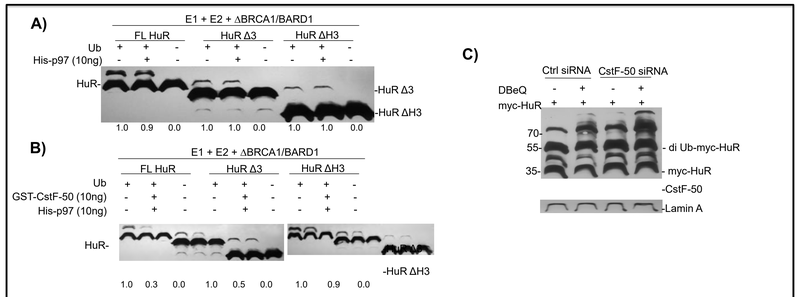

Figure 5: The escort factor p97 associated to CstF-50 inhibits HuR ubiquitination by BRCA1/BARD1 at hinge region. A) *In vitro* ubiquitination reactions of three HuR derivatives were conducted as in Fig. 2 but adding His-p97. Samples were fractionated by SDS-PAGE and immunoblotted with anti-HuR antibodies. **B)** In vitro ubiquitination reactions of three HuR derivatives were conducted as in Fig. 2 but with His-p97 and CstF-50. HuR derivatives with different combinations of RRM, and hinge regions were used in the ubiquitination reactions described in Fig 2. **C)** HCT116 cells were transfected with myc-HuR construct and with either control or CstF-50 siRNA. Cells were treated with DBeQ (10mM), an ATPase activity inhibitor of p97 and allowed to recover for 4 h. Nuclear extracts immunoblotted with anti-myc antibody.

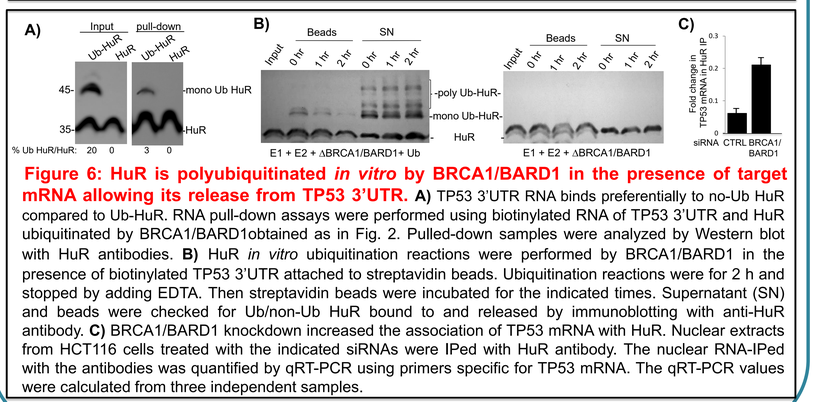

Figure 6: HuR is polyubiquitinated *in vitro* by BRCA1/BARD1 in the presence of target mRNA allowing its release from TP53 3'UTR. A) TP53 3'UTR RNA binds preferentially to no-Ub HuR compared to Ub-HuR. RNA pull-down assays were performed using biotinylated RNA of TP53 3'UTR and HuR ubiquitinated by BRCA1/BARD1obtained as in Fig. 2. Pulled-down samples were analyzed by Western blot with HuR antibodies. **B)** HuR *in vitro* ubiquitination reactions were performed by BRCA1/BARD1 in the presence of biotinylated TP53 3'UTR attached to streptavidin beads. Ubiquitination reactions were for 2 h and stopped by adding EDTA. Then streptavidin beads were incubated for the indicated times. Supernatant (SN) and beads were checked for Ub/non-Ub HuR bound to and released by immunoblotting with anti-HuR antibody. **C)** BRCA1/BARD1 knockdown increased the association of TP53 mRNA with HuR. Nuclear extracts from HCT116 cells treated with the indicated siRNAs were IPed with HuR antibody. The nuclear RNA-IPed with the antibodies was quantified by qRT-PCR using primers specific for TP53 mRNA. The qRT-PCR values were calculated from three independent samples.

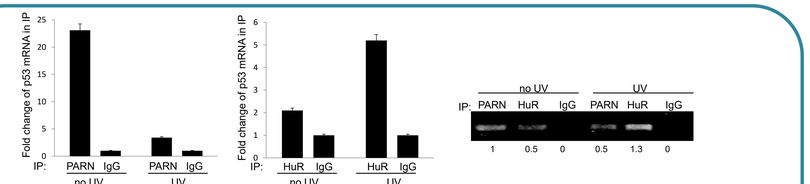

Figure 7: While PARN associates with p53 mRNA under normal conditions, HuR association with p53 mRNA is favored after UV treatment. Nuclear extracts from crosslinked HCT116 cells were used in RNA-immunoprecipitation assays. The extracts were IPed with either with anti-PARN, anti-HuR or IgG antibodies. The endogenous nuclear RNA IPed with the antibodies was quantified by qRT-PCR using primers for p53 mRNA.

Model:

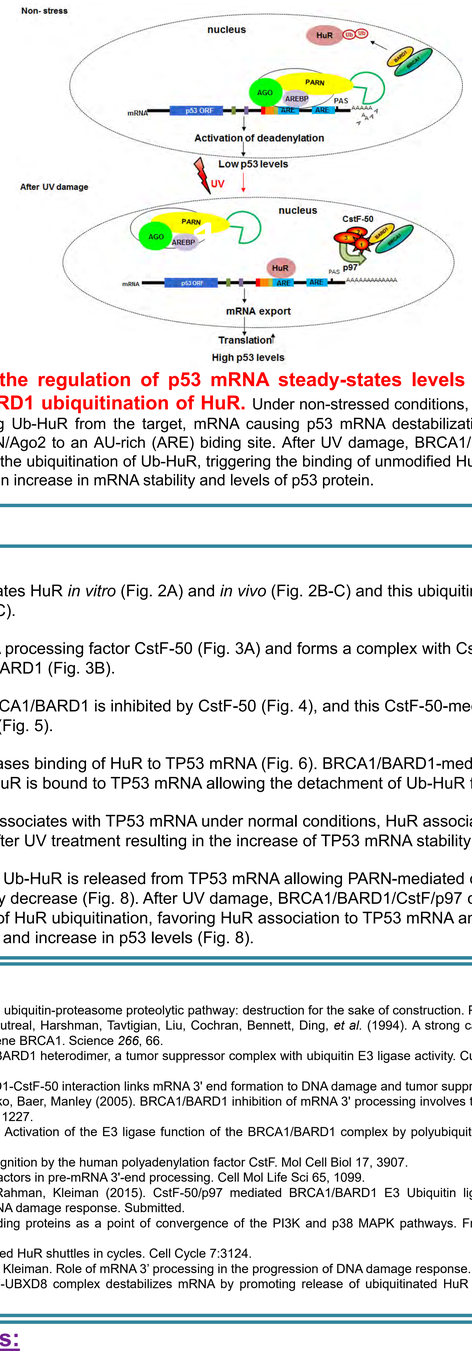

Figure 8: Model for the regulation of p53 mRNA steady-states levels by CstF-50/p97 regulated BRCA1/BARD1 ubiquitination of HuR. Under non-stressed conditions, HuR is ubiquitinated by BRCA1/BARD1 releasing Ub-HuR from the target, mRNA causing p53 mRNA destabilization and degradation through the binding of PARN/Ago2 to an AU-rich (ARE) biding site. After UV damage, BRCA1/BARD1/CstF-50/p97 complex is formed inhibiting the ubiquitination of Ub-HuR, triggering the binding of unmodified HuR to the ARE site in p53 mRNA and resulting in an increase in mRNA stability and levels of p53 protein.

Conclusions:

- ✧ BRCA1/BARD1 ubiquitinates HuR *in vitro* (Fig. 2A) and *in vivo* (Fig. 2B-C) and this ubiquitination is inhibited after UV exposure (Fig.2C).
- ✧ HuR binds directly mRNA processing factor CstF-50 (Fig. 3A) and forms a complex with CstF-50, escort factor p97, BRCA1 and BARD1 (Fig. 3B).
- ✧ HuR ubiquitination by BRCA1/BARD1 is inhibited by CstF-50 (Fig. 4), and this CstF-50-mediated inhibition is further increased by p97 (Fig. 5).
- ✧ HuR ubiquitination decreases binding of HuR to TP53 mRNA (Fig. 6). BRCA1/BARD1-mediated ubiquitination of HuR can occur while HuR is bound to TP53 mRNA allowing the detachment of Ub-HuR from the RNA.
- ✧ While PARN deanylase associates with TP53 mRNA under normal conditions, HuR association with TP53 mRNA is favored after UV treatment resulting in the increase of TP53 mRNA stability (Fig. 7).
- ✧ At non-stress conditions, Ub-HuR is released from TP53 mRNA allowing PARN-mediated deadenylation and resulting in mRNA stability decrease (Fig. 8). After UV damage, BRCA1/BARD1/CstF/p97 complex is formed resulting in the inhibition of HuR ubiquitination, favoring HuR association to TP53 mRNA and resulting in the stabilization of the mRNA and increase in p53 levels (Fig. 8).

References:

Glickman, Ciechanover (2002). The ubiquitin-proteasome proteolytic pathway: destruction for the sake of construction. Physiol Rev *82*, 373.
Miki, Swensen, Shattuck-Eidens, Futreal, Harshman, Tavtigian, Liu, Cochran, Bennett, Ding, *et al.* (1994). A strong candidate for the breast and ovarian cancer susceptibility gene BRCA1. Science *266*, 66.
Baer, Ludwig (2002). The BRCA1/BARD1 heterodimer, a tumor suppressor complex with ubiquitin E3 ligase activity. Curr Opin Genet Dev *12*, 86.
Kleiman, Manley (2001). The BARD1-CstF-50 interaction links mRNA 3' end formation to DNA damage and tumor suppression. Cell 104, 743.
Kleiman, Wu-Baer, Fonseca, Kaneko, Baer, Manley (2005). BRCA1/BARD1 inhibition of mRNA 3' processing involves targeted degradation of RNA polymerase II. Genes Dev 19, 1227.
Mallery, Vandenberg, Hiom (2002). Activation of the E3 ligase function of the BRCA1/BARD1 complex by polyubiquitin chains. EMBO J 21, 6755.
Takagaki, Manley (1997). RNA recognition by the human polyadenylation factor CstF. Mol Cell Biol 17, 3907.
Mandel, Bai, Tong (2008). Protein factors in pre-mRNA 3'-end processing. Cell Mol Life Sci 65, 1099.
Fonseca, Baquero, Mashadova, Rahman, Kleiman (2015). CstF-50/p97 mediated BRCA1/BARD1 E3 Ubiquitin ligase activity facilitates chromatin remodeling during the DNA damage response. Submitted.
Venigalla, Turner (2012). RNA-binding proteins as a point of convergence of the PI3K and p38 MAPK pathways. Frontiers in Immunology 3:398.
Kim, Gorospe (2008). Phosphorylated HuR shuttles in cycles. Cell Cycle 7:3124.
Devany, Fonseca, Zhang, Persaud, Kleiman. Role of mRNA 3' processing in the progression of DNA damage response. (2014, in preparation).
Zhou, Geng, Lou (2013). The p97-UBXD8 complex destabilizes mRNA by promoting release of ubiquitinated HuR from mRNP. Genes & Development 27: 1046.

Acknowledgements:

I would like to thank everybody that has supported me and this work. This work was supported by National Institute of Health, grant R21 CA175794-02 to FEK. This work was partially supported by Yalow Scholars Program.
Special thanks to Dr. Richard Baer, Dr. D. Fonseca, Dr. E. Devany, Jorge Baquero, Michael Murphy, Martha Ordonez, Karole Oblena and George Zakusilo.

Leptin and Leptin Receptor Expression: Associations with Breast Cancer Clinicopathology?

Llanos AAM[1,2], Chekmareva MA[2,3], Chen W[2], Cong L[2], Hong CC[4], Yao S[4], Ganesan S[2,5], Foran DJ[2,3], Ambrosone CB[4], Bandera EV[1,2], and Demissie K[1,2]

[1]Dept. of Epidemiology, Rutgers School of Public Health; [2]Rutgers Cancer Institute of New Jersey; [3]Dept. of Pathology and Laboratory Medicine, Robert Wood Johnson Medical School; [4]Dept. of Cancer Prevention and Control, Roswell Park Comprehensive Cancer Center; and [5]Depts. of Medicine and Pharmacology, Robert Wood Johnson Medical School.

Introduction

The adipokine, leptin (LEP) and its receptor (LEPR), are hypothesized to play a role in breast cancer (BrCa) outcomes disparities. However, at present, limited epidemiologic data are available on these relationships.

Research questions:

1. *Are there associations between LEP expression (protein and gene expression) specimens in breast tumor specimens and BrCa clinicopathologic features?*
2. *Are there associations between LEPR expression (protein and gene expression) in breast tumor specimens and BrCa clinicopathologic features?*

Methods

- Immunohistochemistry and NanoString digital, multiplexed assays were used to assess protein and gene expression, respectively, of LEP and LEPR in breast tumor tissue microarrays in the Women's Circle of Health Study.
  - LEP: protein expression, n= 711; gene expression, n=156
  - LEPR: protein expression, n=621; gene expression, n=156
- Protein expression was scored semi-quantitatively by a board-certified pathologist as well as analyzed using an automated, quantitative method.
- Non-parametic (Wilcoxon-Mann Whitney[a] and Kruskal Wallis[b] tests), preliminary analyses, where P <0.05 was considered statistically significant, were used to examine bivariate associations between breast tumor LEP and LEPR expression profiles, and sociodemographic, anthropometric and breast tumor features.

Results

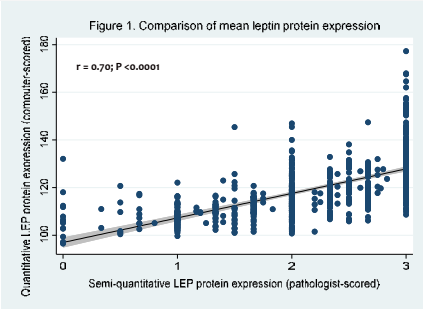

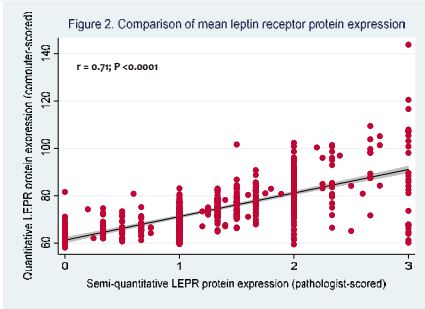

Leptin findings:

- **Lower LEP protein expression** observed among Black women and in breast tumors that are **higher grade, ER-, and Luminal B or triple-negative (TNBC) subtype.**
- **Lower LEP gene expression** observed in breast tumors that are **higher grade, higher stage, larger size, ER-, PR-, and Luminal B or TNBC subtype.**

Leptin receptor findings:

- Higher LEPR protein expression observed in Black women, older women, and women with higher BMI; **lower LEPR protein expression** observed breast tumors that are **higher grade, higher stage, larger size, ER-, PR-, and non-luminal HER2-expressing or TNBC subtype.**
- Lower LEPR gene expression observed in women with higher WHR, and in breast tumors that are **higher grade, ER-, PR-, and subtypes other than Luminal A.**

Table 1. Mean leptin protein and gene expression, by select sociodemographic, anthropometric, and tumor clinicopathologic characteristics among Women's Circle of Health Study participants

Characteristic		Leptin protein expression (semi-quantitative)		Leptin protein expression (quantitative)		Leptin gene expression (quantitative)	
	n	mean±SD	P	mean±SD	P	mean±SD	P
Race[a]	-	-	**0.03**	-	**0.0009**	-	0.22
Black	491	2.12±0.71	-	118.07±10.92	-	663.78±1146.56	-
White	145	2.25±0.72	-	122.11±13.82	-	495.10±378.45	-
Age (years)[b]	-	-	0.25	-	0.79	-	0.10
23-48	227	2.22±0.70	-	118.81±11.67	-	465.82±554.14	-
49-58	211	2.11±0.74	-	119.52±12.29	-	529.98±439.07	-
59-75	198	2.12±0.71	-	118.66±11.31	-	829.56±1646.65	-
BMI (kg/m²)[b]	-	-	0.26	-	0.11	-	0.06
<25.00	140	2.19±0.70	-	120.24±11.63	-	365.94±340.94	-
25.00-29.99	181	2.06±0.76	-	117.85±11.44	-	504.84±554.52	-
≥30.00	315	2.18±0.69	-	119.10±11.96	-	767.45±1366.79	-
WHR[b]	-	-	0.95	-	0.88	-	0.33
0.49-0.84	208	2.15±0.71	-	119.29±11.48	-	632.30±632.99	-
0.84-0.91	209	2.16±0.72	-	119.14±12.76	-	400.44±323.34	-
0.91-1.13	208	2.15±0.70	-	118.76±11.19	-	751.32±1557.27	-
Tumor grade[a]	-	-	0.08	-	**0.02**	-	**0.02**
Well/moderately differentiated	329	2.20±0.71	-	120.19±12.46	-	546.31±432.80	-
Poorly differentiated	309	2.11±0.72	-	117.88±10.77	-	611.29±1249.28	-
Tumor stage (AJCC stage)[b]	-	-	0.71	-	0.14	-	**0.0002**
Stage I	262	2.14±0.75	-	119.93±12.11	-	834.40±1442.19	-
Stage II	270	2.17±0.72	-	118.31±11.71	-	480.41±543.87	-
Stage III	99	2.12±0.69	-	119.56±11.61	-	258.65±187.72	-
Tumor size (cm)[b]	-	-	0.94	-	0.07	-	**<0.0001**
0.03-1.50	256	2.17±0.74	-	120.36±12.29	-	824.99±1333.94	-
1.60-2.50	211	2.18±0.70	-	119.32±12.38	-	601.50±852.45	-
2.60-19.80	201	2.16±0.71	-	117.93±10.95	-	221.66±54.07	-
ER status[a]	-	-	**0.01**	-	**0.01**	-	**0.005**
Negative	184	2.06±0.75	-	117.17±10.43	-	408.35±462.06	-
Positive	525	2.21±0.70	-	120.05±12.22	-	693.70±1195.70	-
PR status[a]	-	-	0.06	-	0.16	-	**0.03**
Negative	243	2.10±0.74	-	118.41±11.37	-	510.10±748.17	-
Positive	466	2.20±0.71	-	119.77±12.06	-	646.97±1160.07	-
HER2 status[a]	-	-	0.92	-	0.62	-	0.17
Negative	564	2.16±0.71	-	119.20±11.82	-	623.09±1084.15	-
Positive	120	2.18±0.71	-	118.44±10.65	-	415.15±460.84	-
Breast cancer subtype[b]	-	-	0.13	-	**0.04**	-	**0.007**
Luminal A	448	2.19±0.72	-	119.90±12.16	-	743.90±1300.18	-
Luminal B	63	2.15±0.72	-	117.78±10.36	-	347.84±283.32	-
Non-luminal HER2-expressing	57	2.20±0.69	-	119.17±11.02	-	474.98±577.39	-
Triple-negative	116	2.05±0.69	-	116.53±10.01	-	421.76±519.12	-

Table 2. Mean leptin receptor protein and gene expression, by select sociodemographic, anthropometric, and tumor clinicopathologic characteristics among Women's Circle of Health Study participants

Characteristic		Leptin receptor protein expression (semi-quantitative)		Leptin receptor protein expression (quantitative)		Leptin receptor gene expression (quantitative)	
	n	mean±SD	P	mean±SD	P	mean±SD	P
Race[a]	-	-	**0.002**	-	**0.0002**	-	0.57
Black	447	1.35±0.72	-	75.38±11.08	-	462.83±334.70	-
White	111	1.12±0.72	-	71.09±8.19	-	484.68±310.98	-
Age (years)[b]	-	-	**0.002**	-	**0.0003**	-	0.45
23-48	205	1.18±0.67	-	72.82±9.91	-	467.89±285.72	-
49-58	177	1.33±0.71	-	73.91±10.38	-	487.71±345.27	-
59-75	176	1.43±0.77	-	77.13±11.43	-	448.97±361.91	-
BMI (kg/m²)[b]	-	-	**0.04**	-	**0.0005**	-	0.73
<25.0	120	1.17±0.71	-	71.84±10.29	-	504.99±330.21	-
25.0-29.99	152	1.32±0.74	-	74.06±10.25	-	459.36±327.04	-
≥30.0	286	1.36±0.71	-	75.90±10.89	-	456.47±331.35	-
WHR[b]	-	-	0.36	-	**0.02**	-	**0.02**
0.49-0.84	177	1.24±0.70	-	72.80±9.34	-	506.43±274.41	-
0.84-0.91	186	1.30±0.72	-	74.65±11.40	-	446.95±241.44	-
0.91-1.13	185	1.35±0.75	-	75.96±11.08	-	453.42±429.06	-
Tumor grade[a]	-	-	**<0.0001**	-	**<0.0001**	-	**0.0002**
Well/moderately differentiated	283	1.49±0.74	-	76.36±11.28	-	592.64±373.80	-
Poorly differentiated	275	1.12±0.72	-	71.95±9.66	-	414.54±312.12	-
Tumor stage (AJCC stage)[b]	-	-	**0.0008**	-	**0.008**	-	0.23
Stage I	220	1.45±0.75	-	75.52±10.84	-	539.42±361.14	-
Stage II	238	1.21±0.71	-	73.31±10.54	-	430.48±267.90	-
Stage III	89	1.14±0.75	-	71.80±8.79	-	541.89±455.02	-
Tumor size (cm)[b]	-	-	**0.0001**	-	**0.0006**	-	0.0006
0.03-1.50	207	1.46±0.72	-	75.95±10.23	-	585.90±375.50	-
1.60-2.50	194	1.33±0.79	-	74.68±12.19	-	430.54±302.22	-
2.60-19.80	180	1.15±0.71	-	72.11±8.92	-	404.35±335.48	-
ER status[a]	-	-	**<0.0001**	-	**<0.0001**	-	**0.0001**
Negative	150	0.88±0.66	-	68.83±6.07	-	367.62±267.74	-
Positive	470	1.47±0.70	-	76.18±11.17	-	557.34±371.92	-
PR status[a]	-	-	**<0.0001**	-	**<0.0001**	-	**0.02**
Negative	206	1.07±0.72	-	71.06±8.81	-	439.17±342.67	-
Positive	414	1.45±0.71	-	76.06±11.08	-	522.57±346.84	-
HER2 status[a]	-	-	0.35	-	0.23	-	0.29
Negative	493	1.33±0.74	-	74.68±10.99	-	512.56±379.83	-
Positive	104	1.25±0.68	-	72.84±8.70	-	376.99±162.89	-
Breast cancer subtype[b]	-	-	**<0.0001**	-	**<0.0001**	-	**0.003**
Luminal A	396	1.43±0.71	-	76.10±11.49	-	591.20±402.33	-
Luminal B	56	1.41±0.64	-	75.06±9.77	-	370.50±117.73	-
Non-luminal HER2-expressing	48	1.07±0.68	-	70.25±6.43	-	382.76±197.99	-
Triple-negative	97	0.89±0.70	-	68.88±5.72	-	381.49±299.74	-

Conclusions

- These preliminary findings suggest that LEP and LEPR protein and gene expression profiles within breast tumor specimens are associated with BrCa clinicopathology, as well as with some sociodemographic and anthropometric characteristics among women with BrCa
- LEP and LEPR expression profiles may serve as biomarkers contributing to interindividual differences in prognostic indicators and are important for understanding breast tumor heterogeneity and outcomes disparities.
- The next step is to explore the multivariable-adjusted associations between LEP and LEPR expression and BrCa clinicopathology.

Acknowledgments

This work was supported by grants from the NCI (K01 CA193527, P01 CA151135, R01 CA100598, R01 CA185623, and P30 CA072720) and by the Biomedical Informatics and the Biospecimen Repository and Histopathology Service shared resources of Rutgers Cancer Institute of New Jersey (supported by P30 CA072720). Tumor samples were received, processed and tracked under the auspices of the Roswell Park Comprehensive Cancer Center DataBank and BioRepository Shared Resource (supported by P30CA16056)

TIGAR induces breast cancer tumor growth with multi-compartment tumor metabolism by modulating Fructose 2,6 bisphosphate levels

Ying-Hui Ko[1], Marina Domingo-Vidal[1], Megan Roche[1], Zhao Lin[1], Diana Whitaker-Menezes[1], Patrick Tassone[1], Joseph Curry[1], Madalina Tuluc[1], Erin Seifert[1], Ramon Bartrons[2], Jaime Caro[1], Ubaldo Martinez-Outschoorn[1]*

[1]Sidney Kimmel Cancer Center, Thomas Jefferson University, Phila, PA, USA

[2]Department of Physiological Sciences, University of Barcelona, Barcelona, Spain

Abstract

A subgroup of breast cancers has several metabolic compartments. However, the mechanisms by which metabolic compartmentalization develop in tumors are poorly characterized. TP53 Induced Glycolysis and Apoptosis Regulator (TIGAR) is a Fructose 2,6 bisphosphatase which is highly expressed in carcinoma cells in the majority of human breast cancers. Glycolysis is reduced by TIGAR by reducing levels of Fructose 2,6 bisphosphate (Fru-2-6-P_2) which is the allosteric regulator of Phosphofructokinase 1. We set out to determine the effects of TIGAR expression on tumor growth and the metabolic phenotype of the different types of tumor cells. Overexpression of this bisphosphatase in carcinoma cells induces expression of enzymes and transporters involved in the catabolism of lactate and glutamine. TIGAR overexpressing carcinoma cells have higher oxygen consumption rates and ATP levels when exposed to glutamine, lactate or the combination of glutamine and lactate compared to control cells. TIGAR overexpressing carcinoma cells induce reciprocal changes in fibroblasts with glycolysis via HIF activation with increased glucose uptake, increased 6-Phosphofructo-2-kinase/fructose-2,6-bisphosphatase-3 (PFKFB3) and LDH-A expression. Conversely, carcinoma cells overexpressing TIGAR have reduced glucose uptake and lactate production. TIGAR overexpression in carcinoma cells increases tumor growth with increased proliferation rates. A catalytically inactive variant of TIGAR which does not reduce Fru-2-6-P_2 levels did not induce tumor growth. Hence, TIGAR expression in breast carcinoma cells promotes metabolic compartmentalization and tumor growth with a mitochondrial metabolic phenotype with lactate and glutamine catabolism. Targeting TIGAR holds promise as a therapy for breast cancer.

Introduction

TIGAR reduces apoptosis and is associated with many aggressive cancers. It is highly expressed in human breast cancer. TIGAR is the only known phosphatase glycolytic modulator regulated by TP53. It reduces glycolysis and increases flux through the pentose phosophate pathway by modulating the activity of PFK1. It is unknown if TIGAR modulates catabolism of other substrates such as lactate and glutamine which have been shown to be alternate catabolites to glucose for carcinoma cells. We hypothesize that TIGAR expression in carcinoma cells induces aggressive disease with utilization of alternative catabolites to glucose and metabolic compartmentalization.

Methods

Culture Media contained 5 mM glucose and 1 mM pyruvate. To study the effect of lactate and glutamine, control conditions were compared to those with 2 mM glutamine; or 10 mM lactate; or 2 mM glutamine plus 10 mM lactate.

Co-culture system. Fibroblasts and carcinoma cells were seeded at a 3:1 fibroblast to carcinoma cell ratio and the total number of cells per well was 1x10^5. As controls, cultures of fibroblasts and carcinoma cells alone were plated in parallel with the same number of cells of a given type as in coculture (7.5 x 10^4 fibroblasts and 2.5 x 10^4 carcinoma cells).

Oxygen consumption rate (OCR) assessment was performed with a Seahorse Bioscience XF96 Extracellular Flux Analyser.

ATP assay. Intracellular ATP levels were measured using the ATP-sensitive fluorochrome quinacrine by flow cytometry.

HIF1A Luciferase activity. NIH3T3 fibroblasts stably transfected with a HIF luciferase reporter (RC0017, Panomics) were seeded in co-culture with carcinoma-control or carcinoma-TIGAR carcinoma cells.

Fru-2,6-P_2 determination was determined and normalized for protein concentration.

Immunohistochemistry was performed and quantitative analysis of immunohistochemistry was performed employing Aperio software.

Animal studies. Oophorectomy and 17β-estradiol pellet placement (0.72 mg/pellet) was performed. Mammary fat pad injections of cancer cells were performed on athymic NCr nude mice at 6 weeks of age.

Results

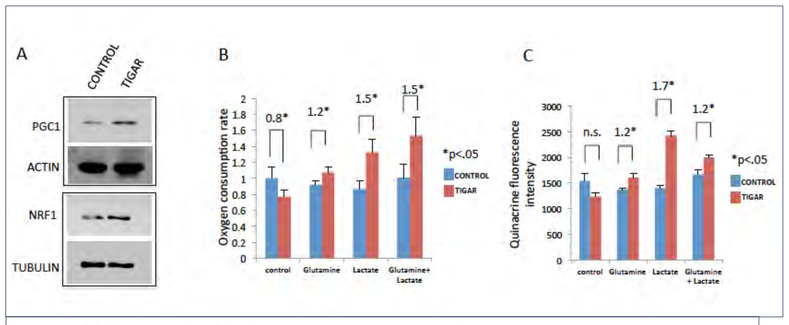

Fig 1. Effect of TIGAR on markers of mitochondrial biogenesis and metabolism. T47D cells overexpressing TIGAR and control cells were cultured and lysed and subjected to immune-blot analysis for (A) PGC1 and NRF1; (B) Oxygen consumption was measured in control T47D cells (blue bar) and with TIGAR overexpression (red bar), relative concentration is shown. Cells were cultured with control media, control with 2mM glutamine, control with 10mM lactate or control with 2mM glutamine and 10 mM lactate; (C) ATP levels measured by quinacrine fluorescence intensity in TIGAR overexpressing and control cells.

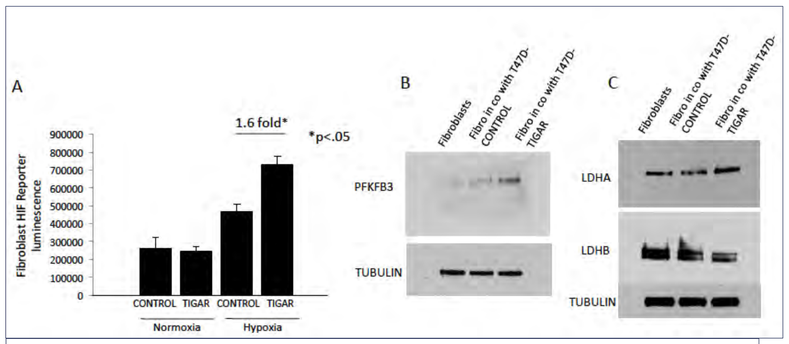

Fig 2. Effect of carcinoma TIGAR expression on fibroblast glycolysis. (A) HIF luciferase reporter in fibroblasts in coculture with carcinoma cells overexpressing TIGAR or control vector. Coculture was performed in normoxia (21% O2) or hypoxia (0.5% O2). (B-C) Fibroblasts with a GFP tag were cocultured with T47D cells either overexpressing TIGAR or control vectors. Fibroblasts were then lysed and immune-blot for PFKFB3, LDHA and LDHB .

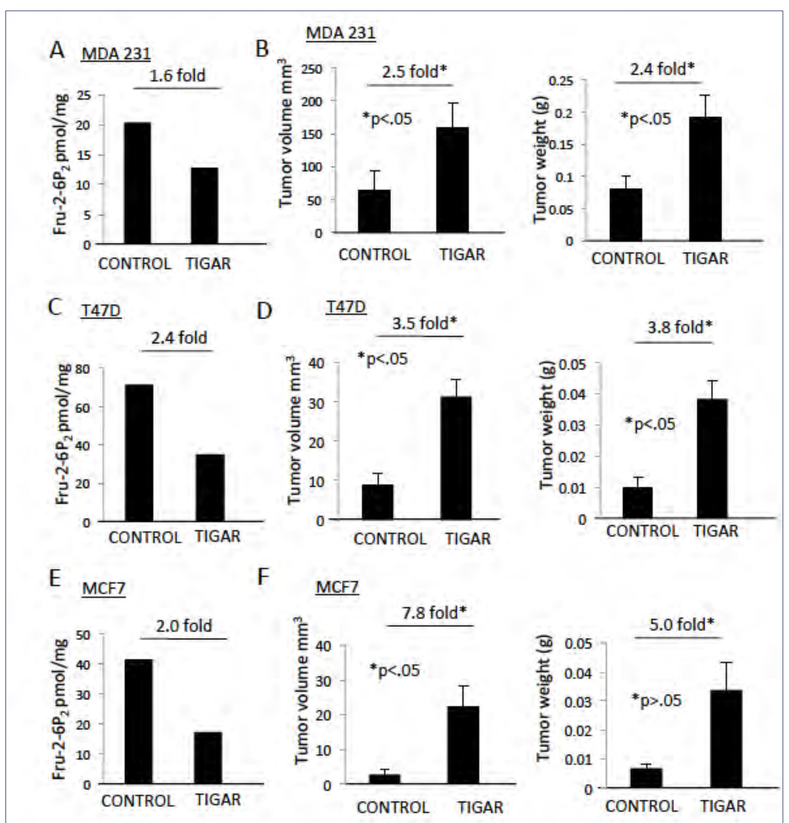

Fig 3. Effect of TIGAR in carcinoma cells on Fru-2,6-P_2 levels and orthotopic tumor growth.

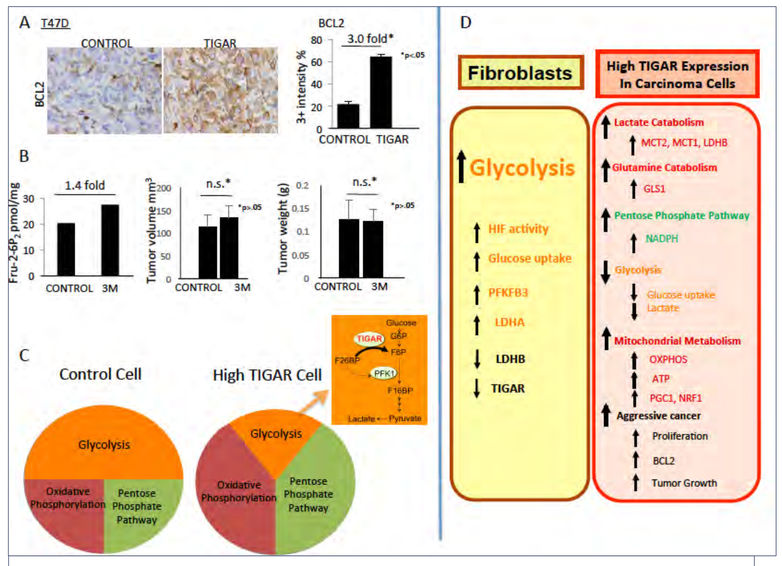

Fig 4. TIGAR and BCL2, tumor growth with catalytically inactive TIGAR and models of TIGAR effects on carcinoma and fibroblast cells. (A) BCL2 expression. Tumor sections were stained by immunohistochemistry for BCL2. The percentage of cells with the strongest BCL2 protein expression was quantified by Aperio digital pathology (3+ intensity percentage). (B) Fru-2,6-P_2 levels and tumor growth. MDA-MB-231 cells overexpressing triple mutant TIGAR with H11A/E102A/H198A mutations (MDA-MB-231-TIGAR-3M) or empty vector control were cultured and Fru-2,6-P_2 levels measured. MDA-MB-231 cells overexpressing triple mutant TIGAR (MDA-MB-231-TIGAR-3M) or empty vector control were injected into the mammary fat pad of nude mice. Tumor volume and weight were measured after resection at 4 weeks post-injection. No statistically significant change in volume or weight was noted between triple mutant TIGAR and control cells. (C) A model is shown of how TIGAR expression in carcinoma cells reduces glycolysis, increases the pentose phosphate pathway activity and increases mitochondrial oxidative phosphorylation. (D) High TIGAR expression in carcinoma cells alters their metabolic state and induces cancer aggressiveness. Conversely, fibroblasts in proximity to carcinoma cells have reciprocal metabolic changes.

Discussion

The current study delineates the role of TIGAR in OXPHOS and glycolytic metabolic reprogramming in breast cancer. We have discovered that TIGAR promotes the growth of breast invasive ductal carcinoma in vivo, and with utilization of lactate and glutamine as substrates mitochondrial OXPHOS metabolism and ATP generation in cancer cells. We also demonstrate that TIGAR expresssion in carcinoma cells induces reciprocal metabolic changes in fibroblasts. The increased fibroblast glycolysis in the current study occurred in the context of increased PFKFB3 and LDH-A expression with hypoxia inducible factor 1 alpha (HIF1A) activation. It has been shown that glycolytic fibroblasts increase breast cancer aggressiveness and tumor growth. Our finding that TIGAR promotes growth of breast invasive ductal carcinoma is relevant to human disease because high TIGAR expression is found in the majority of patients with these tumors. A catalytically active TIGAR is required to promote tumor growth. However, other activities of TIGAR may also influence the biological properties of tumor cells.

Conclusion

TIGAR modulates mitochondrial metabolism and orthotopic breast cancer tumor growth.

Funding acknowledgement

This work was supported by NCI K08-CA175193, P30 CA-56036, Instituto de Salud Carlos III - FIS (PI13/0096) and Fondo Europeo de Desarrollo Regional (FEDER).

Molecular and metabolic pathways involved in oral cancer chemoprevention by black raspberries

***Steve Oghumu*[1,2]*, Thomas J. Knobloch*[2,3] *Lei Bruschweiler-Li*[4]*, Rafael Bruschweiler*[4] *and Christopher M. Weghorst*[2,3]

[1]Department of Pathology, College of Medicine, Ohio State University Wexner Medical Center, Columbus, OH, USA
[2]Ohio State University Comprehensive Cancer Center, Ohio State University Columbus OH, USA
[3]Division of Environmental Health Sciences, College of Public Health, Ohio State University Columbus OH, USA
[4]Department of Chemistry and Biochemistry, College of Arts and Sciences, Ohio State University Columbus OH, USA

The James
THE OHIO STATE UNIVERSITY
COMPREHENSIVE CANCER CENTER

INTRODUCTION

Oral cancer accounts for about 50,000 new cases and 10,000 new deaths in the US every year. This amounts to about one person every hour every day [1]. To combat this public health challenge, there is a need to identify agents that prevent oral cancer development and fully characterize their mechanisms of action. Preclinical and clinical studies demonstrate the ability of black raspberries (BRBs) to inhibit oral carcinogenesis [2-4]. We recently showed that in an experimental model of rat oral carcinogenesis using the carcinogen 4 nitroquinoline-1-oxide (4NQO), BRB reduces oral lesion incidence and multiplicity [5]. However, understanding how the bioactive compounds in BRBs drive the metabolic and molecular pathways that lead to oral cancer chemoprevention remains unclear.

In this study, we determined the potential metabolites and molecular pathways associated with BRB mediated chemoprevention of oral carcinogenesis using the well-established carcinogen induced rat oral cancer model.

METHODS

Male F344 rats were divided into 4 groups: Sentinel group, 4NQO only group, 4NQO + 5% BRB group, and 4NQO + 10% BRB group. 4NQO was administered in drinking water (20ug/ml) for 10 weeks after which regular drinking water was provided for 6 weeks. BRBs were incorporated into rat diets at 5% or 10% concentrations and fed to the rat treatment groups for the last 6 weeks after 4NQO treatment. Sentinel animals did not receive 4NQO or BRB. At terminal sacrifice, urine samples from all groups were harvested and analyzed by NMR and Mass Spectrometry based metabolomics. RNA was extracted from rat tongue samples and used for RNA sequencing analysis.

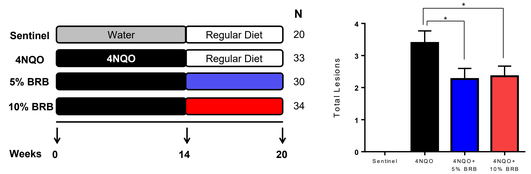

Figure 1. Model of rat oral carcinogenesis and chemoprevention. **(A)** Rats were exposed to oral carcinogen 4-nitroquinoline-1-oxide (4NQO, 20ug/ml in drinking water) for 14 weeks. Administration of the chemopreventive agent Black raspberry (BRB, 5% or 10% incorporated into diet) began at week 14 and continued for 6 weeks. Animals were sacrificed at week 20 for gross and histological analysis of tongue lesions and examinations of cellular and molecular markers of carcinogenesis. N represents number of rats per group. (B) Total lesion counts in tongues of Rat groups described in Figure 1A. (*$p < 0.05$)

METABOLOMICS WORKFLOW

- NMR Metabolomics: Metabolites in urine samples were identified by 'Complex Mixture Analysis by NMR' (COLMAR) followed by 2D ^{13}C-^{1}H HSQC NMR quantitative analysis.
- Mass Spectrometry: Urine metabolites were identified by Orbitrap mass spectrometry and processed using the Progenesis QI package via peak picking algorithms and filtering features (possible metabolites) to p-values below 0.005.

RESULTS

Metabolomic analysis of urine samples from carcinogen induced rats with/without black raspberry treatment

Metabolite	4NQO	4NQO + 5% BRB	4NQO + 10% BRB
Phenethylamine	Unique	Not Detected	Not Detected
Inosine	Unique	Not Detected	Not Detected
L-Gulonolactone	Unique	Not Detected	Not Detected
Dehydroascorbic acid	Unique	Not Detected	Not Detected
4 Hydroxyphenethyl alcohol	Unique	Not Detected	Not Detected
Muramic acid	Unique	Not Detected	Not Detected
Glycerophosphocholine	Present	Up-regulated	Up-regulated
Alpha-hydroxyhippuric acid	Present	Up-regulated	Up-regulated
DL-alpha-Glycerol-phosphate	Present	Up-regulated	Up-regulated
myo-Inositol	Present	Up-regulated	Up-regulated
D-Mannose	Present	Up-regulated	Up-regulated
D-Fructose	Present	Up-regulated	Up-regulated
D-Galacturonic acid	Present	Down-regulated	Down-regulated
Allantoin	Present	Down-regulated	Down-regulated
D-Glucosamine	Present	Down-regulated	Down-regulated
Imidazole	Present	Down-regulated	Down-regulated
Methylguanidine	Present	Down-regulated	Down-regulated
Dimethylamine	Present	Down-regulated	Down-regulated

Table 1: Table showing examples of (i) uniquely identified metabolites detected only in the 4NQO group, (ii) metabolites that were increased in carcinogen exposed rat groups treated with 5% and 10% BRB compared to 4NQO only group, and (iii) metabolites that were decreased in carcinogen exposed rat groups treated with 5% and 10% BRB compared to 4NQO only groups, as determined by NMR.

NMR Metabolomics: 4NQO only administered rats showed highest overall intensity, which was about 2.5 times higher than 4NQO + BRB treated rats. 171 metabolites were identified in urine samples of 4NQO only administered rats while 101 and 90 metabolites were identified in 4NQO administered rats that were treated with 10% and 5% BRB respectively. About 31 'unique' metabolites were identified in 4NQO only administered rat urine samples but were absent in BRB treated groups. Fourteen additional metabolites were increased and 11 metabolites were decreased following BRB treatment of 4NQO administered rats compared to rats administered with 4NQO only.

Mass Spectrometry: This is currently under investigation. Our preliminary PCA analysis demonstrates clustering of sentinel, 4NQO only and 4NQO + BRB groups.

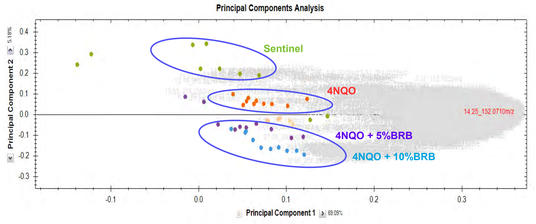

Figure 2: PCA plot showing all features ($p<0.005$) identified using an LTQ Orbitrap XL mass spectrometer. Note clustering of Sentinel group (cluster 1), 4NQO group (cluster 2) and 4NQO + 5% BRB and 4NQO + 10% BRB groups (cluster 3). Features are currently being identified based on fragmentation for determination of differentially expressed metabolites

Transcriptomic analysis of tongues from carcinogen induced rats with/without black raspberry treatment

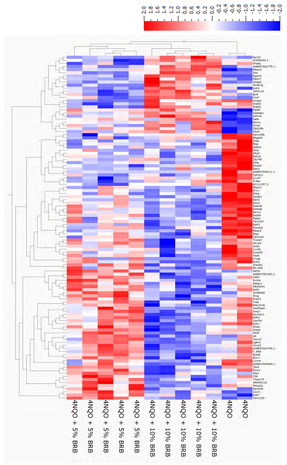

Figure 3. Heat map showing differentially expressed genes between carcinogen only exposed rat group (4NQO) and carcinogen exposed rats treated with 5%or 10% BRBs (4NQO + 5% BRB and 4NQO + 10%BRB), derived from RNA sequencing data.

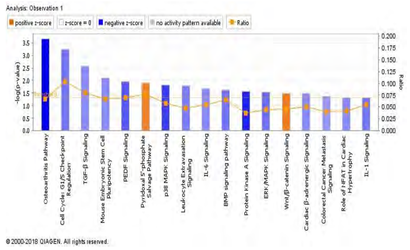

Figure 4. Top canonical pathways modulated by BRB intervention during oral carcinogenesis, determined by Ingenuity Pathway Analysis (IPA) of RNA sequencing data from Rat tongue RNA from 4NQO groups and 4NQO + 10% BRB group. Of interest are cell cycle- and MAP kinase-associated pathways.

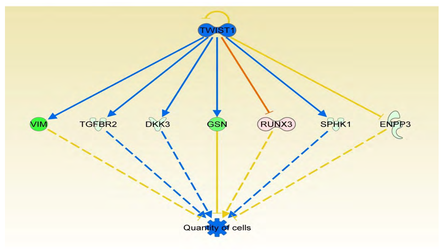

Figure 5. IPA generated hypothesis of a potential mechanism by which BRB mediates inhibition of cellular proliferation during oral carcinogenesis. Inhibition of the upstream regulator TWIST1 drives gene expression changes that result in a reduction in cellular proliferation in the oral tissue of carcinogen induced rats treated with 10%BRB.

Transcriptomics: Based on RNA sequencing data, over 662 genes were identified to be differentially expressed among 4NQO group, 4NQO + 5% BRB and 4NQO + 10% BRB ($p< 0.05$). Genes involved in cancer development, cell cycle regulation and MAP kinase signaling pathways were regulated in a manner that supports a chemo-preventive role for BRB during oral carcinogenesis. Our results demonstrate that multiple pathways are involved in BRB mediated oral cancer chemoprevention. Additional studies are underway to determine the most important molecular pathways that can potentially be targeted for oral cancer treatment.

CONCLUSIONS

- Dietary administration of BRB induces significant metabolic changes that are associated with oral cancer chemoprevention.
- BRB administration in oral carcinogen induced rats results in modulation of pathways associated with cell cycle regulation, and MAP kinase signaling.
- Our metabolomic and transcriptomic analyses reveal distinct molecular and metabolic markers and pathways that potentially drive BRB mediated oral cancer chemoprevention.
- These pathways can potentially be targeted in oral cancer treatment strategies.

CURRENT AND FUTURE WORK

Potential Bioactive Phytochemicals in BRB

- Utilize metabolomics approaches to determine major bioactive metabolites of BRBs.

Identification of novel molecular targets for oral cancer chemoprevention

- Utilize transcriptomics, metabolomics and systems biology related approaches to define molecular pathways and cellular mechanisms of BRB mediated chemoprevention.
- Identification of potential targets for chemoprevention for oral carcinogenesis..

REFERENCES

1. Siegel RL, Miller KD, Jemal A. Cancer statistics, 2016. CA: A Cancer Journal for Clinicians **2016**;66(1):7-30 doi 10.3322/caac.21332.
2. Han C, Ding H, Casto B, Stoner GD, D'Ambrosio SM. Inhibition of the growth of premalignant and malignant human oral cell lines by extracts and components of black raspberries. Nutr Cancer **2005**;51(2):207-17 doi 10.1207/s15327914nc5102-11.
3. Knobloch TJ, Uhrig LK, Pearl DK, Casto BC, Warner BM, Clinton SK, *et al.* Suppression of Proinflammatory and Prosurvival Biomarkers in Oral Cancer Patients Consuming a Black Raspberry Phytochemical-Rich Troche. Cancer Prev Res (Phila) **2016**;9(2):159-71 doi 10.1158/1940-6207.capr-15-0187.
4. Casto BC, Kresty LA, Kraly CL, Pearl DK, Knobloch TJ, Schut HA, *et al.* Chemoprevention of oral cancer by black raspberries. Anticancer Res **2002**;22(6C):4005-15.
5. **Oghumu S**, Casto B, Ahn-Jarvis J, Weghorst L, Maloney J, Geuy P, Horvath K, Bollinger C, Warner B, Summersgill K, Weghorst C, Knobloch T (2017) Inhibition of pro-inflammatory and anti-apoptotic biomarkers during experimental oral cancer chemoprevention by dietary black raspberries *Frontiers in Immunology.* 2017 doi: 10.3389/fimmu.2017.01325 Epub 2017 Sep 29

ACKNOWLEDGEMENTS

This study was supported in part by grant K01CA207599-01A1, and Foods for Health (FFH) Discovery Theme & Food Innovation Center (FIC) Seed Grants.

NATIONAL CANCER INSTITUTE CENTER TO REDUCE CANCER HEALTH DISPARITIES

CURE NCI Study Group Rockville, MD

African genetic ancestry is associated with BRAF-mutated colorectal tumors and distal location in Puerto Rican Hispanics with Colorectal Cancer

Julyann Pérez-Mayoral[1], Marievelisse Soto[1,2], Maria del Mar Gonzalez-Pons[2], Belisa Suarez[2], Myrta I. Olivera[1], Ebony Shah[3], Rick Kittles[3], Marcia Cruz-Correa[1,2]

[1]University of Puerto Rico Comprehensive Cancer Center, San Juan, PR; [2]University of Puerto Rico Medical Sciences Campus, San Juan, PR; [3]City of Hope Comprehensive Cancer Center, Duarte, CA

Background

❖Colorectal cancer (CRC) is the 1st cause of cancer deaths in Puerto Rico (PR), with 26.5% of cancer deaths being caused by CRC [1].

❖When compared to non-Hispanic whites, Hispanics in general have lower incidence rates of CRC and are diagnosed at an earlier age, with more advanced disease and with worse prognosis.[2]

❖However, even between Hispanic subgroups, there are differences in the incidence and mortality rates of CRC (Figure 1)

Figure 1: Incidence and mortality cumulative risk estimates for CRC in Latin America as reported by the GLOBOCAN project (2012).

❖Puerto Rican Hispanics (PRH) are an admixed population of three ancestral races: European, West African and Amerindian[3].

❖This mixture of races vary according to the Hispanic subpopulation under study, which could account, at least in part, for the differences observed in the CRC mortality rates of PRH.

❖Furthermore, increased presence of African ancestry in the genetic background of an individual has been associated with increased risk of colorectal adenoma in Colombian Hispanics[4].

Objective

❖The **objective** of this project was to assess the role of genetic ancestry in CRC risk and clinicopathological features of CRC tumors in the PRH population.

❖The study will have a ***significant impact*** in tailoring screening and treatment recommendations for PRH, both in PR and those living in the US, which in turn, will reduce CRC incidence and mortality rates for PRH.

❖Furthermore, the knowledge obtained will aid in elucidating the role of genetics in susceptibility to CRC in Hispanics.

Methods

❖***Samples:*** A total of 406 PRH CRC cases and 425 controls were recruited from the PURIFICAR population based registry. Genomic DNA was extracted from peripheral blood lymphocytes (PBLs) following the protocol provided by the QIAmp DNAMini Kit (Qiagen).

❖***Laboratory methods:***

Figure 2: Summary of methods.

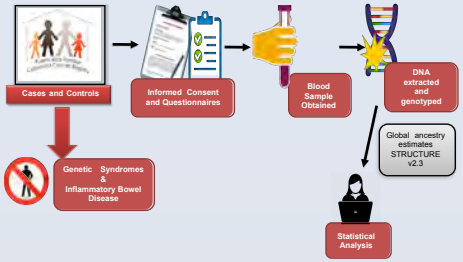

❖***Data analysis:*** Comparison of demographic and clinical characteristics according to CRC status were evaluated using Pearson's Chi Square or Fisher's Exact test as appropriate. Logistic regression models were fitted to estimate the unadjusted and adjusted odds ratio (OR) and its 95% confidence interval (CI) for the association of CRC status and ancestry. Logistic regression models were adjusted by age at recruitment, gender, education, and family history of CRC. Among CRC cases, comparison of tumor characteristics according to the mean of ancestry markers were evaluated using Pearson's Chi Square or Fisher's Exact test as appropriate. Logistic regression models were fitted to estimate the unadjusted and adjusted odds ratio (OR) and its 95% confidence interval (CI) for the association of ancestry and tumor characteristics. Logistic regression models were adjusted by age at recruitment, gender, smoking, drinking and BMI. All statistical analyses were done using STATA 14.0

Results

Figure 3: Ancestral Populations Proportions in the Study Population

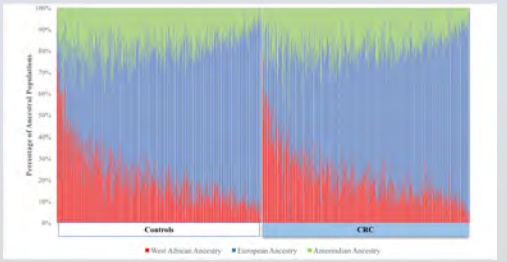

Mean ancestry proportions for the study population are:
61% European, 21% African and 18% Amerindian

Results

Table 1. Demographics and clinical characteristics by participant status by participant status (n=831)

Characteristic	Control (n=425) n (%)	CRC (n=406) n (%)	p-value* *
Age at recruitment			< 0.0001
< 60 years	293 (68.9)	198 (48.8)	
≥ 60 years	132 (31.1)	208 (51.2)	
Gender			< 0.0001
Male	120 (28.2)	211 (52.0)	
Female	305 (71.8)	195 (48.0)	
Educational level*			< 0.0001
≥ 12 years	155 (61.0)	123 (43.0)	
< 12 years	99 (39.0)	163 (57.0)	
Marital Status*			0.502
Single/divorced/widowed	86 (35.4)	75 (32.5)	
Married	157 (64.6)	156 (67.5)	
Health Insurance*			0.067
Private	119 (68.8)	184 (65.7)	
Public	54 (31.2)	88 (31.4)	
Other	0 (0.0)	8 (2.9)	
Family History of CRC*			0.026
No	226 (67.3)	285 (74.8)	
Yes	110 (32.7)	96 (25.2)	
Current Drinker*			< 0.0001
No	263 (63.1)	286 (78.1)	
Yes	154 (36.9)	80 (21.9)	
Ever Smoked 100 Cigarettes			0.022
No	290 (69.71)	228 (61.96)	
Yes	126 (30.29)	140 (38.04)	
BMI*			0.711
< 20	11 (2.7)	14 (3.6)	
20-24	116 (28.2)	99 (25.1)	
25-29	155 (37.7)	152 (38.6)	
30	129 (31.4)	129 (32.7)	
European Ancestry			0.993
≤0.61	204 (48.0)	195 (48.0)	
>0.61	221 (52.0)	211 (52.0)	
African Ancestry			0.854
≤0.21	258 (60.7)	249 (61.3)	
>0.21	167 (39.3)	157 (387)	
Amerindian Ancestry			0.230
≤0.18	252 (59.3)	224 (55.2)	
>0.18	173 (40.7)	182 (44.8)	

*Counts varies due to missing information; *P-value from Chi-square or Fisher's exact test.

Table 2: Association of genetic ancestry (categorical variable) with CRC status.

Ancestry	CRC $OR_{unadjusted}$	CRC $OR_{adjusted*}$	CRC $OR_{adjusted**}$
European Ancestry			
≤ (0.61)	1.0	1.0	1.0
> (0.61)	0.99 (0.76 – 1.31)	0.97 (0.64 – 1.46)	0.99 (0.65 – 1.52)
African Ancestry			
≤ (0.20)	1.0	1.0	1.0
> (0.20)	0.97 (0.73 – 1.29)	1.22 (0.81 – 1.86)	1.26 (0.82 – 1.95)
Amerindian Ancestry			
≤ (0.18)	1.0	1.0	1.0
> (0.18)	1.18 (0.90 – 1.55)	0.89 (0.59 – 1.33)	0.84 (0.55 – 1.28)

*POR's adjusted by age at recruitment, gender, education, and family history of CRC.
** POR's adjusted by age at recruitment, gender, education, and family history of CRC, smoking and drinking.

Table 3: Association of genetic ancestry (continuous variable) with CRC status.

Ancestry	CRC $OR_{unadjusted}$	CRC $OR_{adjusted*}$	CRC $OR_{adjusted**}$
European Ancestry	1.22 (0.43 – 3.43)	3.59 (0.77 – 16.83)	3.76 (0.79 – 17.93)
African Ancestry	0.74 (0.24 – 2.22)	0.41 (0.08 – 2.02)	0.45 (0.09 – 2.28)
Amerindian Ancestry	1.08 (0.16 – 7.34)	0.18 (0.01 – 3.69)	0.10 (0.01 – 2.19)

*POR's adjusted by age at recruitment, gender, education, and family history of CRC.
** POR's adjusted by age at recruitment, gender, education, and family history of CRC, smoking and drinking.

Table 3: Association of tumors characteristics with ancestral markers (categorical variable) among patients with CRC.

Tumor Characteristic	African Ancestry OR unadjusted (95% CI)	African Ancestry OR adjusted* (95% CI)
Tumor Location		
Proximal	1.0	1.0
Distal	2.36 (1.33 – 4.20)	**2.61 (1.38 – 4.96)**
Tumor Stage		
0/ I/II	1.0	1.0
III/IV	0.70 (0.39 – 1.23)	**0.51 (0.28 – 0.91)**
Other/Unknown	0.61 (0.33 – 1.15)	0.61 (0.26 – 1.40)
Tumor differentiation		
High	1.0	1.0
Moderate	3.08 (1.52 – 6.24)	3.11 (1.43 – 6.66)
Low	2.81 (1.03 – 7.68)	2.40 (0.76 – 7.57)
Microsatellite Status		
Stable	1.0	1.0
Low/High	**	**
CIMP Status		
0	1.0	1.0
Low	0.53 (0.12 – 2.27)	0.36 (0.07 – 1.81)
***KRAS* Mutation Status**		
Wild type	1.0	1.0
Mutated	1.17 (0.52 – 2.62)	1.14 (0.47 – 2.73)
***BRAF* Mutation Status**		
Wild type	1.0	1.0
Mutated	4.17 (0.80 – 21.71)	**7.16 (1.21 – 42.45)**

*POR's adjusted by age at recruitment, gender, smoking, drinking and BMI.
**POR can't be calculated given the limited sample size.

European and Amerindian Ancestry proportions were evaluated and were not found to be associated with Colorectal Tumor characteristics.

Conclusions

❖Our results showed that differences in the proportion of ancestral populations have a role in CRC carcinogenes is in the admixed population of PRH.

❖European ancestry (as a continuous variable) was found to show a trend for increased risk of CRC.

❖We found that **increased** levels of African ancestry were associated with distal colon located tumors, tumors with moderate differentiation and *BRAF*-mutated tumors.

❖Additionally, **low levels** of African ancestry were associated with a protective effect against Stage III/IV tumors.

❖These results support a role of genetic ancestry in the susceptibility of being diagnosed with CRC subtypes depending on the levels of African admixture present in the individual.

Acknowledgments

This work was partially supported by: 8U54MD007587-03 and U54MD007587; 5K22CA115913-03, R21CA167220-01, 5R03CA130034-02, and U54CA096297; G12MD007600. In addition, the authors will like to thank the patients involved in the study for their treasured contribution.
Contact: julyann.perez@upr.edu

References

1. Tortolero-Luna, G. et al. 2013.
2. Siegel, R.L. et al. 2015 CA CancerJ Clin,65(6):p.457-480
3. Avena, S. et al. 2012 PLoSONE,7(4):e.34695
4. Hernandez-Suarez, G. et al. 2014 EurJ HumGenet, 22(10) p.1208-1216

Deficiency of CD47 regulates metabolism and hypoxia in the tumor microenvironment

Katherine L. Cook, Tiffany Newman, Adam Wilson, Liliya Yamaleyeva,
David R. Soto-Pantoja

Wake Forest School of Medicine Comprehensive Cancer Center
Winston-Salem, NC 27157

Abstract

Macrophage mediated elimination of cancer cells is critical for control of tumor growth. CD47 is a cell surface receptor well characterized as a checkpoint inhibitor of innate immunity as it binds to the signal regulatory protein-α (SIRPα) on macrophages to inhibit phagocytosis. However, the regulation of cell signaling and metabolism by CD47 binding its ligand, thromsbospondin-1 (TSP1), or by autonomous regulation is largely understudied. We have demonstrated that absence of CD47 regulates glycolytic and mitochondrial metabolism in T cells in response to stress. We now show that blockade of CD47 with anti-sense morpholino reduced the mitochondrial and glycolytic metabolism of murine and human breast cancer cells as measured by oxygen consumption rate (OCR) and extracellular acidification rate (ECAR), suggesting that targeting CD47 may regulate tumor cell metabolism to impact carcinogenesis. Interestingly, blockade of CD47 on macrophages enhanced mitochondrial metabolism and glucose uptake suggesting for the first time a role of CD47 expression on macrophage function. A similar response was observed in CD47 deficient T cells when compared to WT. These data suggests that targeting CD47 may differentially regulate metabolism in the tumor microenvironment enhancing anti-tumor immunity. To test whether targeting CD47 would prevent tumor growth we developed a model of DMBA-induced mammary carcinogenesis in wild-type (WT) and CD47 null mice ($CD47^{-/-}$). We observed delayed tumor onset in $CD47^{-/-}$ when compared with WT mice (9 weeks post DMBA versus 4 weeks post DMBA in WT mice). Moreover, tumor incidence is significantly reduced in CD47 deficient mice (25%) when compared with WT mice (60%), indicating that absence of CD47 reduces tumor burden. Examination of tumor sections shows an over 50% reduction in Ki67 immunoreactivity in $CD47^{-/-}$ tumors demonstrating reduced tumor proliferation. Using an untargeted metabolomics approach, we determined that deficiency of CD47 influences energy metabolite consumption when compared to WT tumors. The metabolic changes were associated with a reduction in oxygen tension in $CD47^{-/-}$ tumors as measured *in vivo* by photoacoustic imaging. The regulation of metabolism and hypoxia in the tumor microenvironment was associated with differences in immune cell infiltration as well as macrophage polarization with increased anti-tumor M1 infiltrate in CD47 deficient tumors. Overall, our results indicate a new role of CD47 in the control of metabolite consumption in the microenvironment regulating both tumor and immune cells actions resulting in reduction of breast tumor burden.

Background

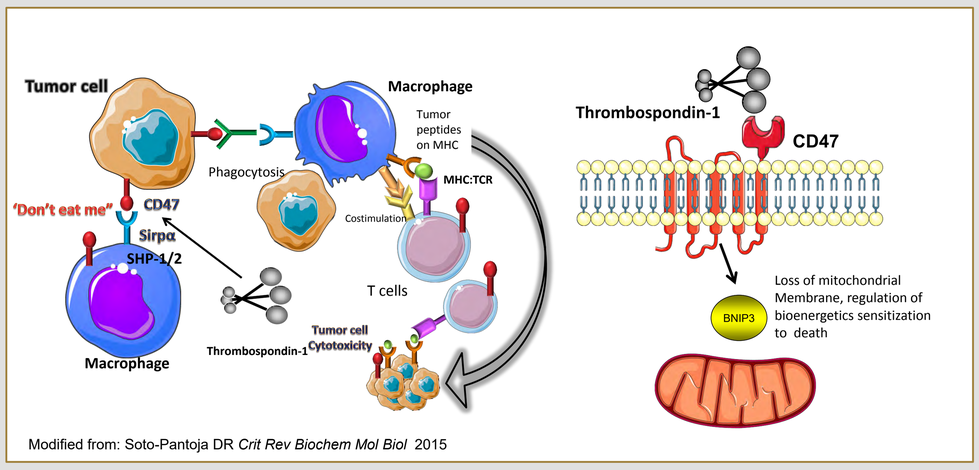

Modified from: Soto-Pantoja DR *Crit Rev Biochem Mol Biol* 2015

Figure 1. CD47 Signaling Pathways. (A) Engagement of tumor cells CD47 ("don't eat me" signal) with macrophages SIRP-α causes activation and phosphorylation of SIRP-α ITIM motifs and the recruitment of SHP-1 and SHP-2 phosphatases preventing myosin-IIA accumulation at the phagocytic synapse inhibiting tumor cell phagocytosis. By blocking the CD47:SIRP-α engagement an increase in tumor cell phagocytosis by APCs is observed. The engulfed tumor cells are then processed, and tumor-associated antigens are presented by these APCs on their MHC causing antigen-specific tumor cell cytotoxicity on cancer cells. (B) Thrombospondin-1 engages CD47 which causes the release of BNIP3 which intercalates in the mitochondrial membrane reducing membrane potential which may cause changes in cell bioenergetics and sensitization to apoptosis.

Methods

DMBA Mouse Model: Wild-type (WT) and CD47 -/- mice were given a single 15 mg subcutaneous dose of medroxyprogesterone acetate (MPA, Pfizer) at 6 weeks of age followed by 4 consecutive doses of 1 mg 7,12-dimethylbenz[a]anthracene (DMBA, Sigma) by oral gavage on weeks 7,8,9, and 10 to induce mammary carcinogenesis (See Figure 2A for schematic).

Cell Culture: 4T1 mouse breast cancer cells were cultured in RPMI medium supplemented with 10% FBS, penicillin/streptomycin, and glutamine at 37˚C and 5% CO_2.

Immunohistochemistry: Staining of tissue sections was performed as previously shown (Soto-Pantoja et al. *Autophagy* 2012;). Slides were be incubated with specific antibodies Ki67 (proliferation), CD80 (M1 macrophage) or CD206. Ki67 staining was done using DAB as chromogen. Fluorescent tag slides where covered in DAPI anti-fade mounting media before analysis.

Cytotoxicity Assays: Cells were plated and left untreated or treated with CD47 morpholino (CD47M). Cytolysis was measured by impedance measured as cell index using an ACEA xcelligence DP instrument.

Cell bioenergetics: 4T1 cells were plated and treated with antisense CD47 morpholino (CD47M). Mitochondrial metabolism (OCR) and Glycolytic flux (ECAR) was measured using a Seahorse XF-96 analyzer.

Metabolomics: Metabolomic profiling analysis was performed by Metabolon. Samples were prepared using the automated MicroLab STAR® system. The resulting extract was divided into four fractions: one for analysis by UPLC/MS/MS (positive mode), one for UPLC/MS/MS (negative mode), one for GC/MS, and one for backup.

In vivo oxygen saturation: Vevo ultrasound system was used for the 3D assessments of tumor vasculature and oxygenation by measuring oxygen saturation (sO_2) and hemoglobin concentration (Hb).

Results

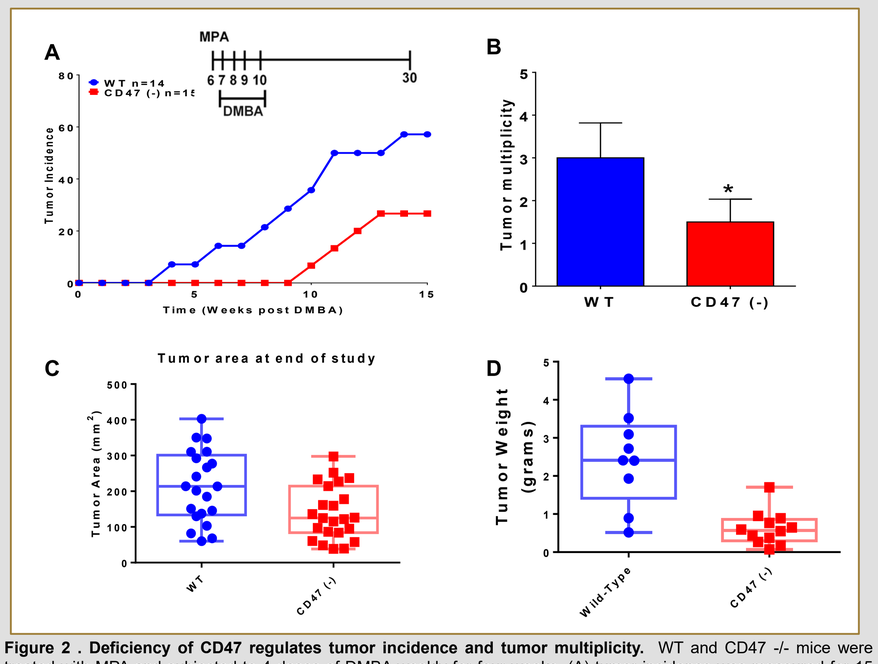

Figure 2 . Deficiency of CD47 regulates tumor incidence and tumor multiplicity. WT and CD47 -/- mice were treated with MPA and subjected to 4 doses of DMBA weekly for four weeks. (A) tumor incidence was measured for 15 weeks post DMBA. (B) Tumor multiplicity was counted in each animal at the end of the study (C) Tumor diameter was measured with caliper and area was calculated (D) Tumor weight at time of death (n=10-12) , *p<0.05.

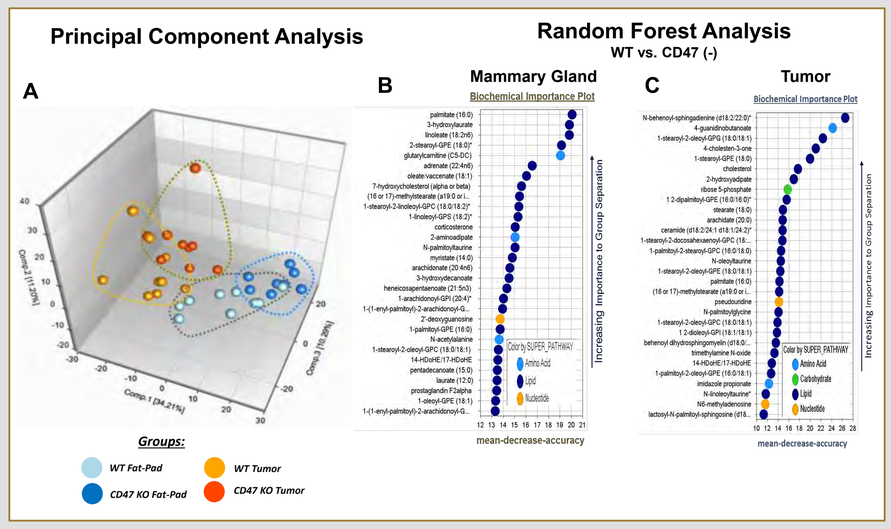

Figure 3 . Metabolite comparison between WT and CD47 (-) mammary gland and tumors. (A) Principal component analysis revealed major separation between the tumor and mammary fat pad. Within the two types of samples, there appeared to be some degree of separation based on genotype, with mammary fat pad showing greater separation. Random forest analysis of WT vs. CD47 deficient (B) mammary gland and (C) Tumors. Random Forest analysis attempts to bin individual samples into groups based on their metabolite similarities and differences. Comparison for WT vs. CD47 (-) mammary glands resulted in a predictive accuracy of 90%, analysis between WT Tumor and CD47 (-) tumor samples showed a predictive accuracy of 70% between genotypes n=9 for each group.

Sub Pathway	Biochemical Name	Tumor Fat Pad WT	Tumor Fat Pad CD47 KO	CD47 KO WT Fat Pad	CD47 KO WT Tumor
Phospholipid Metabolism	choline	1.34	1.35	0.79	0.80
	choline phosphate	2.07	3.27	0.84	1.33
	cytidine 5'-diphosphocholine	5.64	10.71	0.60	1.14
	glycerophosphorylcholine (GPC)	1.66	2.04	0.84	1.03
	phosphoethanolamine	1.16	1.98	0.71	1.21
	cytidine-5'-diphosphoethanolamine	3.77	7.17	0.77	1.46
	glycerophosphoethanolamine	1.86	2.45	0.80	1.05
	glycerophosphoserine*	1.01	1.39	0.97	1.33
	glycerophosphoinositol*	1.97	2.08	1.14	1.21
	trimethylamine N-oxide	1.02	1.68	1.65	2.72
Phosphatidylcholine (PC)	1-myristoyl-2-palmitoyl-GPC (14:0/16:0)	2.74	2.17	1.24	0.98
	1-myristoyl-2-arachidonoyl-GPC (14:0/20:4)*	3.96	3.65	0.81	0.75
	1,2-dipalmitoyl-GPC (16:0/16:0)	1.97	1.59	0.99	0.80
	1-palmitoyl-2-stearoyl-GPC (16:0/18:0)	4.27	1.85	1.00	0.43
Phosphatidylethanolamine (PE)	1,2-dipalmitoyl-GPE (16:0/16:0)*	10.26	2.14	1.40	0.29
	1-palmitoyl-2-oleoyl-GPE (16:0/18:1)	2.45	1.37	0.89	0.49
Phosphatidylserine (PS)	1-stearoyl-2-oleoyl-GPS (18:0/18:1)	1.87	1.22	0.81	0.53
	1-stearoyl-2-linoleoyl-GPS (18:0/18:2)	1.27	1.03	0.79	0.64
	1-stearoyl-2-arachidonoyl-GPS (18:0/20:4)	1.30	1.18	0.78	0.71
Phosphatidylglycerol (PG)	1-palmitoyl-2-oleoyl-GPG (16:0/18:1)	3.50	1.92	0.91	0.50
	1-palmitoyl-2-linoleoyl-GPG (16:0/18:2)	1.87	1.25	0.94	0.63
	1-stearoyl-2-oleoyl-GPG (18:0/18:1)	6.02	1.56	0.93	0.24
Phosphatidylinositol (PI)	1-palmitoyl-2-oleoyl-GPI (16:0/18:1)*	8.60	2.21	1.44	0.37
	1-stearoyl-2-linoleoyl-GPI (18:0/18:2)	2.39	1.02	0.91	0.39
	1,2-dioleoyl-GPI (18:1/18:1)	1.61	0.65	0.88	0.36
	1-stearoyl-2-arachidonoyl-GPI (18:0/20:4)	1.48	0.99	0.84	0.56

Figure 4 . Deficiency of CD47 regulates lipid metabolism. Top metabolites resulting from clustering analyses in mammary fat pad and tumor tissue point heavily to changes in lipid metabolism between WT and CD47 (-) mice

Sub Pathway	Biochemical Name	Tumor Fat Pad WT	Tumor Fat Pad CD47 KO	CD47 KO WT Fat Pad	CD47 KO WT Tumor
Glycolysis and Pyruvate Metabolism	glucose	0.54	0.69	0.76	0.97
	glucose 6-phosphate	2.09	3.73	0.39	0.69
	2-phosphoglycerate	1.15	1.05	0.31	0.28
	3-phosphoglycerate	1.45	0.87	0.74	0.44
	phosphoenolpyruvate (PEP)	1.38	0.76	0.78	0.43
	pyruvate	2.42	4.00	0.74	1.23
	lactate	2.70	2.66	0.98	0.97
Pentose Phosphate Pathway	6-phosphogluconate	1.14	1.65	0.94	1.37
	ribose 5-phosphate	1.33	0.87	0.54	0.36
	ribose 1-phosphate	1.85	4.92	0.45	1.20
	sedoheptulose-7-phosphate	1.17	1.56	0.75	1.01
	erythrose 4-phosphate	2.11	3.36	1.03	1.64

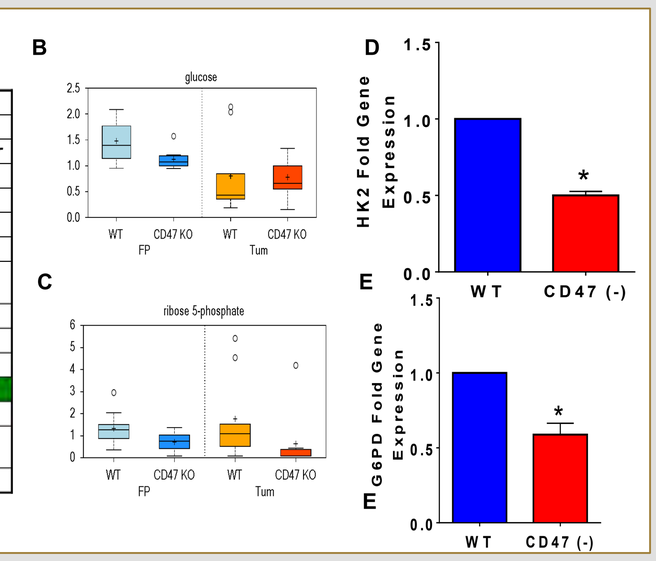

Figure 5 . Deficiency of CD47 regulates glycolytic metabolism. (A) Summary of metabolite regulation between WT and CD47(-) tumors and mammary gland (n=9). (B) Decreases in glucose were observed in the mammary gland (*p<0.05) in CD47 (-) when compared to WT but no difference was observed in tumors. (C) A significant decrease gland (*p<0.05) in ribose 5-phosphate was noted in CD47 (-) tumors in relation WT tumor. Tumor extracts were examined by RT PCR to determine gene expression of (D) Hexokinase and (E) Glucose-6-phosphate dehydrogenase in tumors (n=6 *p<0.001).

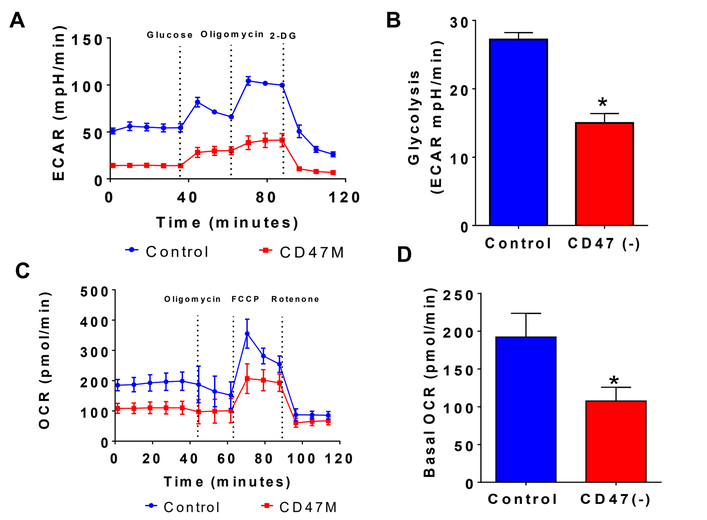

Figure 6. Blockade of CD47 regulates cell bioenergetics. 4T1 breast cancer cells where plated for 24h and were left untreated or administered 10 um CD47 morpholino (CD47M). Extracellular Acidification Rate profile (D) and glycolysis (B) measured by addition of glucose was measured using a Seahorse XF-96 bioanalyzer. Oxygen consumption rate (OCR- C, D) was measured by XF-96 to determine mitochondrial function*p<0.05.

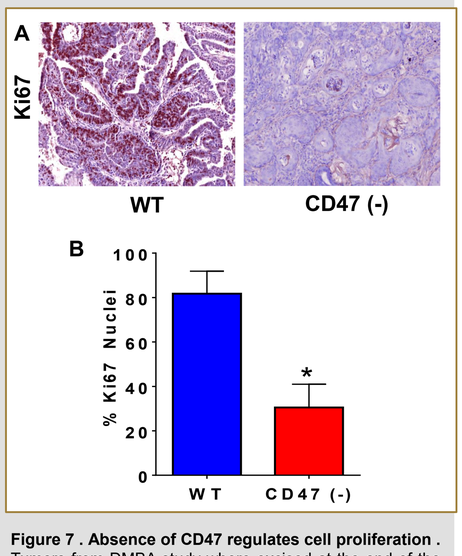

Figure 7 . Absence of CD47 regulates cell proliferation . Tumors from DMBA study where excised at the end of the study. Tissues where fix and paraffin embedded. Sections from WT and CD47 -/- where stained with a Ki67 antibody (A) incubated with DAB (brown stain). Positive nuclei was counted under bright field microscope N=4 , *p<0.05.

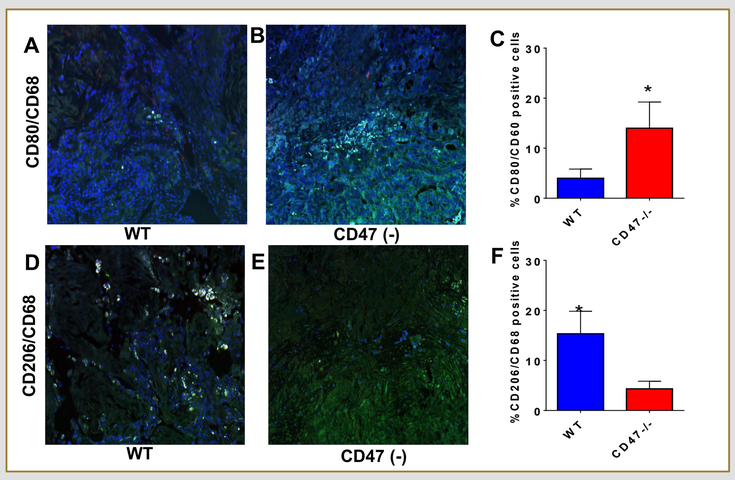

Figure 8 . Absence of CD47 regulates macrophage polarization. Tumors from DMBA model where excised at the end of the study. Tissues where fix and paraffin embedded. Sections from WT (A,D) and CD47 -/- (B,E) where stained with a fluorescent CD68 antibody (green) and CD80 (red) to stain for M1 type macrophage. Another set of sections was stained with CD68 green and CD206 antibody red to stain for M2 type macrophage. Sections where stained with DAPI (Blue to detect nuclei). Positive cells for CD80 (C) or CD206 (F) where counted using mantra quantitative pathology software (Stained with DAPI/CD68). N=3 , *p<0.05.

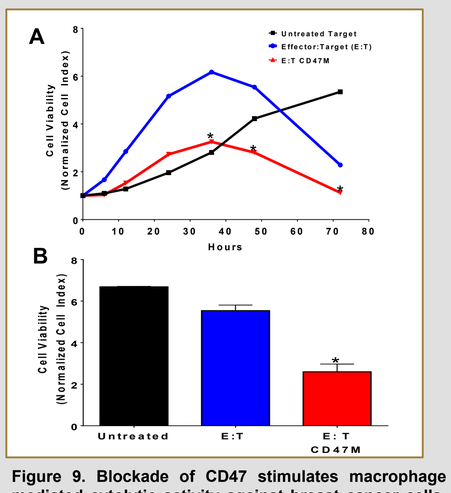

Figure 9. Blockade of CD47 stimulates macrophage mediated cytolytic activity against breast cancer cells. 4T1 breast cancer cells where plated for 24h, cells where co-cultured RAW.267mouse macrophages. Cytolytic activity was measure by cell impedance using ACEA xcelligence system (A), (B) Cell index at 48h . N=3, *p<0.05

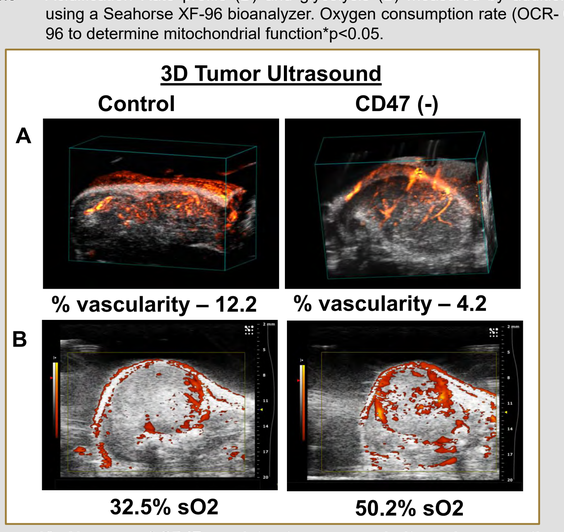

Figure 10. Absence of CD47 regulates tumor vascularity and oxygenation. (A) Power Doppler analysis using photoacoustic imaging was used to measure tumor vascularity, (B) Photoacoustic mode with OxyZated and HemoMeasure software of the Vevo was used for the 3D assessments of tumor volume and oxygenation by measuring sO_2 and Hb concentration.

Summary

- Absence of CD47 in the microenvironment reduces tumor burden in a carcinogen-induced mammary carcinogenesis model.
- Untargeted metabolomics analysis shows absence of CD47 shifts metabolite consumption in the tumor microenvironment.
- Inhibition of CD47 resulted in down regulation of both mitochondrial metabolism and glycolytic flux.
- Knockdown of CD47 on macrophages resulted in increased tumoricidal activity against breast cancer cells.
- Absence of CD47 reduces tumor vascularity and increases Oxygen saturation *in vivo.*

Targeting CD47 shifts bioenergetics of the tumor microenvironment, to reduce tumor burden and enhance anti-tumor immunosurveillance.

Acknowledgments: DSP is supported by a The NCI Transition Career Development award K22 (1K22CA181274-01A1) & MetaVivor Foundation Young Investigator Award

ATF4 mediates metabolic reprogramming and survival during MYC-induced lymphomagenesis

Feven Tameire[1], Ioannis Verginadis[1], Nektaria-Maria Leli[1], Andreas Czech[2], Christine Polte[2], Crystal S. Conn[3], Maria Monroy[1], Andrew Kossenkov[4], Zoya Ignatova[2], Serge Y. Fuchs[5], J. Alan Diehl[6], Davide Ruggero[3] and Constantinos Koumenis[1]

[1]Department of Radiation Oncology, [2] Institute for Biochemistry and Molecular Biology, University of Hamburg, Martin-Luther-King-Platz , Hamburg 20146, Germany, [3]School of Medicine and Department of Urology, Helen Diller Family Comprehensive Cancer Center, UCSF,[4]Center for Chemical Biology and Translational Medicine, The Wistar Institute, Philadelphia, PA 19104, USA, [5]Department of Biomedical Sciences, School of Veterinary Medicine, [6]Department of Biochemistry and Molecular Biology and Hollings Cancer Center, Medical University of South Carolina, Charleston, SC, 29425, [1]Perelman School of Medicine, University of Pennsylvania, Philadelphia, PA 19104

Abstract

The proto-oncogene c-Myc is often deregulated in human tumors and particularly in lymphomas, its overexpression due to translocations, associates with poor prognosis. While c-Myc is a potent activator of pro-tumorigenic pathways, it can also induce anti-tumorgenic pathways such as apoptosis. However, in c-Myc driven cancers the anti-tumorigenic state is evaded via a yet poorly understood pro-survival mechanism. We previously reported that activation of the PERK arm of the Integrated Stress Response (ISR) is one such pro-survival mechanism induced by c-Myc to resist c-Myc induced apoptosis. We also demonstrated enhanced activation of the PERK/p-eIF2α arm of the UPR in a mouse model of lymphoma and in B-cells obtained from B cells isolated from patients with Burkitt's lymphoma compared to normal B cells.

The Integrated Stress Response (ISR) pathway is essential in cancer cell adaptation to extrinsic stresses such as hypoxia and nutrient deprivation both *in vitro* and *in vivo*. The ISR kinases, PERK and GCN2, phosphorylate eIF2α, transiently inhibiting protein translation during times of stress. Phosphorylation of eIF2α promotes the preferential translation of the transcription factor ATF4, which activates a gene expression program that enhances uptake and synthesis of amino acids, antioxidant defense and chaperone expression to promote recovery from nutrient deprivation and ER stress. Here, we demonstrate the critical role ATF4 plays in promoting the survival of c-Myc overexpressing cells both in vitro and in vivo.

In vitro, we demonstrate that ATF4 depletion significantly sensitized cells to apoptosis following c-Myc activation in mouse and human cells. ATF4 expression was dependent on the ISR kinases PERK and GCN2. Using tRNA microarray, we discovered that c-Myc activation leads to significant accumulation of uncharged tRNAs. Accumulation of uncharged tRNAs led to activation of GCN2 in RNA Polymerase III dependent manner. ChIP-seq analysis of ATF4 and c-Myc identified gene targets that MYC and ATF4 co-occupied. These targets showed enrichment for pathways involved in tRNA charging, amino acid transport and amino acid biosynthesis. Targeted analysis of intracellular metabolites showed a significant decrease in glycolytic and TCA cycle metabolites in cells depleted of ATF4 following c-Myc activation. Consistent with our in vitro data, we observe higher levels of p-eIF2α and ATF4 in lymphoma cells compared to WT B cells in vivo in a mouse model of c-Myc driven Burkitt's lymphoma. Importantly, acute deletion of ATF4 significantly delayed MYC-driven lymphomagenesis and promoted survival of Eμ-myc lymphoma bearing mice. Our findings establish that ATF4 cooperates with c-Myc in supporting metabolism as well as regulating pro-survival pathways and therefore can be targeted as a therapy modality in MYC driven lymphomas.

The Integrated Stress Response

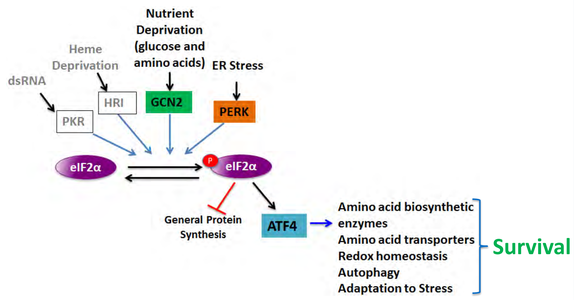

Figure 1: The Integrated Stress Response and Cancer. The ISR is mediated by four kinases, PERK, general control nonderepressible 2 (GCN2), RNA-dependent protein kinase (PKR) and heme regulated inhibitor (HRI) that converge on phosphorylation of eIF2α. Each kinase is activated by specific cellular stresses, but the common target of the ISR is phosphorylation of eIF2α which culminates in the translation of ATF4. ATF4 is critical for inducing a transcriptional response tailored for each stress. The GCN2/PERK/eIF2α/ATF4 signaling is elevated in primary human liver, breast, lung and head and neck tumors and has been shown to support tumor growth *in vivo*.

Results

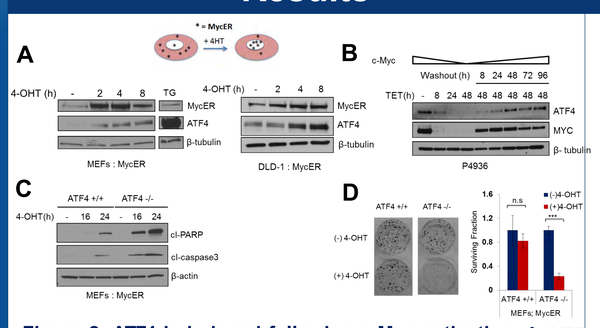

Figure 2. ATF4 is induced following c-Myc activation. A. MEFs (left panel) and DLD-1 cells (right panel) expressing MycER construct were treated with 4-hydroxytamoxefen (4-OHT) to activate c-Myc. Indicated nuclear proteins were assessed by immunobloting. Thapsigargin (0.5uM for 4hrs) treated cells were used as a positive control for ATF4 induction. **B.** Western blot of P4936, human burkitt's lymphoma cells, with tetracycline-off c-Myc, treated with tet (0.1ug/ml) for indicated times. **C.** Immunoblot showing increased levels of apoptosis markers after c-Myc activation in ATF4 deficient MEFs. **D.** ATF4+/+,MycER and ATF4-/-,MycER MEFs were treated with 4HT. Clonogenic survival was assessed (left panel) and surviving fractions counted from three independent experiments are shown normalized to untreated control for each (right panel).

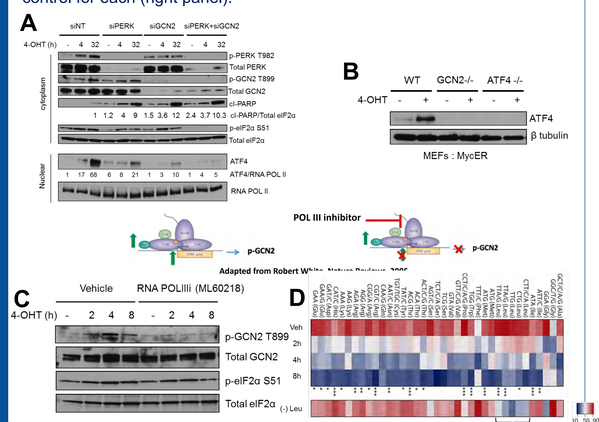

Figure 3. Loss of GCN2 enhances apoptosis after c-Myc activation. Both PERK and GCN2 are required for phosphorylation of eIF2α after c-Myc activation. A. Immunoblot of indicated protein levels in DLD-1 cells after siRNA mediated knockdown of PERK and GCN2. Knockdown of both GCN2 and PERK suppresses phosphorylation of eIF2α after c-Myc activation. **B.** Immunoblot analysis of nuclear lysates from GCN2 +/+ or GCN2-/- MEFs after c-Myc activation. **C.** Western blot showing protein levels of p-GCN2 after c-Myc activation in the presence or absence of of RNA POLIII inhibitor (ML-60218). DRB, RNA POLII inhibitor, is used as a negative control. **D.** Microarray of aminoacyl–tRNAs in DLD-1; MycER cells assessing charging of tRNAs after c-Myc induction at indicated times, three independent experiments, ANOVA, *, p<0.05; **, p<0.01; ***, p< 0.001. Line indicates Leu isoacceptors that are uncharged upon Leucine deprivation conditions.

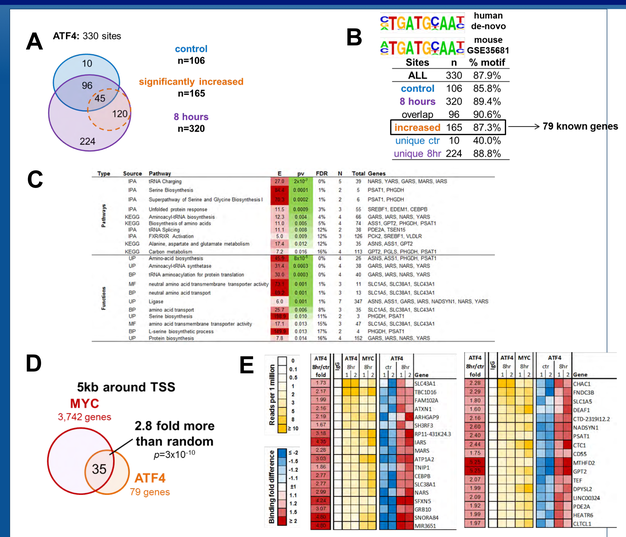

Figure 4. ATF4 and c-Myc bind to common target genes. **A.** ATF4 ChIP-seq identified 330 binding sites for ATF4. Binding sites occupied by ATF4 in control (without 4-OHT) are shown in blue. Binding sites that are bound by ATF4 following c-Myc activation are shown in purple. Binding sites that are significantly increased after 8 hours of c-Myc activation are shown in orange. **B.** Motif enriched within 330 ATF4 binding sites (human de-novo) and within ATF4 mouse experiment from GSE35681 dataset. Table shows percent of binding sites containing the motif for different site groups. **C.** Functions and pathways significantly enriched among genes bound by ATF4 within 5kb from TSS and upregulated at 8 hours of c-Myc activation, E=enrichment, FDR=false discovery rate, UP=Uniprot, MF=molecular function, BP=biological process. **D.** Overlap between ATF4 and c-Myc binding sites that are significantly increased following MYC activation. **E.** An overlapping ATF4 and c-Myc binding sites. List of genes that contain ATF4 or c-Myc binding sites within 5kb from TSS.

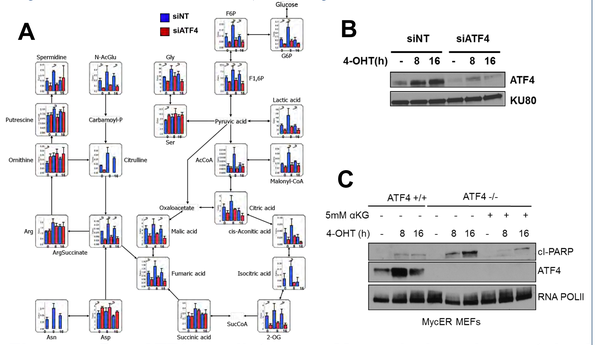

Figure 5. ATF4 mediates c-Myc induced metabolic adaptation by regulating glucose uptake and TCA cycle intermediates. A. Capillary electrophoresis mass spectrometry (CE-MS) based quantitative analysis of metabolites in the indicated pathways shown following c-Myc activation for 8 and 16hrs in siNT (blue bars) and siATF4 (red bars). n=3, two tailed student t-test, *p<0.05. **B.** immunoblot showing knockdown level of ATF4 for the metabolite analysis, representative of three independent experiments. **C.** Representative western blot of MEFs treated with αKG at earlier time points of c-Myc activation.

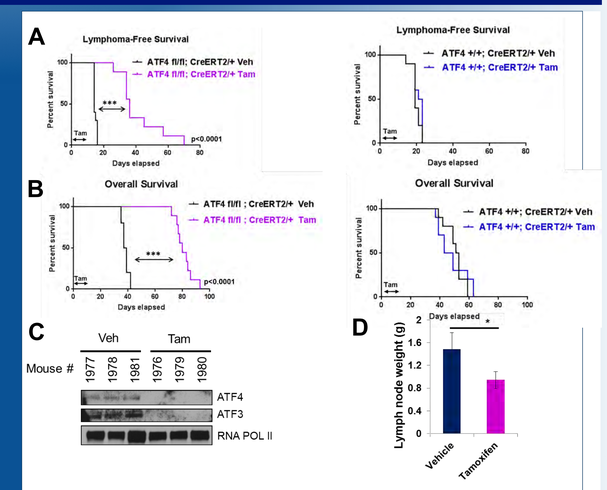

Figure 6. Acute ablation of ATF4 significantly delays c-Myc driven Lymphomagenesis. A. Lymphoma-free survival of mice bearing Eμ-Myc; ATF4 fl/fl lymphoma (left) or Eμ-Myc; ATF4 +/+ lymphoma (right) treated with either vehicle (veh) or tamoxifen (tam). **B.** Overall survival in A. n = 8-9 mice per group, Mantel Cox test,*** p<0.0001. **C**. Immunoblot of B cells isolated from Eμ-Myc; ATF4 fl/fl lymphoma bearing mice. **D.** lymph node weight of mice in Fig C, n=3, student t-test, p<0.03.

Working Model

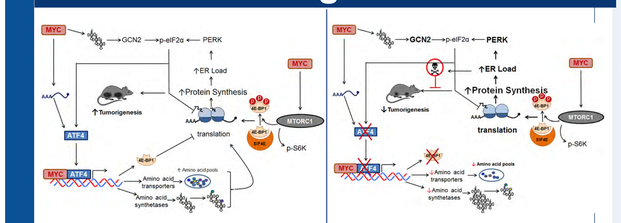

Acknowledgment

This research is supported by National Cancer Institute grant PO1-CA165997. F.T is supported by F31CA183569 .

Penn Radiation Oncology

Penn Medicine

Defining the crossroads of neural stem cell regulation and brain tumor formation

Jesse Garcia Castillo, Hector Gomez, David Aguilar, Samuel J. Pleasure, and Odessa R. Yabut *

Department of Neurology, University of California San Francisco, San Francisco, California

*E-mail: odessa.yabut@ucsf.edu | Phone: 415-514-4949

INTRODUCTION

Brain tumors arise from postnatal neural stem cell (NSC) niches[1]

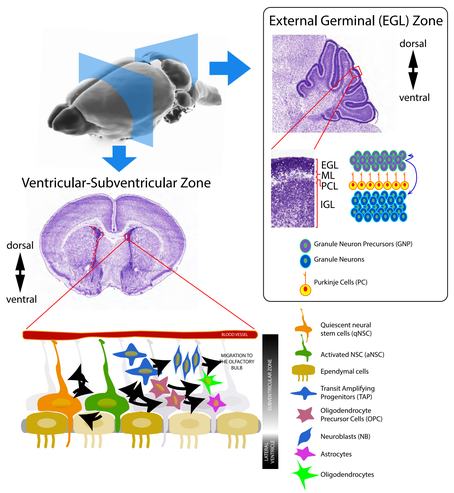

Suppressor of Fused (Sufu): a tumor suppressor gene

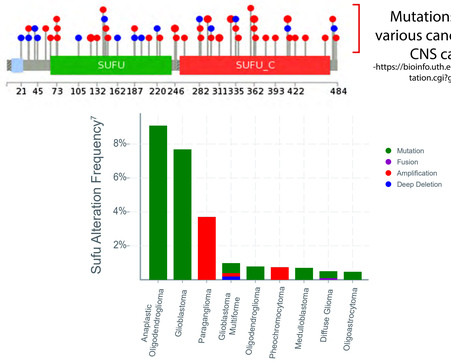

- Sufu controls the formation of various CNS regions at embryonic stages.
- In the embryonic neocortex, Sufu functions to specify and maintain cortical progenitors[2, 3].
- Sufu mutations cause medulloblastoma, affecting approximately 35% of all infant cases of MB[4].
- Loss of function Sufu mutations are present in glioblastoma subtypes[7].

REFERENCES

1. Yabut OR, Pleasure SJ. The Crossroads of Neural Stem Cell Development and Tumorigenesis. Opera Med Physiol. 2016 Dec;2(3-4):181-187.
2. Yabut OR, Fernandez G, Huynh T, Yoon K, Pleasure SJ. Suppressor of Fused Is Critical for Maintenance of Neuronal Progenitor Identity during Corticogenesis. Cell Rep. 2015 Sep 29;12(12):2021-34.
3. Yabut OR, Ng HX, Fernandez G, Yoon K, Kuhn J, Pleasure SJ. Loss of Suppressor of Fused in Mid-Corticogenesis Leads to the Expansion of Intermediate Progenitors. J Dev Biol. 2016 Dec;4(4).
4. Kool M et al. ICGC PedBrain Tumor Project. Genome sequencing of SHH medulloblastoma predicts genotype-related response to smoothened inhibition. Cancer Cell. 2014 Mar 17;25(3):393-405.
5. Pospisilik, J. et al. (2010). Drosophila genome-wide obesity screen reveals hedgehog as a determinant of brown versus white adipose cell fate. Cell. 140(1):148-160.
6. Zhuo, L. et al. (2001). hGFAP-cre transgenic mice for manipulation of glial and neuronal function in vivo. Genesis 31, 85–94.
7. Gao et al. Integrative analysis of complex cancer genomics and clinical profiles using the cBioPortal. Sci Signal. 2013 Apr 2;6(269):pl1. doi: 10.1126/scisignal.2004088.

HYPOTHESIS

Similar to the known roles of Sufu in regulating neural progenitors in the embryonic neocortex[2], **we hypothesize that Sufu continues to regulate neural stem/progenitors in postnatal neurogenic niches. We also hypothesize that dysfunction of Sufu in these regions are likely critical contributors of tumor initiation and maintenance.**

These studies advance our understanding of the mechanisms that permit and support tumor growth, and will ultimately aid in the design of effective therapies for brain tumors.

APPROACH

conditional deletion of Sufu in neural stem/progenitors

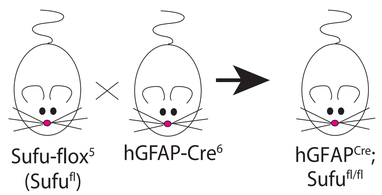

Analyze NSC behavior in neurogenic niche where Sufu expression has been ablated

RESULTS

1. Loss of SUFU leads to the expansion of dorsal V-SVZ and EGL

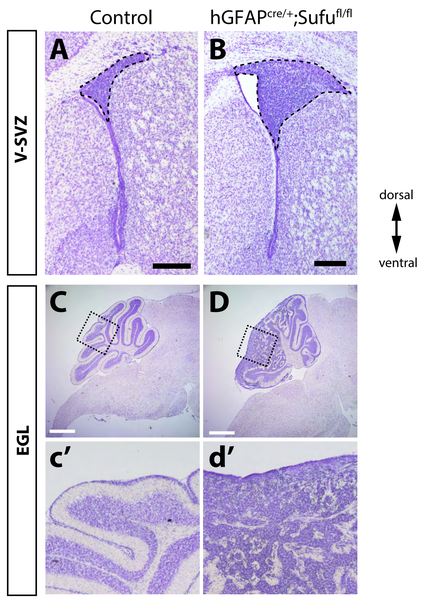

(A, B) Coronal sections from the Postnatal day (P)7 control and mutant V-SVZ were subjected to Nissl staining. The total area of the dorsal V-SVZ (outlined) were measured and compared between mutants and control littermates and showed significant expansion. Scale bars: 250 μm. n=3 mice per genotype, ***=p-value 0.01
(C, D) Loss of Sufu in the cerebellum similarly results in the expansion of the EGL in P14 mutant mice (E) unlike controls (D). Scale bars: 500 μm.

RESULTS

2. Highly proliferative neural stem/progenitors in the neonatal *hGFAP$^{cre/+}$;Sufu$^{fl/fl}$* dorsal V-SVZ

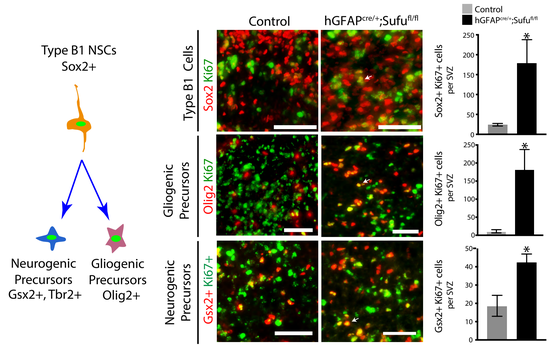

Double-immunostaining with the proliferation marker, Ki67 show that Sox2+ NSCs, neurogenic, and gliogenic precursors co-express Ki67 more frequently in mutants than in littermate controls Scale bars: 50 μm. n=3 controls, n=3 mutants, *p-value < 0.05.

3. Accumulation of cells in the dorsal V-SVZ of the neonatal *hGFAP$^{cre/+}$;Sufu$^{fl/fl}$* mice

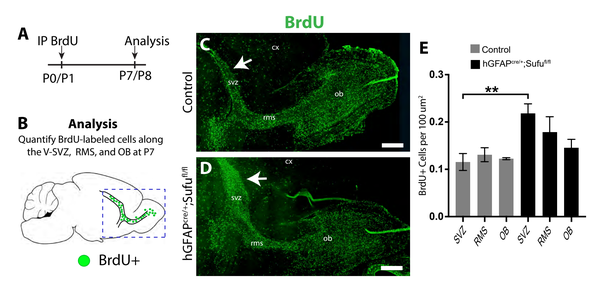

(A, B): Intraperitoneal (IP) injection of the thymidine analog, BrdU, was conducted to label proliferating cells in the V-SVZ of the P0 control and mutant mice for analysis at P7.
(C, D, E): Sagittal sections were immunostained for BrdU and showed BrdU+ cells along the V-SVZ, RMS, and OB of both control and mutant P7 mice. Accumulation of BrdU-labeled cells were observed in the V-SVZ of mutants but not controls (arrows). Graph show significant increase in BrdU-labeled along the V-SVZ. Scale bars: 500 μm. n=4/genotype

4. Cells in the dorsal V-SVZ fail to survive in the *hGFAP$^{cre/+}$;Sufu$^{fl/fl}$* mice

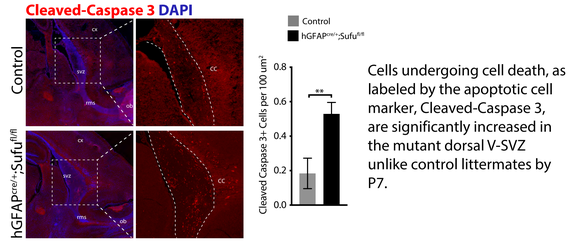

Cells undergoing cell death, as labeled by the apoptotic cell marker, Cleaved-Caspase 3, are significantly increased in the mutant dorsal V-SVZ unlike control littermates by P7.

ACKNOWLEDGEMENTS

This research is supported by NIH/NCI K01CA201068 (O.R.Y.), NIH/NINDS R01MH077694 (S.J.P.) and Diversity Supplement (H.G.).

RESULTS

5. Granule neuron precursors are highly proliferative and fail to differentiate in the neonatal *hGFAP$^{cre/+}$;Sufu$^{fl/fl}$* EGL

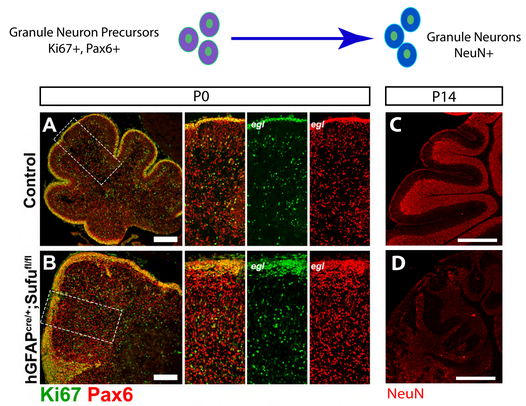

(A, B): Double-immunostaining with the proliferation marker, Ki67, show a greater number of Pax6+ granule neuron precursors in the EGL co-expressed Ki67 more frequently in mutants than in littermate controls at P0.
(C, D): NeuN+ differentiated granule neurons are markedly reduced in the P14 cerebellum of mutant mice unlike controls.

6. Cell death is prevalent in the EGL of the neonatal *hGFAP$^{cre/+}$;Sufu$^{fl/fl}$* mice

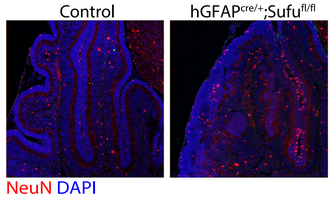

Cells undergoing cell death, as labeled by the apoptotic cell marker, Cleaved-Caspase 3, are significantly increased in the mutant EGL unlike control littermates by P7.

7. Tumor formation in the cerebellum of *hGFAP$^{cre/+}$;Sufu$^{fl/fl}$;p53$^{fl/fl}$* mice

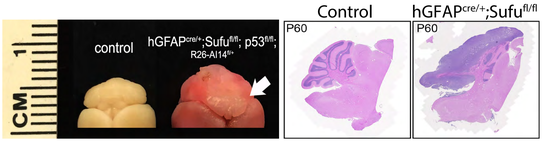

Sufu and p53 deletion promotes tumorigenesis by P60 in the mutant mice.

CONCLUSIONS

Sufu is controls proliferation of neural stem/progenitor populations and **maintains the lineage identity of stem/progenitors into mature neuronal and glial subtypes**. Failure to do can result in tumor formation, as is the case in the cerebellum.

These findings underscore the importance of maintaining the differentiation potential of neural stem/progenitor cells to prevent tumor formation.

Exploring therapeutic strategies that direct tumorigenic cells, particularly those with stem cell properties, towards a differentiated phenotype could be a promising treatment preventing brain tumor growth and malignancy.

A case study examining recruitment of health care providers as qualitative research participants: how long does it take?

Felder TM[1,2], Heiney SP[1], Friedman DB[2,3], Franco R[4], Hebert JR[2,5], Ford ME[6,7]

1.College of Nursing, University of South Carolina, Columbia, South Carolina; 2.Cancer Prevention and Control Program, Arnold School of Public Health, University of South Carolina, Columbia, South Carolina; 3. Department of Health Promotion, Education, and Behavior, Arnold School of Public Health, University of South Carolina, Columbia, South Carolina; 4.Center for Integrative Oncology & Survivorship, Cancer Institute, Greenville Health System, Greenville, South Carolina; 5. Department of Epidemiology and Biostatistics, Arnold School of Public Health, University of South Carolina, Columbia, South Carolina; 6. Department of Public Health Sciences, Medical University of South Carolina, Charleston, South Carolina

Background and Significance

- Promising research approaches, such as implementation science and multilevel interventions, often require involving health care providers (HCPs) as research participants.
- Growing evidence documents the significant impact that the patient-provider relationship has on many patient health outcomes, such as adherence to hormonal therapy.
- Given that HCPs may be difficult to recruit as research participants, due to their heavy workload and busy schedules, there is a need to better understand the time and resources needed to achieve HCP recruitment success.

Study objective

To quantify the time spent to recruit and interview HCPs about their perspective on key considerations for a future multilevel intervention aiming to improve adherence to adjuvant hormonal therapy.

Methods

Case study recruitment and eligibility

- PI (Felder) sent an email invitation letter to key professional associations, statewide organizations and K01 project consultants.
- Interested HCPs contacted the PI (**Figure 1**) by telephone or email, and were screened for eligibility. If eligible, an interview was scheduled.
- HCPs received $50 for completed interviews.

Figure 1. HCP Enrollment Process

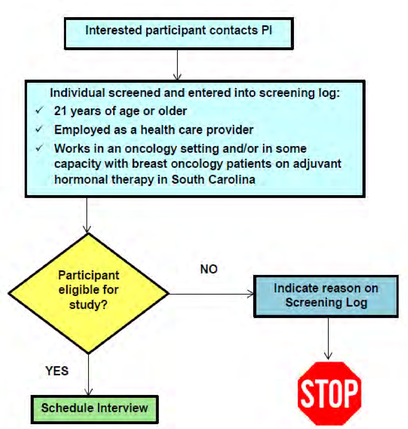

Methods (cont.)

Case study recruitment data source

- The PI tracked and maintained a recruitment database of communications (phone and electronic) to/from potential participants and sites. This database included lists of participant email addresses, email correspondences and phone call logs.

Data analysis

- We adapted Hysong et al.'s (2013) recruitment process mapping framework to guide and define three key recruitment outcomes:
  1. *Reaching participants* = days from initial contact to potential HCPs to eligibility screening.
  2. *Gaining entry* = days and contact attempts from initial contact to obtaining authorization to recruit at a given site.
  3. *Interviewing participants* = days and contact attempts from initial contact to completing HCP interviews.
- We analyzed records from the PI's recruitment database to summarize and calculate recruitment outcomes.

Results

- The PI's email invitation letter reached 199 disclosed recipients and led to 23 completed HCP interviews (**Table 1**).

Table 1. Summary of Health Care Provider Recruitment Through Sending Initial Email Invitation Letter to Key Professional Networks

Contact	# Email Recipients	# Study Inquiries	# HCPs Interviewed*
State Cancer Coalition	Undisclosed	3	2
State Coalition Workgroup	64	0	0
Professional Nursing Organization	84	4	3
Professional Social Work Organization	Undisclosed	2	1
State Cancer Control Program	28	1	0
Cancer Center 1	17	10	13
Cancer Center 2	3	2	2
Cancer Center 3	Undisclosed	1	1
Cancer Center 4		0	0
Pharmacy Consultant	3	1	1
TOTAL	**199**	**24**	**23**

Results (cont.)

- Most HCP participants were non-Hispanic White (n=20, 87%) and female (n=19, 83%).
- HCPs represented a range of current positions, such as nurses (n=13, 57%), oncologists (n=4, 19%) and social workers (n=2, 9%). Many HCPs had been in their professions for 15 years or more (n=11, 48%).

Table 2. Summary of health care provider recruitment outcomes

Outcome	Metric	Median	Mean	SD	Min-Max	n
Obtaining IRB authorization or site permission	Cycle time in calendar days from initial contact to establishing authorization to recruit at a given site.	21	42	54	0-150	7
	Number of contact attempts to site needed to establish authorization to recruit at a given site.	4	3	1	1-4	7
Reaching participants	Cycle time in calendar days from initial contact to potential participants to eligibility screening.	21	62	74	0-230	25
Scheduling participants	Cycle time in calendar days from initial contact to interview completion for those agreeing to participate.	21	62	75	0-233	23

- The average time to reach HCP participants was 68 ± 76 days [range: <1-233 days] **(Table 2)**.
- Thirteen HCPs were recruited from one large, collaborating site that facilitated institutional review board approval [*gaining entry*= 150 days].

Conclusions & Implications

- Obtaining site authorization led to the greatest delays in recruitment. However, the site with the highest number of days to establishing authorization yielded the highest number of HCP interviews.
- Establishing collaborations with large sites can help facilitate HCP recruitment.

This study was approved by the University of South Carolina and Greenville Hospital System's Institutional Review Boards. Study funding: Mentored Research Scientist Development Award to Promote Diversity from the NCI/NIH (PI: Felder - K01CA193667)

Expanding the Story of Survival: Faith, Family, and Genetic Counseling in African American Women with a Family History of Breast Cancer

Vida Henderson, PhD, PharmD, MPH, MFA[1]; Beverly Chukwudozie, MPH[1]; Angela Odoms-Young, PhD[2]; Karriem Watson, DHSc, MS, MPH[1]; DeLawnia Comer-Hagans, PhD[3]; Shirley Spencer, PhD, MS[3]; Vickii Coffey, PhD, MSA[3]; Giesela Grumbach, PhD, MSW, LCSW[3]; Catherine Balthazar,PhD[3]; Robert Winn, MD[1]; Kent Hoskins, MD[4]

[1] University of Illinois Cancer Center; [2]University of Illinois at Chicago College of Applied Health Sciences; [3]Governors State University; [4] University of Illinois at Chicago College of Medicine

UNIVERSITY OF ILLINOIS CANCER CENTER
Bench to Community

The GUIDE Project

Background

Breast cancer (BC) mortality is higher for African American women (AAW) than for any other race or ethnicity. Increasing uptake of genetic counseling among AAW with increased BC risk is a key step in reducing racial disparities in BC. We are developing a culturally-sensitive intervention that provides educational information designed to motivate AAW with genetic risk for BC to engage in genetic counseling. To identify themes that are culturally relevant and salient to the target population, multiple qualitative methods were used to identify barriers, motivating factors, and familial experiences related to BC that impact the desire and ability of AAW to access genetic counseling.

Racial Segregation & Breast Cancer Mortality in Chicago

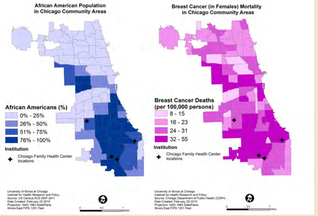

Genetic Counseling & Genetic Testing Is "Standard of Care"

- National practice guidelines and professional societies recommend **women with breast cancer** that have high risk personal or family history features undergo genetic counseling and *genetic* testing of the *BRCA1* and *BRCA2* genes
- US Preventive Services Task Force recommendation: women **without breast cancer** whose "family history is associated with an increased risk for mutations in *BRCA1* or *BRCA2* genes should be referred for genetic counseling and evaluation for genetic testing."

Women with personal history of breast cancer

- Population-based study in FL and PA of over 3,000 women diagnosed w/ breast cancer 2007-2009
- Black women 44% less likely to have genetic testing recommended
- Black women 56% less likely overall to have genetic testing performed (24% less likely when doctor recommended it)

Women with family history of breast/ovarian cancer

- Study of 408 women with strong family history breast cancer
- Black women 72% less likely to undergo genetic counseling even after controlling for mutation risk and patient attitudes toward *genetic* testing

McCarthy et al. J Clin Oncol, Aug 1, 2016; Armstrong et al. JAMA, April 13, 2005

Methods

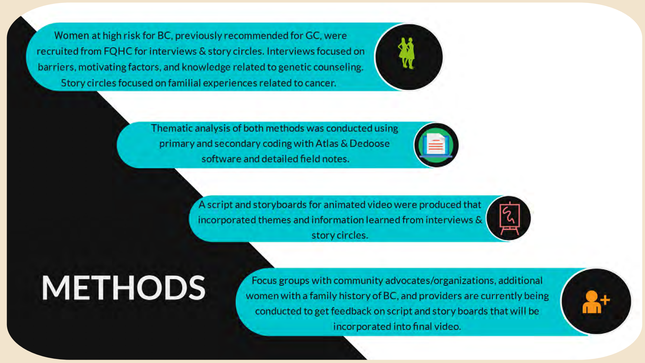

Research was supported by the National Cancer Institute (NCI) under Award Numbers P20CA202907 & P20CA202908. The content is solely the responsibility of the authors and does not necessarily represent the official views of the National Institutes of Health.

Theoretical Model

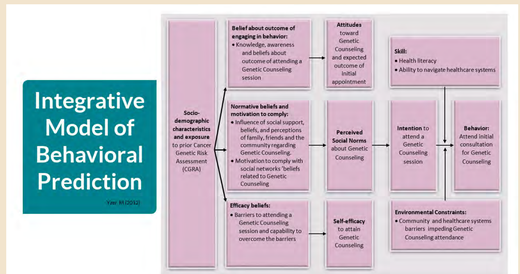

Results

Interview Participants

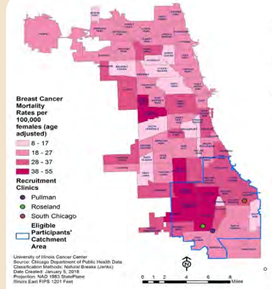

- Interview participants recruited from foundational work in which Cancer Genetic Risk Assessment (CGRA) using a Breast Risk Screening tool was performed at FQHC on South side of Chicago
- Eligibility: AAW 25 to 69 years; no personal history of BC; received recommendation for GC; consented to be contacted for future studies
- n=61 met eligibility criteria and were referred to GC by their PCP; n=20 participated in interviews
- Out of 20 women interviewed:
  - Attended GC (n=3)
  - Scheduled GC appointment, but did not attend (n=5)
  - Did not schedule a GC appointment (n=12)
- Interviews were facilitated by interview guide that assessed constructs related to GC in IMBP (attitudes, beliefs, knowledge, perceived social norms, self-efficacy, barriers)
- Conducted May to July 2017

Story Circle Participants

- 2 story circles were conducted with a subset of women interviewed (n=11)
- Story circle guide was developed that asked women to share different aspects of familial experiences related to BC and GC
- Conducted August to September 2017

THEMES

1. Trust, Relationships, Communication with Providers
Lack of trust and poor communication with providers was prevalent among women. Women often felt talked "about" and not talked "to" by their providers and they desired more comprehensive, honest, and open discussions with their providers so that they could share in decision-making regarding their health.

2. Health Education/ Health Literacy
Due to limited trust in providers, women believed that higher levels of health literacy facilitated relationships and communication with providers because it enabled them to critically assess the information given to them by providers.

3. Health Beliefs
Women acknowledged that many people automatically associate cancer with death but they felt that knowing the status of one's health was better than not knowing. Women believed in a mind-body connection in regard to health; negative thoughts result in negative health outcomes and positive thoughts motivate women to take measures to prevent negative health outcomes. There was also a general belief that medication caused more harm than good and this belief extended to cancer treatments.

4. Motivators/ Facilitators for Breast Care
Having family members with a history of cancer empowered some women to utilize preventive services and be proactive in their healthcare, while others utilized services due to fear.

THEMES

5. Family
Family and social support were extremely important to women, both in receiving and giving social and emotional support when dealing with cancer. Familial secrecy and nondisclosure of cancer diagnoses were highly prominent among women. Familial secrecy was cyclical, multi-directional and paradoxically associated with guilt or anger.

6. Religion/ Spirituality
Religion and spirituality played multiple roles in women's health beliefs. Religious/spiritual beliefs and prayer served as coping mechanisms in dealing with hardships and stress; tools to receive signs or answers in knowing how to act and making decisions; the root causes of positive health outcomes; and the root causes for negative health outcomes (e.g., punishment for prior behaviors).

7. Barriers
Barriers related to healthcare and breast health were mostly psychosocial barriers that included: "s" of seeing a provider or screening results; "s" associated with cancer diagnoses or the cancer journey; social support to others; and lack of familial or social support. Other stereotypes; guiltedness; lack of healthcare knowledge; discrimination faced within the healthcare system; healthcare system complexity; sub-par or poor healthcare; and lack of insurance or costs were also barriers that women encountered related to their health and healthcare.

8. Genetic Counseling
Many of the women equated genetic counseling with detection or a diagnosis of breast cancer. Consequently, the emotional responses associated with being diagnosed with breast cancer (e.g. fear, embarrassment, denial) were also cited as a barriers to African American women receiving genetic counseling. After learning about genetic counseling, most of the women felt that it was something that would be valuable to them, other women, and potentially their families.

Next Steps

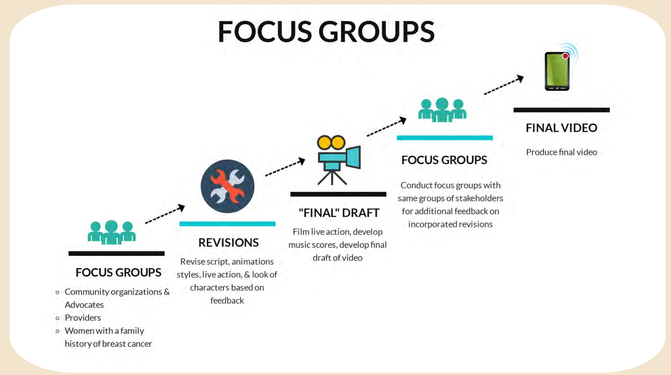

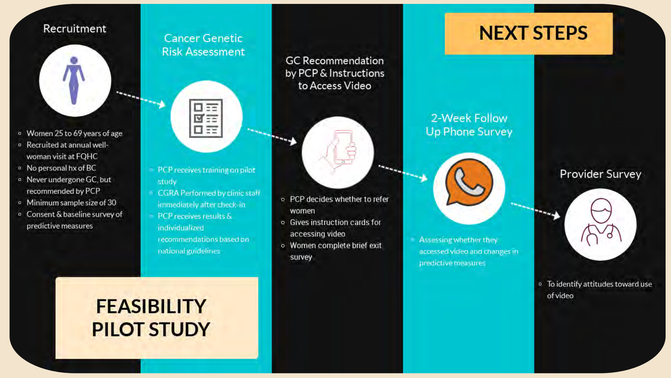

Conclusion

Use of multiple qualitative methods represents an innovative, culturally sensitive approach that provides comprehensive exploration of factors associated with uptake of genetic counseling in high risk populations. Data will inform the creation of an educational intervention by incorporating the "lived experiences" of AA families with BC.

Questioning Dietary Acculturation and Breast Cancer Risk:
The role of food in shaping and maintaining ethnic identity through the acculturation process

A. Susana Ramirez, PhD, MPH

Background

Epidemiological studies: **"Hispanic Acculturation Paradox"**: Increased acculturation is associated with increased consumption of dietary fat and decreased consumption of fruits/vegetables. These diet patterns increase obesity and diet-related breast cancer risk. The paradox is that this shift occurs despite gains in income and education that otherwise suggest a protective effect.

Unclear in the existing literature is how the dietary ac culturation process operates and how food-related cultures relate to general acculturation processes or to maintenance of origin cultures. Deeper understanding of dietary acculturation processes would improve the design of nutrition interventions for the growing population of bicultural Latinos.

Purpose

To examine ethnic identity among bicultural young adult Latinas and how it relates to diet and nutrition knowledge, in order to inform the design of a nutrition communication intervention.

Methods

- Mixed methods: Semi-structured depth interviews + survey
- Mexican-American women ages 18-29 (n=29) in rural California Bi
- cultural; self-identification; English speaking (acculturation proxy)
- Descriptive statistics; thematic analysis of transcripts

Participant Characteristics	
Age (range: 18-29)	M=22.5
Education	
H.S./G.E.D. or less	40.7%
Some coll/technical	37.0%
College+	22.2%
Received food assistance past yr	22.2%

Ethnic Identification (check all)	
Hispanic	67.9%
Latina	42.9%
Mexican-American	67.9%
Mexican	46.4%
Chicana	28.9%

Results

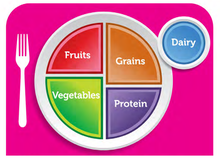

Perceptions of Diet and Health

- ✧ General nutrition principles widely known; e.g.,: portion size; food groups; specific nutrients such as sugar, fat
- ✧ Confusion and misperceptions about diet and disease
- ✧ Desire for more detailed information and specific tips

"Well, I can't speak Spanish, so…the food is…the only thing I can really bond with other Mexicans over…."

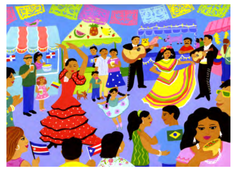

Diet Central to Cultural Identity

- ✧ Time spent with family centered on eating
- ✧ Familial pressure to eat large portions
- ✧ Mexican foods represent comfort

"We like fiestas."

Mexican Foods are Unhealthy

- ✧ Types of foods: Celebration foods, high-fat
- ✧ Large portion sizes
- ✧ But…moms make healthy Mexican foods at home

"Sopes, enchiladas, carne asada, carnitas, your typical trad itional Mexican meals…Big meals like that…. When you know that you're going to go to your family's house,…you don't have an option of eating healthy."

Healthy Foods are "American"

- ✧ Types of foods: Salads
- ✧ Preparation techniques: Grilled chicken
- ✧ Many respondents eat a more American style on their own, lacking skills to cook Mexican foods at home

Discussion

A new paradox?

Participants universally identified eating Mexican foods as an important strategy for expressing and maintaining their Mexican culture, yet these foods were almost equally universally presumed to be unhealthy.

Mexican foods were perceived as less healthy than foods identified as more "American" that also were a regular part of participants' diets.

More research needed:

To examine nutrition patterns prior to migration and subsequ ent dietary acculturation processes. *How does the "traditional" diet change through migration and acculturation?*

Increased consideration of US-born Latinos (2nd, 3rd generation) and complexity of acculturation in nutrition and communication science.

Interrogation of food production systems in origin countries: *Are the same foods really the same foods?*

Implications

Communication of nutrition information t o bicultural Latinas depends on better und erstanding of factors that affect diet behaviors and message persuasiveness

How to harness power of culture, identity, and belonging for improved nutrition communication?

Diet-breast cancer link for Latinas?

UCMERCED

www.communicationculturehealth.org

This project was supported by the National Cancer Institute under Award Number K01CA190659.
Content is solely the responsibility of the author and does not necessarily represent the official views of the National Institutes of Health.

Adapting Evidence-Based Intervention Strategies to Reduce Cervical Cancer Disparities Among Women Living with HIV

Principal Investigator: Lisa T. Wigfall, PhD, MCHES®[1]

Mentors: Heather M. Brandt, PhD, CHES®[2]; Daniela B. Friedman, PhD[2]; James R. Hébert, ScD[2]; and Marcia G. Ory, PhD[1] (primary)

Affiliations: [1]Texas A&M University, [2]University of South Carolina

Abstract

Background: Although cervical cancer is one of only a few cancers that are preventable, HIV-positive women (**Figure 1**) are three times more likely to develop cervical cancer than HIV-negative women.[2] The HPV vaccine and Pap/HPV tests are effective cervical cancer prevention tools that are recommended for HIV-positive women.[3]

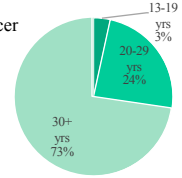

Figure 1. US HIV-positive females[1] (newly diagnosed HIV infections in 2016)

Purpose/Objective: To describe how HPV vaccination and cervical cancer screening evidence-based intervention (EBI) strategies will be adapted for HIV-positive women (new target population). Our objective is to develop (**Aim 2**) and pilot test/evaluate (**Aim 3**) a multicomponent cervical cancer prevention and patient navigation program for HIV-positive women. The program will be delivered by staff at community-based HIV/AIDS service organizations (ASOs) (new setting) located in the South US Census region (**Figure 2**), a geographical area disproportionately affected by HIV/AIDS.

Figure 2. South US Census Region

Methods: In May-June 2016 & July-August 2018, we conducted/will conduct a needs assessment survey with ASO staff to inform adaptation (**Aim 1**). Follow-up interviews and focus group discussions will be conducted in July-December 2018 to inform intervention development (**Aim 2**). Study sites were/will be located in the following geographical areas located in the South US Census region where the 2016 HIV incidence rates (per 100,000 population) were higher than the US rate (12.3): Columbia, SC (**21.7**); Jackson, MS (**25.0**); Houston-The Woodlands-Sugar Land, TX (21.8); and New Orleans-Metairie, LA (**33.3**).

Results: Most SC ASO staff (n=28) who worked with HIV-positive women were willing to: (1) assess screening adherence (100%); (2) ask about (96%) and explain (93%) most recent Pap test result; (3) promote patient-provider communication about cervical cancer screening tests (100%); and (4) provide navigation to free or low-cost cervical cancer care (96%).[4] SC ASO staff's willingness to promote HPV vaccination was similarly positive.[4] See **Table 1**.

Conclusions: Some ASO staff are willing to engage in cervical cancer prevention efforts. A pilot test will be conducted during the next cervical cancer awareness month (January 2019) to evaluate acceptability and feasibility (**Aim 3**). Barriers and facilitators to program implementation will also be identified.

Prevention & Early Detection

Initiation and Completion of the 3-Dose Nonavalent HPV Vaccine Series (18-26 Years old)[3]

Adherence to Cervical Cancer Screening Guidelines For Women Living with HIV[3]

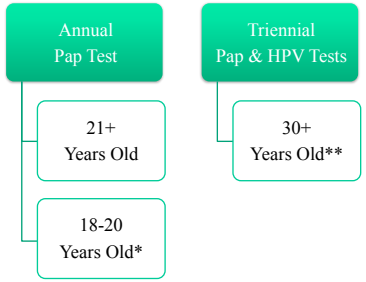

Notes: *Within one year of sexual debut; **HPV testing is not recommended for women living with HIV who are less than 30 years old.

Healthy People 2020 Objectives

HPV Vaccination: Increase the vaccination coverage level of 3 doses of human papillomavirus (HPV) vaccine for females by age 13 to 15 years.[5] [Immunization and Infectious Diseases Objective #11.4]

Cervical Cancer Screening: Increase the proportion of women who receive a cervical cancer screening based on the most recent guidelines.[5] [Cancer Objective #15]

Pilot Randomized Control Trial (RCT)

Outcomes: HPV Vaccine Initiation (secondary) & Cervical Cancer Screening Intentions (primary)

Include:
- HIV-positive
- Female sex at birth
- 18+ years old
- Unvaccinated
- Unscreened/Underscreened

Exclude:
- Diagnosed with cervical cancer
- Cervix removed for a benign reason
- Had a Pap test within past year (or within past three years if Pap and HPV tests were done)
- Completed one or more doses of the HPV vaccine

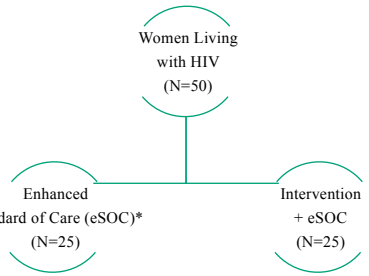

Figure 3. Study Design

Note: *We are currently evaluating the appropriateness of using the Center for Disease Control and Prevention's *Inside Knowledge* campaign materials with HIV-positive women.[4,6]

Preliminary Data

Table 1. ASO staff's willingness to engage in cervical cancer prevention efforts, N=30

Characteristics	(%)
HPV Vaccination	
Promote HPV vaccine uptake	91
Positively influence clients' HPV vaccine decision	68
Promote patient-provider communication about the HPV vaccine	100
Navigate to adult safety net HPV vaccine providers	95
Cervical Cancer Screening	
Assess clients' Pap test screening adherence	100
Ask clients about their most recent Pap test result	96
Help clients understand their most recent Pap test result	93
Promote patient-provider communication about Pap and HPV tests	100
Navigate to free or low-cost cervical cancer care	96

Table 2. Patient and provider-level evidence-based cervical cancer prevention programs

NCI RTIPs	HPV Vaccination	Cervical Cancer Screening
1-2-3 Pap	✓	
A Su Salud en Acción		✓
Cambodian Women's Health Project		✓
DOSE HPV	✓	
Faith Moves Mountains		✓
Give Teens Vaccines	✓	
HPV Vaccine Decision Narratives	✓	
Increasing Breast and Cervical Cancer Screening Among Filipino American Women		✓
Kukui Ahi (Light the Way)		✓
Making Effective HPV Vaccine Recommendations*	✓	
Prevention Care Management		✓
Promoting HPV vaccination Among American Indian Girls	✓	
Tailored Communication for Cervical Cancer Risk		✓
Targeting Cancer in Blacks		✓
The Chinese Women's Health Project		✓
The Forsyth County Cancer Screening Project		✓
The Gateway to Health		✓
Vietnamese Women's Health Project		✓
Woman to Woman		✓

Notes: NCI (National Cancer Institute); RTIPs (research-tested intervention programs); *clinicians

Next Steps

- Work with key stakeholders to systematically select and adapt evidence-based intervention strategies to reduce cervical cancer disparities among women living with HIV.[7]
- Develop an implementation toolkit for ASO staff.

References

1. CDC. *HIV Surveillance Report, 2016* [Table 7a].
2. Hernández-Ramirez RU, Shiels MS, Dubrow R, Engels EA. Cancer risk in HIV-infected people in the USA from 1996 to 2012: a population-based, registry-linkage study. *Lancet HIV.* 2017.
3. US DHHS. *Guidelines for the Prevention and Treatment of Opportunistic Infections in HIV-Infected Adults and Adolescents.*
4. **Wigfall LT**, Bynum SA, Sebastian N, Brandt HM, Ory MG. HPV-associated cancer prevention programs at community-based HIV/AIDS service organizations: Implications for future engagement. Unpublished data. Under review in *Front Oncol.*
5. US DHHS. *Healthy People 2020.*
6. CDC. *Inside Knowledge: Get the Facts About Gynecologic Cancer* campaign.
7. Highfield L, Hartman MA, Mullen PD, Rodriquez SA, Fernandez ME, Bartholomew LJ. Intervention mapping to adapt evidence-based interventions for use in practice: increasing mammography among African American women. *Biomed Res Int.* 2015.

Funding Acknowledgement: Research reported in this poster presentation was 100% supported by the National Cancer Institute of the National Institutes of Health under award number K01CA175239. [Total project cost: $711,544]

Prostate Specific Membrane Antigen promotes prostate tumor progression and survival by conferring resistance to hypoxic stress.

Anisha Lewis BS[1] , Danica Anukam BS[1], Aiyana Ponce BS[2] , Abdulsalam S[3] Linda Shapiro, PhD[1], and **Leslie Caromile, PhD[1]**

1. Center for Vascular Biology, University of Connecticut Health Center, Farmington, CT 06030
2. Dept. of Biological Sciences, The University of Texas at El Paso, El Paso, TX 79968
[3] Dept. of Health and Natural Sciences, University of St. Joseph, West Hartford, CT 06117

Introduction

Cancer cells commonly adapt to the nutrient poor, hypoxic environment created by rapidly growing primary tumors by modifying their metabolism to allow survival. These metabolic alterations are fundamental to their growth *in situ* as well as their progression to metastasis that underlies the majority of disease-related mortality. The transmembrane peptidase Prostate Specific Membrane Antigen (PSMA) is progressively upregulated in ~80% of tumors during prostate cancer (PC) progression where it correlates negatively with prognosis. We have previously reported that expression of PSMA promotes increased tumor cell survival in hypoxic environments. To investigate these PSMA-dependent survival mechanisms we engineered a panel of PSMA-null ($PSMA^{KO}$) human PC cell lines (LnCaP, 22rv1) using CRISPR/Cas9. Loss of PSMA resulted in significantly lower proliferation rates, reduced anchorage-independent colony growth in soft agar and a shift in the balance of the calcineurin-A/NFAT and HIF-1a calcium-associated signal-transduction pathways toward a more hypoxia-sensitive phenotype when compared to wild type controls, supporting PSMA's role as a cell survival gene in primary PC. Furthermore, $PSMA^{KO}$ cells showed decreased cell migrationand invasionwithcorrespondinglysuppressedrateof lung metastasis inNOD/SCID mice. AssayofPSMA^{KO} cells under hypoxic conditions indicated a metabolic switch from the glucose-dependent aerobic glycolysis typical of cancer cells to anaerobic oxidative phosphorylation characteristic of controlled proliferation and decreased resistance seen in less aggressive tumors. *In silico* meta-analysis of publicly available human gene data sets indicated that expression changes in PSMA and calcium-associated genes correlate significantly with PC metastasis to bone and lymph. These results suggest that PSMA expression on tumor cells confers resistance to hypoxia, contributes to tumor progression and increased metastatic potential via adaptive changes in the calcium signal-transduction cascade to promote cell survival, thus supporting completedisruptionofPSMAasapromisingtherapeuticoption in management andtreatment ofPC.

Methods

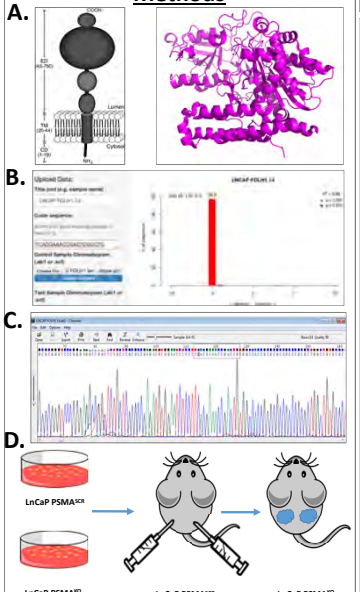

Figure 1: : **A**. Schematic representation of PSMA and the 3-D structure of PSMA (PyMOL, https://www.pymol.org/) was used to generate image of PSMA (PDB ID: 2OOT). **B.** Tracking of Indels by Decomposition; https://tide-calculator.nki.nl/ analysis of LnCaP PSMA^{KO}. **C** Representative sequence of 5bp deletion. **D.** Experimental method for the Xenograft model. SCR= Scramble, KO=Knockout.

Results

Deletion of PSMA in LnCaP and 22Rv1 decreases their metastatic potential in culture.

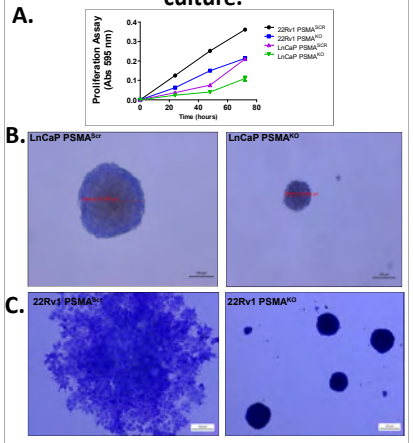

Figure 2. A. Comparison of proliferation rate of LnCaP and 22Rv1 PSMA over 72 hours by MTT assay. **B.** Growth of LnCaP PSMA Scr and KO were monitored over time in soft agar 3D culture. 20x magnification. C. Growth of 22Rv1 PSMA Scr and KO were monitored over time in soft agar 3D culture. 20x magnification. Quantification of stained colonies for both colony size and colony area was done by Image J (not shown). Scale bar is 100-200μM.

LnCaP and 22Rv1 PSMA^{KO} cells showed decreased cell migration and invasion

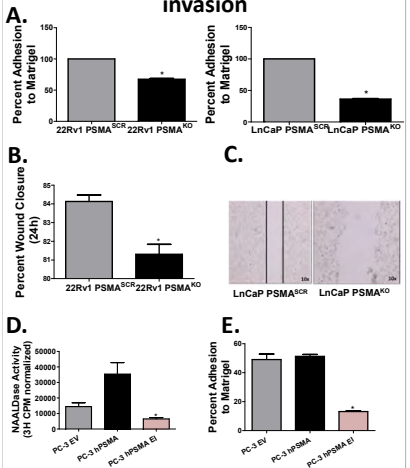

Figure 3. **A.** Percent adhesion of LnCaP and 22Rv1 PSMAScr and KO to Matrigel in 6h as measured by calcein am fluorescence (495nm). Measurements were normalized to Scr control. **B.** Percent wound closure in 22Rv1 PSMA SCR and KO measured over 24h. **C.** Wound assay for LnCaP PSMAScr and KO. **D.** NAALDase activity assay for PSMA activity (EV – empty vector, EI – enzymatically inactive). **E.** Percent adhesion of enzymatically inactive PSMA to Matrigel in 6h as measured by calcein am fluorescence (495nm). * p < 0.005.

Results

Deletion of PSMA in LnCaP inhibits tumorigenesis in *vivo*.

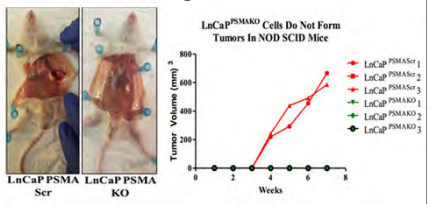

Figure 4: NOD/SCID mouse xenograft model was used to evaluate PSMAs role in tumor growth. NOD/SCID mice injected with LnCaP PSMA scramble (right) and LnCaP PSMA KO cells (left). Xenograft tumor volume progression was monitored for 7 weeks.

$[Ca^{2+}]_i$ is lower in PSMA^{KO} cells under hypoxic conditions

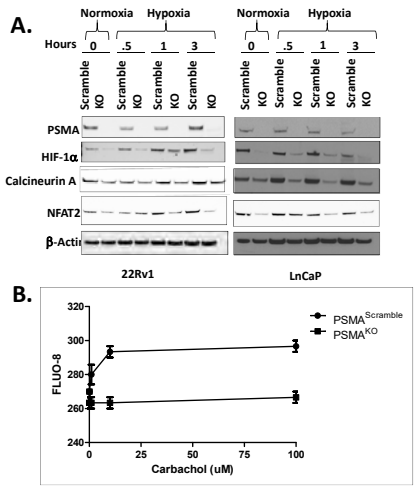

Figure 5 A. Western blot for PSMA, HIF1A, Calcineurin A, NFAT, and β-actin. **B**. Fluo-8 no wash Calcium assay to assess intracellular calcium mobilization. (n=3/sample) *p< 0.005.

Cytoskeleton of PSMA^{KO} cells are less organized under hypoxic conditions

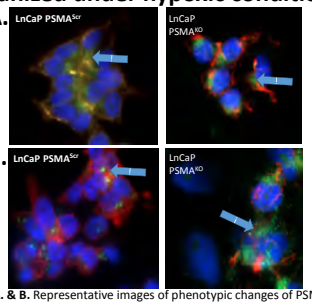

Figure 6 A. & B. Representative images of phenotypic changes of PSMA^{Scr} and PSMA ^{KO} cells treated with 100μM $CoCl_2$ at 24 hr. Dapi, Phalloidin, G-Actin. 63x.

Results

Deletion of PSMA in LnCaP alters metabolic profile under hypoxic conditions

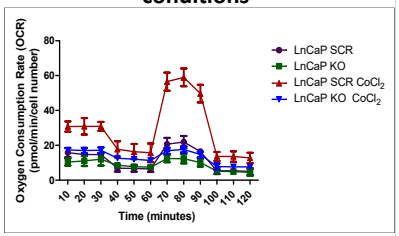

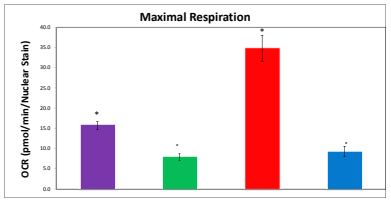

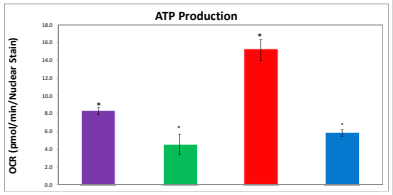

Figure 7. The Seahorse XF Cell Mito Stress Test kit was used to assess mitochondrial function of LnCaP PSMA SCR and KO cells under mimicked hypoxia. Oxygen consumption, maximal respiration and ATP production were measured. * p < 0.005 when compared to control SCR.

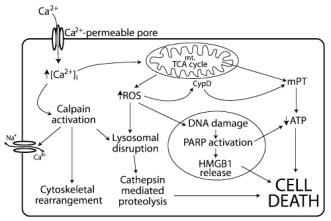

Conclusions/Future Directions

It has been shown that PSMA expression is higher in metastatic lesions of prostate cancer and colon cancer. Dramatic changes in calcium levels are a primary response of many cells to hypoxia and typically stimulate cell death. These results suggest that PSMA expression on tumor cells confers resistance to hypoxia, contributes to tumor progression and increased metastatic potential via adaptive changes in the calcium signal-transduction cascade to promote cell survival, thus supporting complete disruption of PSMA as a promising therapeutic option in management and treatment of PC.

Funding

NIH NCI Mentored Research Scientist Development Award to Promote Diversity (K01CA188412)

Engineering Precision Medicine to Increase Graft-Versus-Lymphoma Activity: Hematopoietic Stem Cells Modified with Chimeric Antigen Receptors

Truscott LC[1,2], Kao RL1,2, Chiou T[1,2], Kohn DB[1,2]and De Oliveira SN[1,2]
[1] Department of Pediatrics, David Geffen School of Medicine at UCLA, Los Angeles, CA, USA
[2] Division of Pediatric Hematology/Oncology, Mattel Children's Hospital-UCLA Medical Center, Los Angeles, CA, USA

Background

- Gene-modified human hematopoietic stem cells (HSC) have been used to introduce genes into organisms
- Here, gene-modified HSC with chimeric antigen receptors (CAR) were used to create multi-lineage immune effectors that directly target cancer cells
- Gene-modified HSC also had suicide gene systems, such as HSV-sr-39TK, or a truncated EGFR (EGFRt) which binds to Cetuximab
- EQ CAR construct obtained through collaboration with Forman lab at City of Hope, that engineers antigen specificity against CD19 and co-delivers EGFRt

Objectives

- Evaluation of anti-lymphoma activity of CAR-modified HSC in vitro and in vivo
- Evaluation of activation of co-delivered suicide gene systems to ablate gene-modified cells

Methods

- *In vitro*

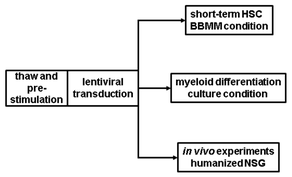

- *In vivo*

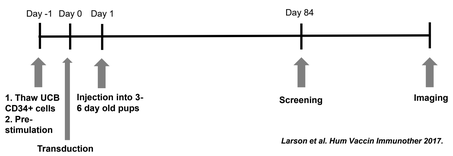

Larson et al. Hum Vaccin Immunother 2017.

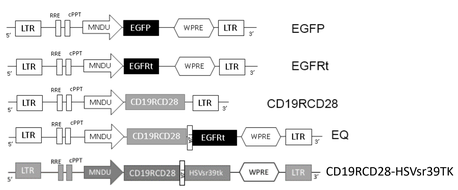

Results

- Gene modification of human HSC did not affect engraftment, proliferation, or differentiation

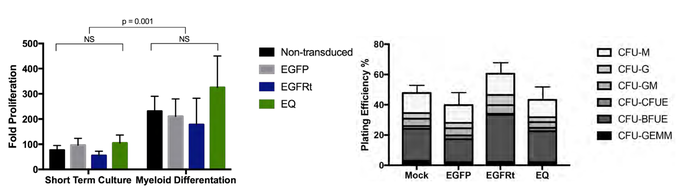

Results, continued

- Specific ablation of gene-modified cells in target cells expressing EGFRt when incubated with Cetuximab

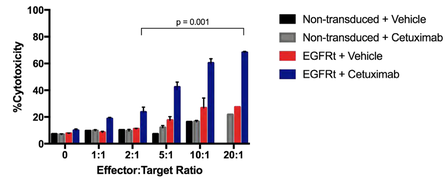

- Humanized NSG had similar engraftment of human cells independently of transgene

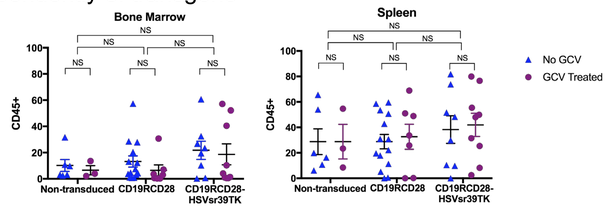

Hum Vaccin Immunother 2017;13(5):1094-1104

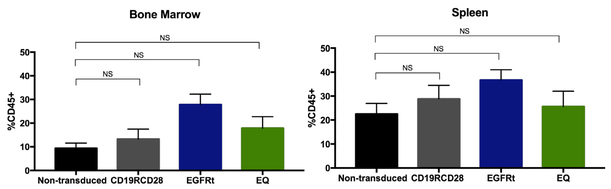

- Mice engrafted with CAR-modified HSC were protected against CD19+ tumors

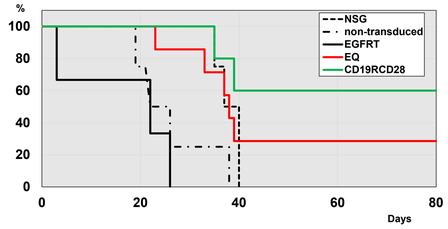

- After treatment with Ganciclovir, gene-modified cells were decreased in bone marrow and spleen

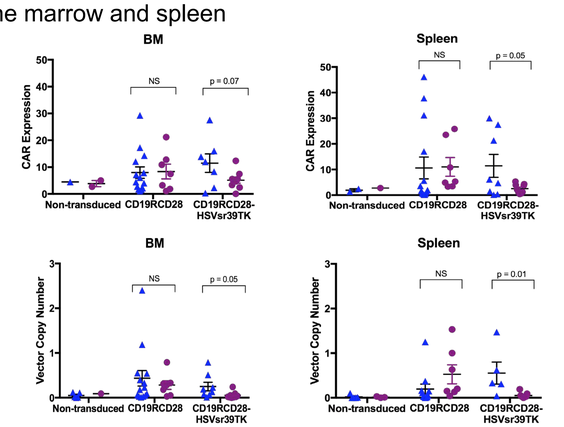

Hum Vaccin Immunother 2017;13(5):1094-1104

Results, continued

- Presence of suicide gene led to significant ablation of gene-modified cells after mice treated with Cetuximab

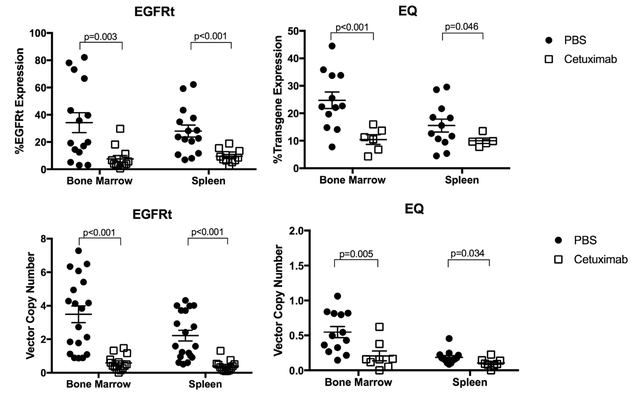

- PET imaging using ^{89}Zr-Cetuximab shows engraftment of gene-modified HSC and their ablation after Cetuximab treatment

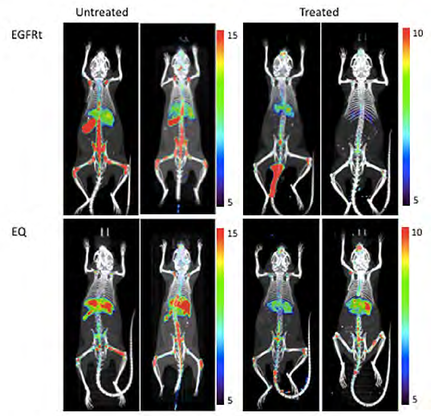

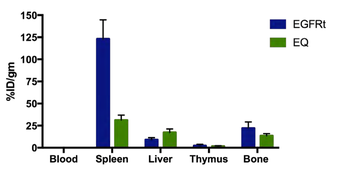

Conclusions

- Modification of HSC with second generation anti-CD19 CAR has provided specific and persistent anti-lymphoma protection
- Addition of the suicide gene systems HSV-sr39TK or EGFRt to the construct did not affect transduction efficiency
- Addition of HSV-sr39TK to the construct did allow significant ablation of gene-modified cells in mouse tissues after treatment with ganciclovir
- Addition of EGFRt to the construct did allow significant ablation of gene-modified cells in mouse tissues after treatment with cetuximab

Funding support: 1K23 CA222659-01, K-12 UCLA Child Health Research Center Development Award (CHRCDA), NIH/NHLBI 2 T32 HL086345-06, Hyundai Hope on Wheels Scholar Hope Grant Award, ASH Scholar Award, St. Baldrick's Foundation.

Corresponding author:
Satiro De Oliveira, MD, sdeoliveira@mednet.ucla.edu,
10833Le Conte Avenue, A2-410 MDCC, MC 175217,
10834Los Angeles, CA 90095-1752, USA

Exposure to a Complex Endocrine Disrupting Chemical Mixture Activates AhR, Proliferation, and Survival Pathways in Breast Cancer Cells

Larisa Gearhart-Serna[1,2], Moises Tacam Jr [1,3], Ulises Jair Nino-Espino[3], Rich Di Giulio[2], and Gayathri Devi[1,2]

[1]Department of Surgery, Duke University School of Medicine, [2]University Program in Environmental Health, Duke University Nicholas School of the Environment, [3]Duke University Trinity School of Arts and Sciences

Background

Polycyclic aromatic hydrocarbons (PAHs)
- Products of inorganic fuel combustion
- Present in tobacco smoke, car exhaust, industrial emissions, grilled and smoked meats, forest fires, volcanic eruptions
- Humans are ubiquitously exposed

PAHs and breast cancer
- In two studies from 2017, PAH levels in the ambient air were linked to higher incidence of breast cancer in the eastern U.S., and PAH levels in human serum were linked to higher risk of breast cancer

The role of EDCs, like PAHs, in breast cancer progression is an understudied yet potentially crucial area of concern

Methods

- Exposure analysis using NHANES PAH metabolite data to determine dose of physiological relevance
- Growth of SUM149 cells as tumor organoids and treatment with Superfund site-derived complex PAH mixture
- Western immunoblot analysis of SUM149 cells for mitogenic (ERK/pERK), and survival (XIAP, SOD1) proteins after PAH treatment

Hypothesis: SUM149 cell derived tumor organoids will exhibit increased growth, as well as mitogenic and survival signaling, upon PAH mixture exposure at physiologically relevant doses

Human PAH Exposure Analysis → PAH Treatment in a 3D Tumor Organoid Model → Protein Analysis of Tumor Cells Treated with PAHs

Relevance of PAHs to Human Exposure

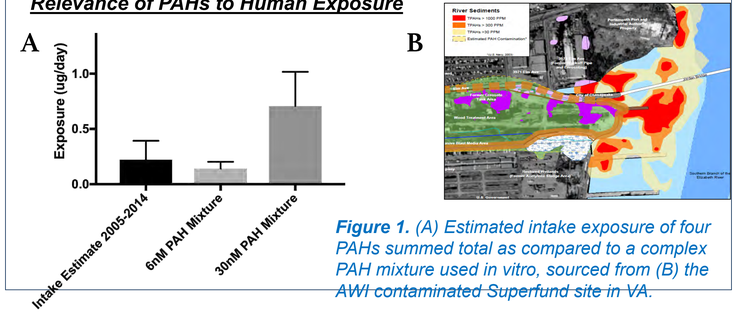

Figure 1. *(A) Estimated intake exposure of four PAHs summed total as compared to a complex PAH mixture used in vitro, sourced from (B) the AWI contaminated Superfund site in VA.*

Results and Figures

Low dose PAH mixture exposure correlates with increased proliferation

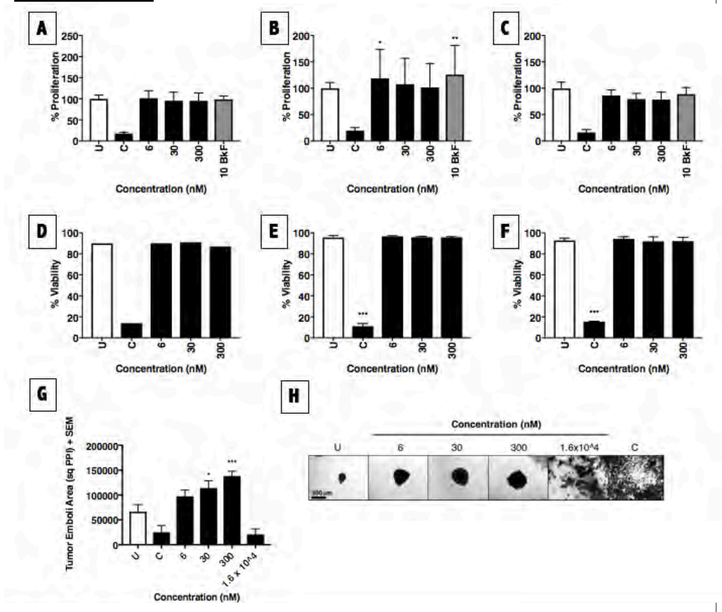

Figure 2. *Proliferation by MTT assay in (A) HME1, (B) MCF-7, and (C) SUM149 cells, and viability counts for (D) HME1, (E) MCF-7, and (F) SUM149 cells following low dose PAH mixture or low dose BkF single chemical exposure for 24 hours. (G) SUM149 inflammatory breast cancer cell line tumor emboli area treated with PAH mixture for 72 hours, and (H) representative images from tumor emboli following treatment for 72 hours. Scale bar = 500um. U = untreated, C = chlorothalonil, cytotoxic chemical control, BkF = benzo[k]fluoranthene. *p<0.05, **p<0.01, ***p<0.001.*

Low dose PAH mixture exposure correlates with increased survival signaling

Figure 3. *(A) Cropped immunoblot of the aryl hydrocarbon receptor (AhR) and EROD assay for CYP1A1 activity for (A-B) MCF-7 and (C-D) SUM149 cells following 24h PAH mixture exposure or exposure to BaP single chemical doses. U = untreated, BaP = benzo[a]pyrene. *p<0.05, ***p<0.001.*

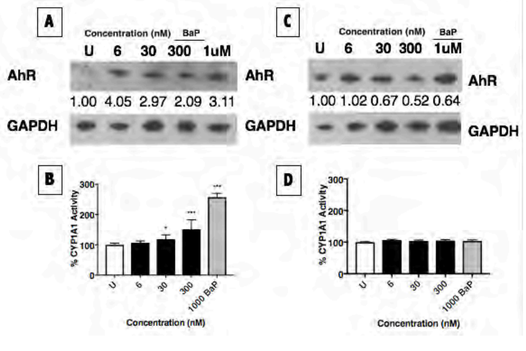

Low dose PAH mixture exposure upregulates components of the AhR toxicant response pathway

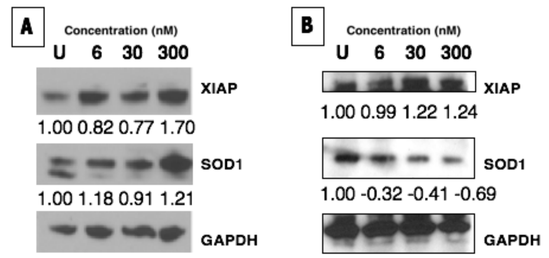

Figure 4. *X-linked inhibitor of apoptosis protein (XIAP) and superoxide dismutase (SOD1) cropped immunoblots, an anti-apoptotic protein and an antioxidant protein, respectively, in (A) MCF-7 cells and (B) SUM149 cells, following 24h exposure to low dose PAH mixture.*

Conclusions and Future Directions

- Low nanomolar, physiologically relevant doses of PAH mixture increase:
  1. 2D breast cancer cell proliferation
  2. Tumor organoid growth
  3. Toxicant Signaling (AhR, CYP1A1)
  4. Survival Signaling (XIAP/SOD1)

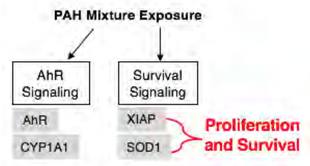

FUTURE DIRECTIONS
- Chronic exposure cell lines reflecting normal and
- vulnerable populations to PAH exposure
- In vitro and in vivo models of metastasis
- PAH analysis in patient tumor tissues using mass spectrometry

References and Acknowledgements

- Allensworth, J.L. et al. (2015). Disulfiram (DSF) acts as a copper ionophore to induce copper-dependent oxidative stress and mediate anti-tumor efficacy in inflammatory breast cancer. Mol. Oncol. 9(6) 1155-1168
- Large, C., & Wei, Y. (2017). Geographic variations in female breast cancer incidence in relation to ambient air emissions of polycyclic aromatic hydrocarbons. Environmental Science and Pollution Research, 1-7.
- Shen, J., Liao, Y., Hopper, J. L., Goldberg, M., Santella, R. M., & Terry, M. B. (2017). Dependence of cancer risk from environmental exposures on underlying genetic susceptibility: an illustration with polycyclic aromatic hydrocarbons and breast cancer. British Journal of Cancer.
- U.S. Environmental Protection Agency (USEPA). 2007. Record of Decision Operable Units 1, 2 & 3. Atlantic Wood Industries, Inc. Superfund Site, Portsmouth, Virginia.

This work was supported in part by development funds from DCI Cancer & Environment Program P3917733 (GRD), Bolognesi Award (GRD), and NIEHS T32-ES021432 (LMGS).

Duke NICHOLAS SCHOOL OF THE ENVIRONMENT

Duke Surgery
Duke University School of Medicine

RIOK2 IS A MEDIATOR OF OBESITY ENHANCED PROSTATE CANCER GROWTH

Everardo Macias[1], David Corcoran[2], Jen-Tsan Chi[3], Stephen Freedland[4,5].

Author Affiliations- [1]Department of Pathology, [2]Duke Center of Genomic and Computational Biology
[3]Department of Molecular Genetics and Microbiology, Duke University Durham, NC
[4]Division of Urology, Department of Surgery, Cedars Sinai, Los Angeles, CA; [5]Section of Surgery, Durham Veterans Administration Hospital, Durham, NC

Abstract

INTRODUCTION AND OBJECTIVES: Obesity is a growing global and U.S. health problem. For 2012, an estimated 117,000 cancer cases in the U.S. were deemed preventable by achieving and maintaining a healthy weight, including 11% of all advanced prostate cancers (PC). Obesity is associated with greater risk of high-grade PC, recurrence after therapy, metastases, and PC specific death. We exploited this link to identify actionable targets by performing a shRNA genomic screen in obese and lean mice targeting the entire kinome. Our functional screen identified multiple kinases, which appear to be essential for obesity-driven PC growth including kinases previously implicated in PC and others not previously studied such as Right Open Reading Frame Kinase 2 (RIOK2).

METHODS: LAPC-4 cells were inoculated with an shRNA library of ~5000 lentivirus targeting 513 kinases. 5x106 cells (~1,000 cells per shRNA) were grafted to chronically obese mice. Tumors were established to ~200 mm3 and a portion collected for reference. Remaining mice were randomized to continue on ad lib WD or 25% CR diet. Genome-integrated shRNA inserts were amplified using nested barcoded primers and sequenced using Illumina Hi-Seq 2000 and quantified. A virtual screen based on a RIOK2 homology model generated using MODELLER based on two RIOK2 crystal structures. Global gene expression analysis of RNA from scramble control and RIOK2 knockdown with two shRNAs in 22RV1 cells was conducted with Affymetrix U133A Plus Array.

RESULTS: RIOK2 expression correlates with Gleason grade in radical prostatectomy tissue and RIOK2 kinase activity is elevated in metastatic vs localized PCs. ENCODE ChIP-seq data shows Androgen Receptor and Myc bind to the RIOK2 promoter and regulate expression. Targeting RIOK2, via newly identified small molecule inhibitors reduces cell viability and soft agar colony growth. Gene set enrichment analysis of RIOK2 depleted PC cells showed reduction of cell cycle, adipogenesis, EMT and cancer stem cell genes. RIOK2 also regulates Neuropeptide Y2 Receptor (NYP2R), which is part of the NPY obesogenic signaling axis that correlates with obesity and worse PC outcomes.

CONCLUSIONS: Our in vivo screen highlighted RIOK2 as an actionable PC target in obese hosts. Targeting RIOK2, pharmacologically with our lead compounds or genetically, drastically reduces PC cell viability. RIOK2 may regulate NPY2R expression, which when coupled with elevated NPY in both obese hosts and PCs can amplify NPY pro-tumorigenic signaling.

Objective

We hypothesize that obesity promotes PC growth via aberrant activity of a small subset of kinases. If we can identify and target obesity associated kinases, we can reduce the excess risk of obesity in PC. **Thus, our objective is to identify and therapeutically target kinases that are required for progression of PC in obese men.** To accomplish this, we have employed state-of-the-art functional genomic kinome screen in obese mice, modeling not only tumor biology, but also the host environment which is reflective of most men with PC.

Methods

LAPC-4 PC cells were transduced by a shRNA kinome library pool of ~5000 shRNAs at an MOI of ~0.3, ensuring a single integration per cell and puromycin-selected. 5x106 cells, ~1,000 cells per shRNA, were injected subcutaneously into obese male CB.17 scid/scid mice. DNA from injected cells collected as reference (Cell time zero: C0) (Fig 1). After tumors reached 200 mm^3 8 mice were sacrificed for reference (Tumor time zero – T0). Of the remaining mice, half were kept on an ad libitum Western diet and the other half were fed a 25% calorically restricted pair-fed diet (25% CR). 25 days after randomization, all mice in both WD and 25% CR were sacrificed. As expected tumor volumes and weights at sacrifice tended to be larger in WD obese mice compared to lean 25% CR mice (Fig 1). Genome-integrated shRNA inserts from each group (C0, T0, WD and CR) were amplified using nested PCR primers with barcoded (6 bp) sequences. Amplified shRNAs were sequenced using Illumina Hi-Seq 2000. We combined 25 bar-coded samples in one sequencing lane, to obtain ~4-5 million reads/sample to cover the ~5000 shRNA in each pool to have enough coverage for most shRNAs. These analyses of shRNA sequencing and abundance were performed with Dr. Corcoran in the 'Omics Analytic Core at Duke University.

Results

In vivo Kinome Screen Identifies RIOK2 as an essential Kinase for Tumor Cell Growth in Obese Mice

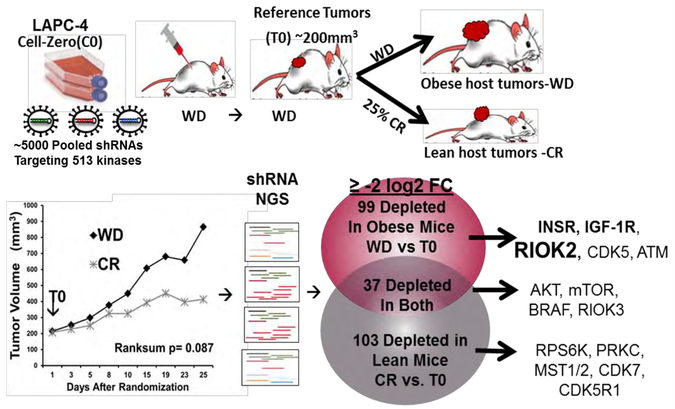

Figure 1. Experimental design of shRNA kinome screen to identify essential (depleted) kinases for PC growth in obese and calorie restricted mice .

RIOK2 Correlates with Prostate Cancer Grade and Lethal Outcome

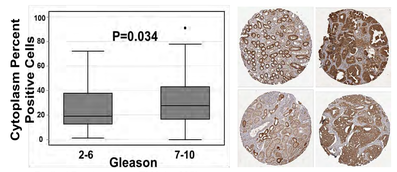

Logistic regression analysis for lethal outcome.

All men (N=419)		
Gene*	Odds ratio (95% CI)	P-value
RIOK2	1.90 (0.99, 3.65)	0.055
Stratified by BMI (kg/m^2)		
BMI <25 (N=199)	1.04 (0.38, 2.80)	0.932
BMI ≥27.5 (N=88)	2.15 (0.63, 7.74)	0.222
BMI ≥30 (N=30)	8.10 (0.23, 518.95)	0.268

*Modeled as continuous variable
Unpublished data courtesy Lorelei Mucci, Harvard

Figure 2. RIOK2 protein expression in A) Radical Prostatectomy TMA and B) logistic regression analysis of gene expression and lethal PC outcome.

RIOK2 is essential for Cell Growth and *de novo* Protein Synthesis

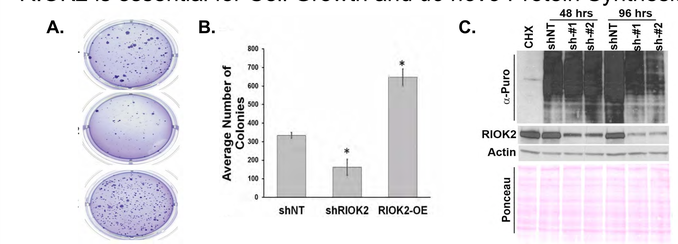

Figure 4. Phenotypic and protein synthesis effects of RIOK2 loss. A) Softagar colonies and B) quantification of RIOK2 knockdown and RIOK2 overexpressing LAPC-4 cells. D) VCaP cells treated with non-targeting or RIOK2 shRNAs for indicated times were treated with puromycin for 15 min, harvested and immunoblotted as indicated.

Gene Expression Analysis of RIOK2 Depleted Cells Identifies Link with NPY Obesogenic Signaling Axis

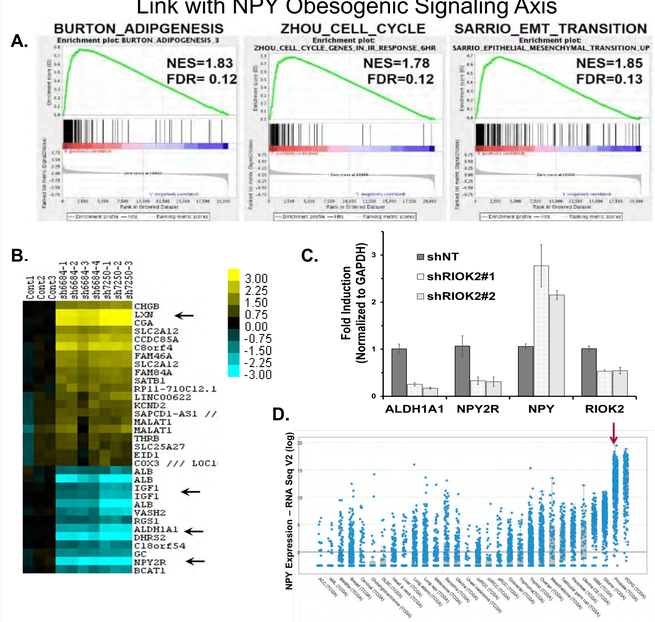

Figure 5. Gene expression analysis of RIOK2 depleted 22RV1 cells. A) Gene set enrichment of analysis of control cells vs. RIOK2 depleted cells. B) Heat map of top upregulated (yellow) and downregulated (blue) genes. C) qRT-PCR validation of denoted genes. Two RIOK2 targeting shRNAs (n=4/shRNA) in gene expression and validation experiments. D) NPY expression in various tumor types.

RIOK2 Lead Compounds Inhibit Prostate Cancer Cell growth, Anchorage Independence and Invasion

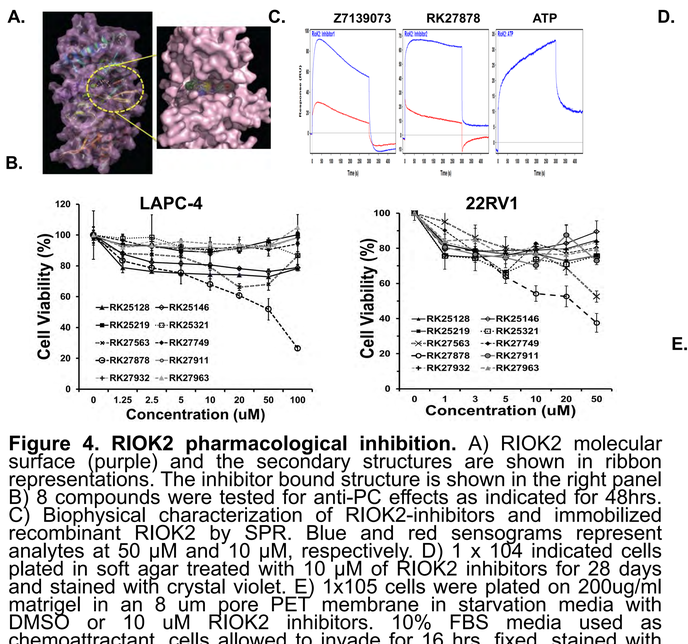

Figure 4. RIOK2 pharmacological inhibition. A) RIOK2 molecular surface (purple) and the secondary structures are shown in ribbon representations. The inhibitor bound structure is shown in the right panel B) 8 compounds were tested for anti-PC effects as indicated for 48hrs. C) Biophysical characterization of RIOK2-inhibitors and immobilized recombinant RIOK2 by SPR. Blue and red sensograms represent analytes at 50 μM and 10 μM, respectively. D) 1 x 104 indicated cells plated in soft agar treated with 10 μM of RIOK2 inhibitors for 28 days and stained with crystal violet. E) 1x105 cells were plated on 200ug/ml matrigel in an 8 um pore PET membrane in starvation media with DMSO or 10 uM RIOK2 inhibitors. 10% FBS media used as chemoattractant, cells allowed to invade for 16 hrs, fixed, stained with crystal violet and quantified (*p≤.05).

Conclusions

- Our kinome screen identified RIOK2, a widely overlooked kinase, as a potential mediator of PC progression in obese hosts.
- RIOK2 expression correlates with Gleason grade and lethal PC.
- Loss of RIOK2 genetically or with small molecules we have identified inhibits PC cell viability and invasion.
- RIOK2 regulates NPY2R expression that may couple NPY obesogenic signaling to PC cancer progression in obese men.

Funding

This study was supported by The Stewart Rahr – 2014 Prostate Cancer Foundation Young Investigator Award (EM) as well as NCI awards 1K22CA207883-01 (EM), R21CA216052-01 (EM) and 5K24CA160653-03 (SJF).

Brain Penetrating Nanoparticles (BPN) and Convection Enhanced Delivery (CED) for gene transfer in the brain

Karina Negron[1]; Namir Khalasawi[2]; Jillian Ho[2]; Justin Hanes, PhD[1-4]; Jung Soo Suk, PhD[2,4]

Johns Hopkins School of Medicine: [1]Pharmacology and Molecular Sciences; [2]Chemical Biomedical Engineering; [3]Biomolecular Engineering; [4]Ophthalmology

Introduction

Significance:

- Clinical trials for localized glioblastoma (GBM) gene therapy have revealed suboptimal therapeutic distribution in the brain as a key limiting factor.
- DNA-loaded nanoparticles (DNA-NP; non-viral polymeric gene vector) as large as 110 nm well-coated with hydrophilic and neutrally charged polyethylene glycol (PEG) efficiently penetrate the brain extracellular matrix (ECM) → "brain-penetrating" nanoparticles (**BPN**s).
- Convection enhanced delivery (**CED**) is an delivery method that facilitates distribution of locally administered therapeutics, including gene therapy, by providing a continuously pressure gradient.
- The combination of CED and BPNs provides a synergistic improvement of therapeutic distribution in the brain.

Specific Aims:

- To determine the optimal amount of PEG needed to achieve widespread distribution of, and subsequent transgene expression by, DNA-NP in the brain *in vivo* following CED.
- To address the lack of correlation between *in vitro* and *in vivo* performances of DNA-NP.

Hypothesis:

- The ability of DNA-NP to penetrate through the brain tissue and to mediate transgene expression in the brain is dependent upon surface PEG density.
- 3D tumor cell spheroid may serve as a *in vitro* model that better reflects an *in vivo* environment.

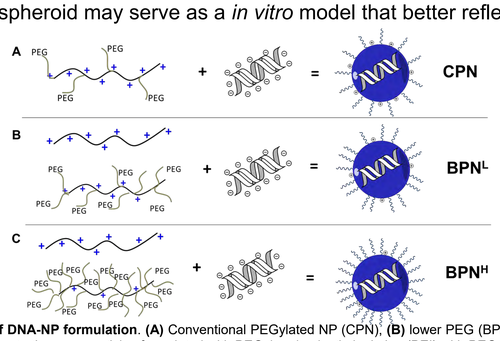

Figure 1. Schematic of DNA-NP formulation. **(A)** Conventional PEGylated NP (CPN), **(B)** lower PEG (BPN^L) and **(C)** higher PEG (BPN^H) density brain-penetrating nanoparticles formulated with PEGylated polyethylenimine (PEI) with PEG:PEI density of 8, 30 and 50, respectively.

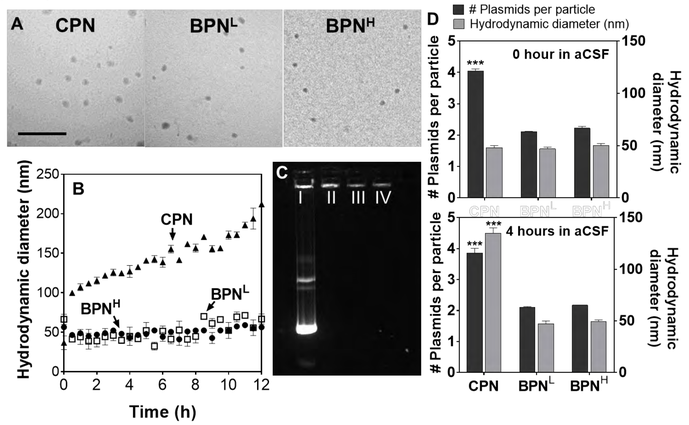

Figure 2. DNA-NP characterization (A) Transmission electron microscopy images of DNA-NP. Scale bar = 250 nm. **(B)** Hydrodynamic diameters over 12 hours in artificial cerebrospinal fluid (aCSF) at 37ºC. **(C)** Compaction of plasmids in DNA-NP shown by electrophoresis: I) free DNA, II) CPN, III) BPN^L, IV) BPN^H. **(D)** Number of plasmids in each DNA-NP and hydrodynamic diameter of DNA-NP when freshly formulated (top) and after a 4 hour incubation in aCSF 37ºC (bottom).

In vitro Transfection Efficiency

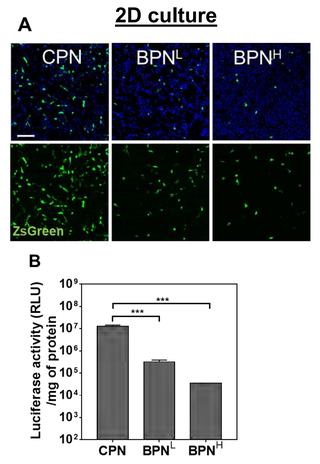

Figure 3. *In vitro* transfection in F98 GBM-based 2D culture. (A) Reporter ZSGreen and **(B)** luciferase transgene expression by DNA-NPs carrying ZSGreen-expressing and luciferase-expressing plasmids, respectively.

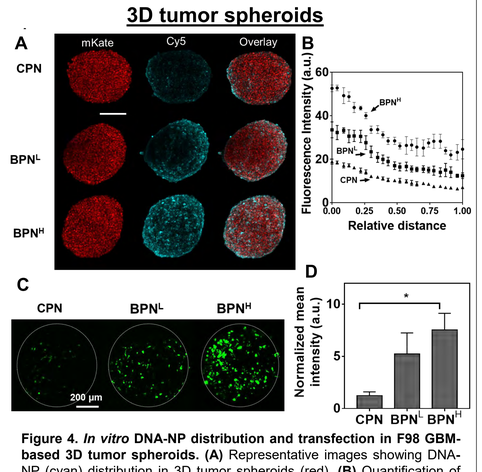

Figure 4. *In vitro* DNA-NP distribution and transfection in F98 GBM-based 3D tumor spheroids. (A) Representative images showing DNA-NP (cyan) distribution in 3D tumor spheroids (red). **(B)** Quantification of radial distribution of DNA-NPs within the spheroids. **(C)** Representative ZSGreen transgene expression (green) by DNA-NPs carrying ZsGreen-expressing plasmids in 3D tumor spheroids. **(D)** Quantification of ZSGreen transgene expression withing the spheroids.

Ex vivo Multiple Particle Tracking (MPT)

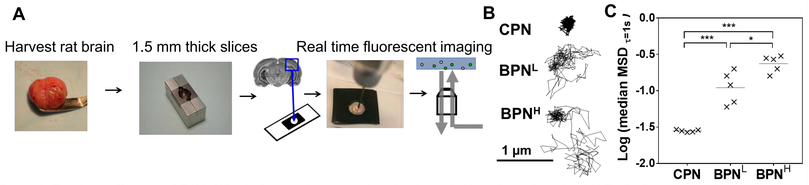

Figure 5. Ex vivo diffusion of DNA-NPs in freshly harvested rat brains. (A) Workflow of ex vivo MPT. **(B)** Representative trajectories of DNA-NP in rat brain tissue over 20 seconds. Scale bar = 1 µm. **(C)** Logarithms of median square displacements (MSD) of DNA-NPs at a time scale of 1 second. Data represent 5 independent experiments with n ≥ 200 particles tracked for each experiment.

In vivo Transfection Efficiency

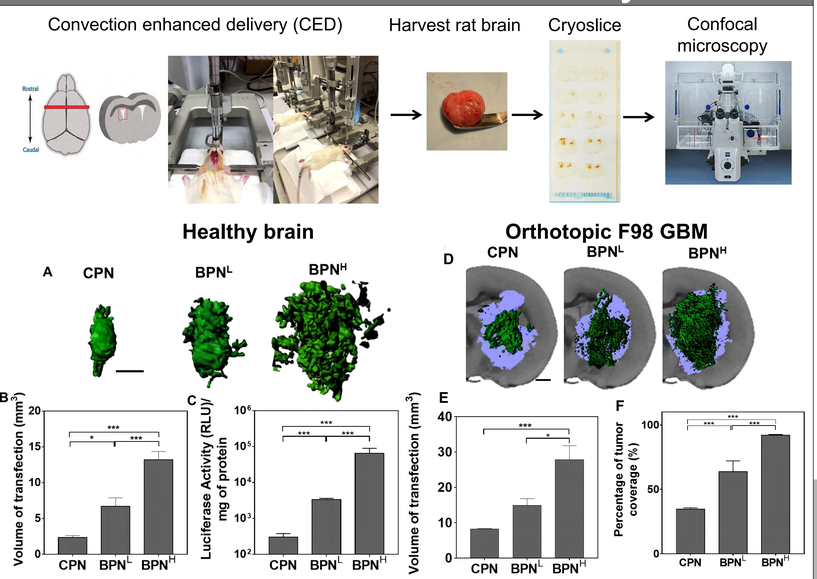

Figure 6. *In vivo* distribution and overall level of transgene expression following CED of DNA-NPs. (A) Workflow of *in vivo* gene transfer study. **(B)** Representative 3D images and **(C)** quantification (n ≥ 6 rats) of volumetric distribution of ZsGreen reporter transgene expression (green) in healthy rat brains. Scale bar = 1 mm. **(D)** Overall level of luciferase transgene expression in healthy rat brains (n ≥ 6 rats). **(D)** . **(E)** Representative 3D images and **(F)** quantification (n ≥ 4 rats) of volumetric distribution of ZsGreen reporter transgene expression (green) in orthotopic brain tumors (light blue). Scale bar = 1 mm. **(F)** Percentage of tumor volume with transgene expression (n ≥ 4 rats).

Transgene Expression Kinetics

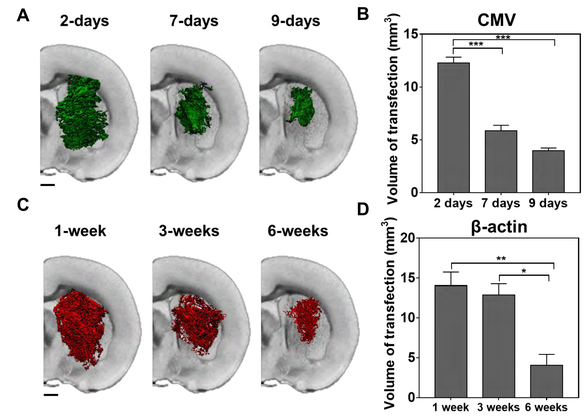

Figure 7. Transgene expression kinetics by DNA-BPN^H. (A) Representative 3D images and **(B)** quantification of volumetric distribution of Zsgreen transgene expression (green) regulated by a CMV promoter in healthy rat brain at varying time points after the administration. **(C)** Representative 3D images and **(D)** quantification of volumetric distribution of mCherry reporter transgene expression (red) regulated by a β-actin promoter in healthy rat brains at varying time points after the administration. Scale bar = 1 mm.

Summary and Conclusions

- BPN^H possesses "brain-penetrating" properties (i.e. ~50 nm particle diameter and near neutral surface charges) which are retained in a physiologically relevant condition.
- BPN^H efficiently penetrates 3D tumor spheroids and mediates widespread transgene expression.
- BPN^H can rapidly penetrate the brain tissue *ex vivo*.
- BPN^H provides more widespread transgene expression in healthy rat brains and orthotopically established brain tumors following CED compared to other formulations with lower PEG contents.
- Transgene expression kinetics of BPN^H can be modulated by the use of different types of expression promoters.
- *In vitro* transgene expression in 3D rat tumor spheroids correlates with *in vivo* transgene expression in orthotopically established rat tumors (BPN^H > BPN^L > CPN).

Special thanks to:

- Prior members of the Center for Nanomedicine at JHU, including Drs. Elizabeth Nance, Panagiotis Mastorakos, Clark Zhang as well as Eric Song, for their guidance.
- F31 Diversity NIH Fellowhip (FCA210610A)
- NIH R01EB020147, R01CA204968 and W.W. Smith Award (J.S.S.)
- Carl Storm Underrepresented Minority (CSURM) Fellowship for supporting my participation in the 2018 Barriers of the CNS GRC

References

1. Negron, K., et al., *Mechanistic studies to enhanced gene transfer in healthy and tumor brain tissue via Convection Enhanced Delivery (CED) of DNA-brain penetrating nanoparticles*. In Preparation
2. Mastorakos, P., et al., *Highly PEGylated DNA Nanoparticles Provide Uniform and Widespread Gene Transfer in the Brain*. Adv Healthc Mater, 2015. **4**(7): p. 1023-33.

mEAK-7 Regulates Self-renewal and Radiation Resistance in Cancer Cells

J.T. Nguyen[1,2,3], F.S. Haidar[1,2,3], A.L. Fox[1,2,3], A. Cho[4], C. Ray[1,2,3], D. Mendonca[1,2,3], H. Amatullah[1,2,3], J.K. Kim[4], and P.H. Krebsbach[1,4]

[1]Biointerfaces Institute, [2]Dept. of Biologic and Materials Sciences, [3]University of Michigan School of Dentistry, and [4]University of California, Los Angeles School of Dentistry.

BACKGROUND

Aberrant mTOR signaling has been observed in a variety of human cancers (*1*). Recently, we identified mEAK-7 (mammalian-enhancer-of-*akt*-1-7) as a novel molecular activator of mTOR signaling in human cells that utilizes the S6K2/4E-BP1 axis (*2*). Further, mEAK-7 exhibits a preferential expression pattern in human cancer cell lines (*2*). While EAK regulates dauer formation and lifespan in nematodes (*3*), the molecular mechanism remains unknown. However, the details of S6K2 signaling has not been extensively studied because S6K1 and S6K2 were widely considered to be redundant kinases (*4*). However, in breast cancer cells, loss-of-function studies demonstrate that S6K1 and S6K2 have several different protein targets (*5*). Additionally, canonical models of mTOR complex 1 (mTORC1) or mTORC2 may not be present in all cells, and have traditionally only been studied in small number of biologically relevant cell types . Most recently, a group identified a novel mTOR complex that forms outside of mTORC1 and mTORC2, which involves GIT1 in astrocytes (*6*). This poses an interesting question as to both the specificity of mTOR complex formation and the possibility that unknown mTOR complexes remain to be discovered.

While it is largely believed that mTOR signaling is suppressed under genotoxic stress through activation of AMPK regulation of TSC2 (*7*), studies demonstrate aberrant activation of mTOR signaling in response to This occurs via one of two phosphorylation pathways: either S6K-mediated phosphorylation of MDM2 to downregulate p53 (*8*), or 4E-BP1 phosphorylation in response to DNA damage (*9*). Sustained radiation treatment to mice activates mTOR signaling and oxidative stress in the intestine (*10*). Chemotherapeutics combined with rapamycin result in an additive cytotoxic effect in breast carcinoma cell lines (*11*). Additionally, normal tissues undergoing radiation stress exhibits activated mTOR signaling long in minipigs (*12*). Thus, we posit that there is major signaling mechanism that regulates genotoxic-induced mTOR signaling, possibly to allow for enhanced survival of cells during and after severe stressors.

mTOR signaling may impact radiation resistance and self-renewal, as seminal work revealed that cancer stem cells existed and were capable of giving rise to mature tumors raised from a single founder cell (*13*). Thus, there is a specific phenotype of cancer cells that contribute to the survival and pathogenicity of human cancers. Additionally, CSCs have been shown to be radiation resistant and thrive under genotoxic stress, but how that mechanism is regulated is unknown (*14, 15*). In a medulloblastoma *in vivo* model of cancer stem cells and radiation resistance, data suggests that PI3K signaling was activated via S6 regulation, a crucial mTOR signaling indicator, is activated in response to DNA damage (*16*). Intriguingly, mTOR signaling has also been indicated to be an essential component of CSC self-renewal in pancreatic CSCs (*17*). Therefore, substantive evidence suggests that mTOR signaling may play an important role in CSC radiation resistance and self-renewal.

Given reports that genotoxic stress is capable of activating mTOR signaling, select CSCs demonstrate radiation resistance, and the fact that CSCs require mTOR signaling for self-renewal, we posited that mEAK-7 plays a role in regulating radiation resistance in cancer cells and their ability to modulate self-renewal. Therefore, we hypothesize that mEAK-7 may be activated in response to DNA damage in order to regulate mTOR signaling in human cells.

ABSTRACT

Objectives:
Recently, we demonstrated that mammalian EAK-7 (mEAK-7) is an alternative activator of mTOR signaling. However, the molecular role of mEAK-7 under genotoxic stressors such as radiation therapy is unknown. The purpose of this study was to identify the role of mEAK-7 in regulating radiation resistance in non-small cell lung carcinoma cell lines.

Methods:
Cell lines were derived from ATCC. Multiple unique siRNAs were utilized. X-irradiation produced by Orthovoltage. Clonogenic assays performed in 2D and 3D. Comet assays prepared according to Cell Biolabs. Flow cytometry utilized for cell sorting of CSCs. mTOR signaling analyzed via immunoblot assays.

Results:
Bioinformatics analysis demonstrated that a subset of human cancers exhibits significant mEAK-7 gene copy number amplification or mRNA upregulation in certain human cancers. H1299 and H1975 cells treated with control or mEAK-7 siRNA, and treated with X-irradiation resulted in a statistically significant decrease in 2D colony formation and 3D spheroid formation. Flow cytometry demonstrated that CSCs derived from the H1299 cell line, defined by CD44+/CD90+, translate more mEAK-7 protein and this correlates with elevated levels of mTOR signaling. mEAK-7 knockdown resulted in a reduction in DNA damage repair, as analyzed by comet assay, and enhanced cell apoptosis after X-irradiation treatment. Immunoprecipitation/mass spectrometry analysis demonstrates that mEAK-7 associates with DNA-PK, and this interaction increases, in response to X-irradiation. DNA-PK signaling promotes the formation of radiation-resistant CSCs through aberrantly enhanced DNA-damage response mechanisms. We demonstrate that DNA-PK inhibitors resulted in further suppressed mTOR signaling in the presence of DNA damage, suggesting that these two signaling pathways cross-talk.

Conclusions:
mEAK-7 regulates alternative mTOR signaling under nutrient stimulation. However, the role of mEAK-7-mediated mTOR signaling in human cancer, was unknown. Thus, this study demonstrates that mEAK-7 is highly expressed in the CSC population, is required for clonogenic self-renewal, enhances the DNA-damage response, and promotes DNA-PK-mTOR cross-talk signaling in human cancer cells.

RESULTS

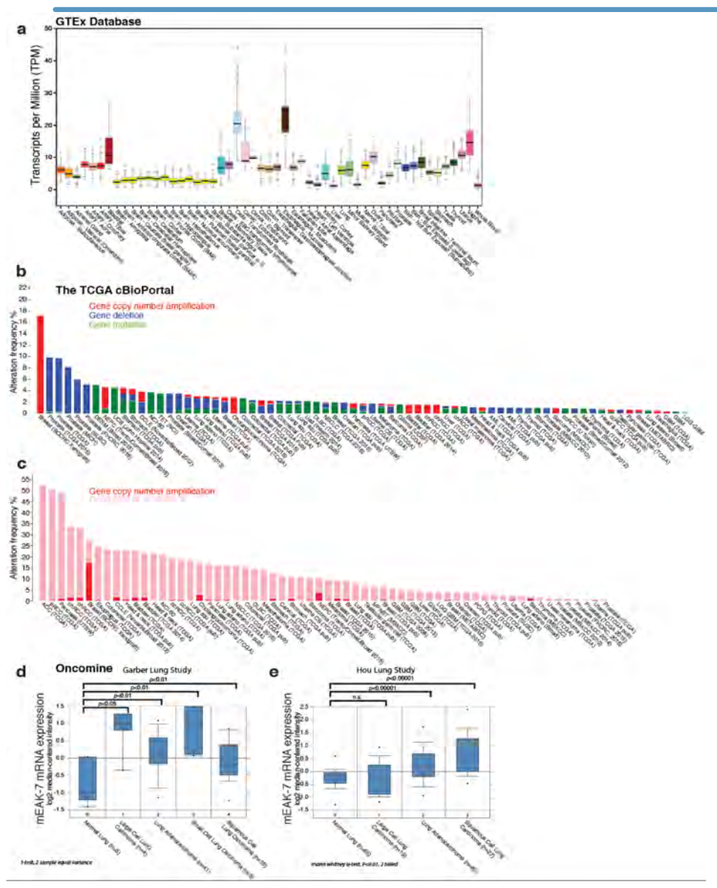

Figure 1. mEAK-7 gene is detected in normal human cells and upregulated in select human cancer types.

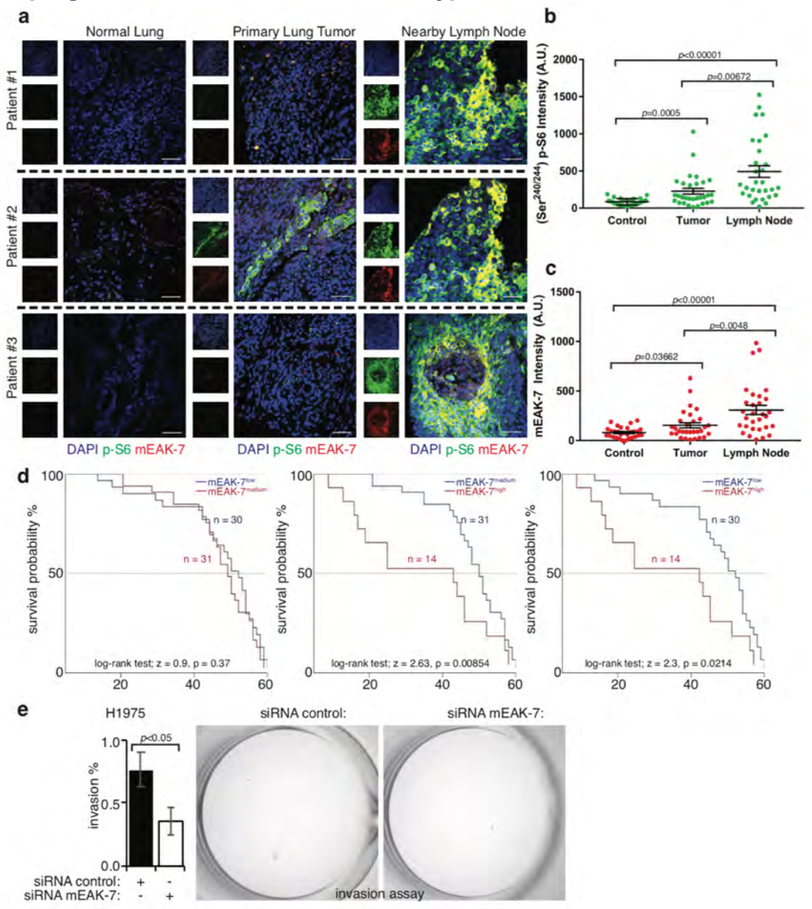

Figure 2. mEAK-7 is highly expressed in nearby lymph nodes of the tumor mass in NSCLC patients.

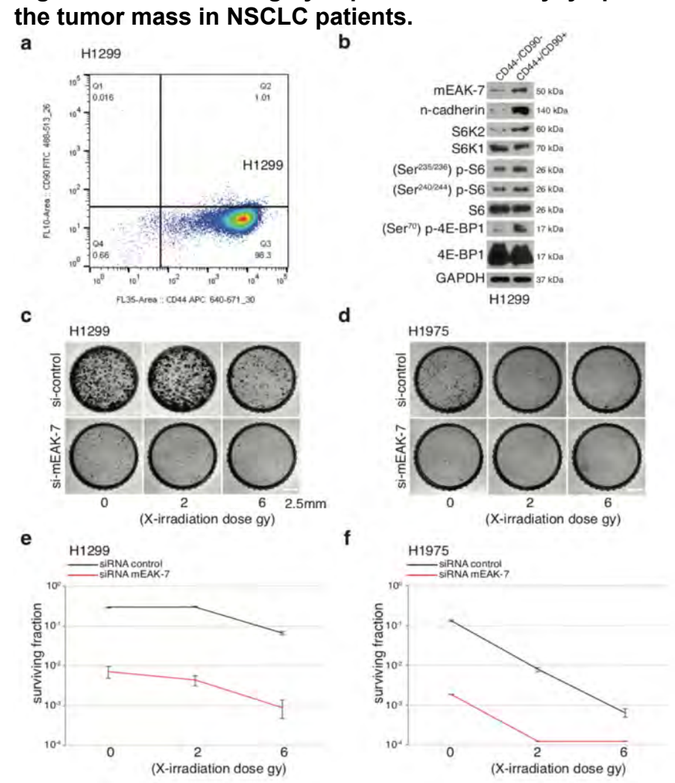

Figure 3. mEAK-7 is expressed in CD44+/CD90+ group, is required for clonogenic potential and radiation resistance.

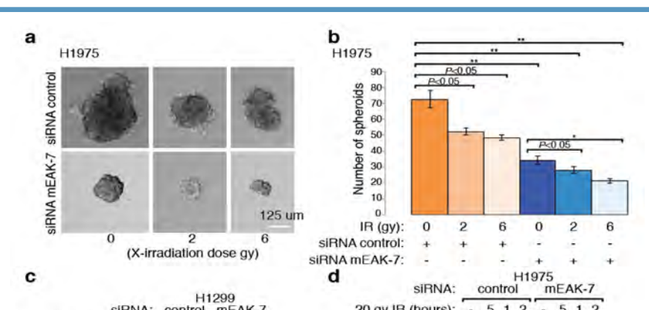

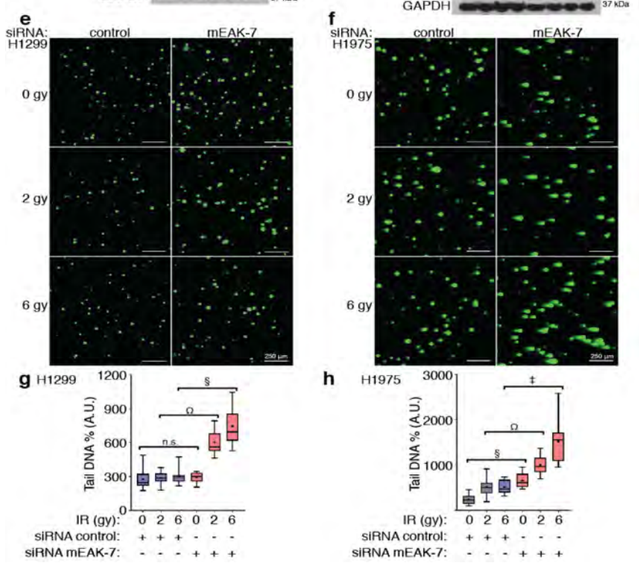

Figure 4. mEAK-7 is required for spheroid formation and is necessary for an effective DNA damage response.

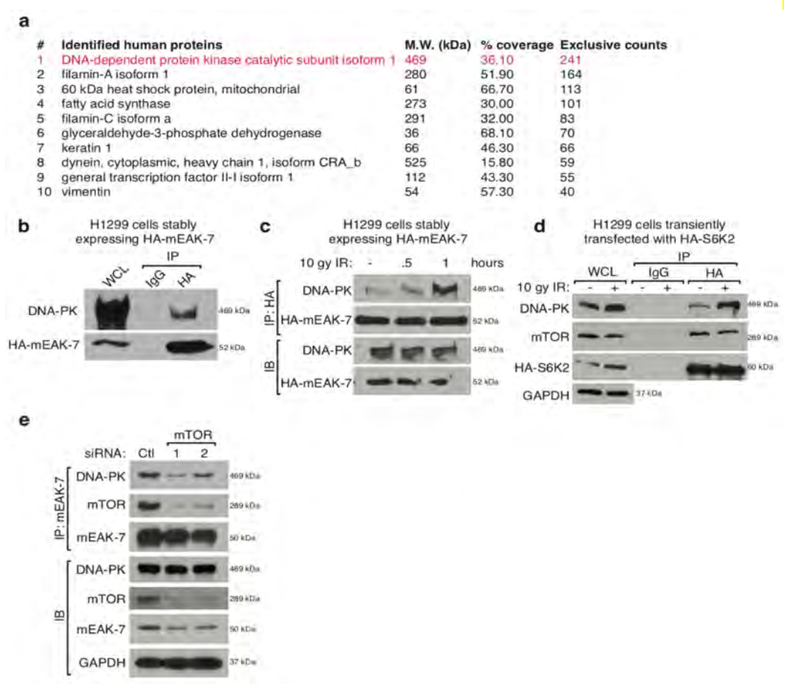

Figure 5. Immunoprecipitation/mass spectrometry analysis demonstrates that mEAK-7 associates with DNA-PK in response to X-irradiation treatment.

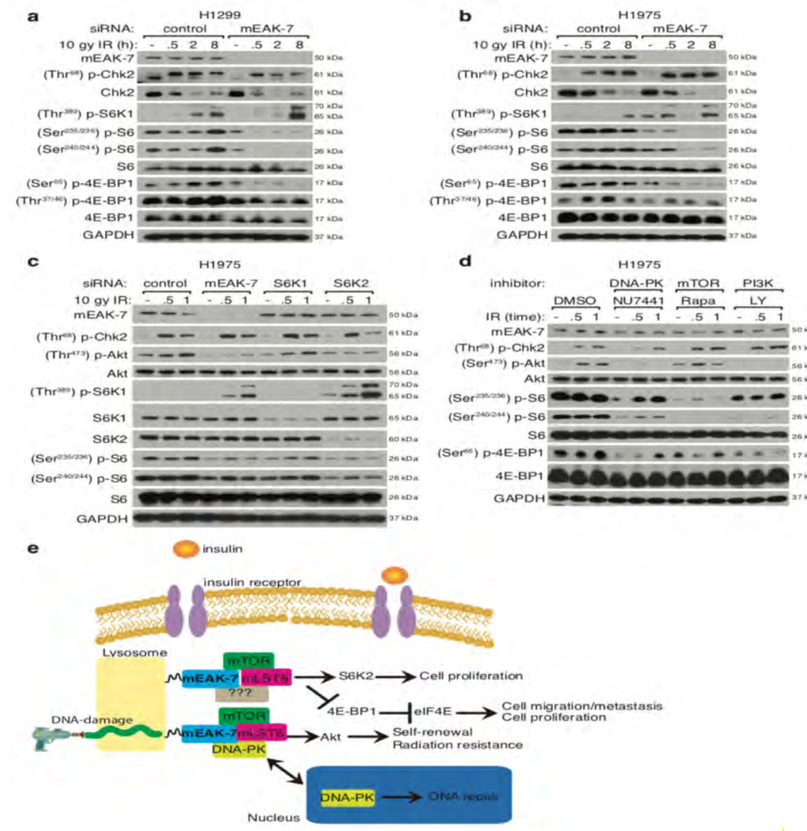

Figure 6. mEAK-7 is required for X-irradiated activation of mTOR signaling to regulate radioresistance through a novel DNA-PK/mTOR complex